Dana-Farber Cancer Institute
Harvard Medical School
Director: Laurie Glimcher, M.D.

and

Kinderklinik und Kinderpoliklinik im Dr. von Haunerschen Kinderspital
Klinikum der Ludwig-Maximilians-Universität München
Vorstand: Prof. Dr. Dr. Christoph Klein

Integration of screening data for the discovery of therapeutic strategies in Ewing sarcoma

Dissertation
zum Erwerb des Doktorgrades der Medizin
an der Medizinischen Fakultät der
Ludwig-Maximilians-Universität zu München

Vorgelegt von
Björn Stolte

aus
München

2021

Authorized by the medical faculty of the Ludwig-Maximilians-Universität München

Berichterstatter:	Prof. Dr. Dr. Christoph Klein
Mitberichterstatter:	Prof. Dr. Lars Lindner
	Prof. Dr. Claus Belka
	Prof. Dr. Thomas Kirchner
Dekan:	Prof. Dr. med. Thomas Gudermann
Tag der mündlichen Prüfung:	21.10.2021

1 - Attestation under oath

LMU LUDWIG-MAXIMILIANS-UNIVERSITÄT MÜNCHEN

Dean's Office
Faculty of Medicine

MMRS

Affidavit

Stolte, Björn

Surname, first name

Street

Zip code, town

Country

I hereby declare, that the submitted thesis entitled

Integration of screening data for the discovery of therapeutic strategies in Ewing sarcoma

is my own work. I have only used the sources indicated and have not made unauthorised use of services of a third party. Where the work of others has been quoted or reproduced, the source is always given.

I further declare that the submitted thesis or parts thereof have not been presented as part of an examination degree to any other university.

Boston, MA, 8 November 2021

Place, date

Björn Stolte

Signature doctoral candidate

2 - Table of contents

3 - Abbreviations

ABL - Abelson murine leukemia viral oncogene homolog 1

BCR - Breakpoint Cluster Region protein

Cas9 - CRISPR associated protein 9

CDK - cyclin dependent kinase

CDKN2A - cyclin-dependent kinase Inhibitor 2A gene

CRISPR - Clustered regularly interspaced short palindromic repeats

DNA - deoxyribonucleic acid

ETS - ETS transcription factor family

EWS - protein encoded by *EWSR1* gene

EWSR1 - Ewing sarcoma breakpoint region 1 gene

FLI1 - Friend Leukemia Virus Integration 1 gene

FLI - protein encoded by *FLI1* gene

gamma-H2AX - phosphorylated histone H2A.X

MDM2 - Murine double minute 2 gene

MDM2 - protein encoded by *MDM2* gene

MDM4 - Murine double minute 4 gene

MDM4 - protein encoded by *MDM4* gene

MYCN - V-Myc Avian Myelocytomatosis Viral Oncogene Neuroblastoma Derived Homolog gene

p53 - protein encoded by *TP53*

PARP - Poly (ADP-Ribose) Polymerase 1 protein

PPM1D - Protein Phosphatase, Mg2+/Mn2+ Dependent 1D gene

RAD51 - RAD51 recombinase gene

STAG2 - Stromal antigen 2 gene

TP53 - Tumor protein 53 gene

USP7 - Ubiquitin-specific peptidase 7 gene

USP7 - protein encoded by *USP7* gene

Wip1 - Wild-Type p53-Induced Phosphatase 1, protein encoded by *PPM1D*

4 - Publications

1. *Genome-scale CRISPR-Cas9 screen identifies druggable dependencies in TP53 wild type Ewing sarcoma*

   Björn Stolte, Amanda Balboni Iniguez, Neekesh Dharia, Amy Saur Conway, Ann Morgan, Gabriela Alexe, Nathan Schauer, Xiaoxi Liu, Gregory Bird, Aviad Tsherniak, Francisca Vazquez, Sara Buhrlage, Loren Walensky, Kimberly Stegmaier

   Journal of Experimental Medicine, August 2018, PMID: 30045945

2. *EWS/FLI confers tumor cell synthetic lethality to CDK12 inhibition in Ewing sarcoma*

   Amanda Balboni Iniguez, **Björn Stolte**, Emily Jue Wang, Amy Saur Conway, Gabriela Alexe, Neekesh Dharia, Nicholas Kwiatkowski, Tinghu Zhang, Brian Abraham, Jaume Mora, Peter Kalev, Alan Leggett, Dipanjan Chowdhury, Cyril Benes, Richard Young, Nathanael Gray, Kimberly Stegmaier

   Cancer Cell, February 2018, PMID: 29358035

5 - Attestation by Laurie Glimcher, M.D.

Laurie H. Glimcher, M.D.
President and CEO, Dana-Farber Cancer Institute

Director, Dana-Farber / Harvard Cancer Center

Richard and Susan Smith Professor of Medicine
Harvard Medical School

450 Brookline Ave., DA1628
Boston, MA 02215-5450
617.632.4266 tel. 617.632.2161 fax
laurie_glimcher@dfci.harvard.edu
www.dana-farber.org

August 23, 2018

Dear Colleagues:

This letter is to acknowledge that Björn Stolte (born November 19th 1991 in Munich, Germany) was a visiting researching medical student in Dr. Kimberly Stegmaier's laboratory at the Dana-Farber Cancer Institute in Boston, MA from May 2015 until July 2018. During his training, he performed experiments for his doctoral thesis work to be granted by the University of Munich, which resulted in a co-authorship on the research paper entitled "EWS/FLI confers tumor cell synthetic lethality to CDK12 inhibition in Ewing sarcoma" published in *Cancer Cell* in 2018, and first-authorship on the research paper entitled "Genome-scale CRISPR-Cas9 screen identifies druggable dependencies in TP53 wild type Ewing sarcoma" published in 2018 in *Journal of Experimental Medicine*.

Sincerely,

Laurie H. Glimcher, M.D.
President & CEO

6 - Introduction

6.1 - Discovery, epidemiology, prognosis, and molecular characteristics of Ewing sarcoma

Ewing sarcoma is a malignant tumor of small, blue, round cells localizing to the bones and soft tissues of mostly children, adolescents and young adults. The disease was discovered by Dr. James Ewing in 1920, who described a “diffuse endothelioma of the bone”. He found that the tumor most commonly affects the diaphysis of long bones, is susceptible to exposure to radium, and has a characteristic appearance on radiologic imaging. These distinct features established the cancer as its own entity that was separate from osteosarcoma, which was known as a neoplastic growth of the bone. The disease was later named “Ewing’s tumor” by Dr. Ewing’s peers and has retained the name since. [1]

The peak incidence age of Ewing sarcoma is 15 years. Boys and young men are more commonly affected with a male to female ratio of 3:2. It is a rare disease with around 3 new diagnoses per million per year and is more common in patients of European descent (1.5 cases per million), than in those of Asian (0.8 cases per million), and African descent (0.2 cases per million). Sites of bone disease include the pelvis, femur, tibia and ribs, and soft-tissue tumor localizations include the thoracic wall, gluteal muscle, pleural cavities, and cervical muscles. [2-8]

Since the first description of the disease in the early 1920s, the prognosis for patients with Ewing sarcoma has dramatically improved, thanks to multi-disciplinary approaches, progress in surgical techniques, innovations in radiation therapy, and new chemotherapy agents and regimens. While one of Dr. Ewing’s first patients, a 14-year-old girl with a tumor of the arm, had the then common fate to quickly succumb to the disease (she died within 30 months of onset of symptoms), today, patients with localized disease and standard risk have 5-year survival rates of 70-80%. The prognosis for patients presenting with more advanced stages, however, is still unfavorable. About a quarter of patients present with metastatic spread at diagnosis and face 5-year survival rates of only about 30%. Similarly, patients with relapsed disease have long-term survival rates of less than 25%. [1, 2, 6, 8, 9]

Ewing sarcoma cells express an aberrant oncogenic fusion transcription factor that drives proliferation. During tumorigenesis, a chromosomal translocation leads to the fusion of EWS and

ETS family proteins, and while different translocations and fusion proteins exist, about 85% of tumors present with a t(11;22)(q24;q12) chromosomal translocation, resulting in the chimeric fusion gene *EWSR1-FLI1* encoding the EWS-FLI protein. The expression of the fusion protein transcription factors leads to oncogenic programs that drive malignant behavior. Adding to the complexity of understanding the disease, the cell of origin of Ewing sarcoma is unknown, with leading hypotheses suggesting development from either mesenchymal stem cells or neural crest cells. [10-15]

The rate of genetic mutations in Ewing sarcoma is remarkably low. With few recurrent mutations, it is one of the most genetically silent human cancers. [16-18] Therefore, and similar to many other genetically silent pediatric cancers, epigenetic dysregulation is being investigated as a contributor to oncogenesis. [19-21]

6.2 - Current therapeutic approach to Ewing sarcoma

The current therapeutic approach to Ewing sarcoma is multi-disciplinary and relies on combinations of surgical resection, local radiation therapy, and multi-agent chemotherapy. Chemotherapy regiments include cytotoxic agents such as etoposide, vincristine, cyclophosphamide, ifosfamide and doxorubicin. Although outcomes have vastly improved since Ewing sarcoma was first described, major challenges remain. Patients with relapsed and metastatic disease still have a dismal prognosis and pediatric oncologists treating these patients have few long-term effective therapies to offer. Furthermore, adverse effects of the treatment, the life-long consequences of surgery at a young age (especially for patients treated with amputation), and the risk of secondary malignancies are short-comings of current treatment strategies. [2, 4, 5, 7-9, 22] It is therefore evident that better treatment options for Ewing sarcoma are needed.

6.3 - The challenge of developing targeted therapies in Ewing sarcoma

The advent of molecular genetics has led to a better understanding of the metabolism and signaling of cancer cells and, in some cases, the identification of molecular vulnerabilities in cancer cells. A molecular vulnerability is conferred by a protein that a cancer cell, but not a normal

cell, heavily relies upon for proliferation, which opens a therapeutic window. The inhibition of these proteins is called targeted therapy. In theory, targeted therapies offer great advantages over the use of non-specific cytotoxic chemotherapy agents, including less adverse effects and lower risk of secondary malignancies. A prime example of a targeted therapy is the inhibition of the BCR-ABL fusion tyrosine kinase in chronic myeloid leukemia (and later acute lymphoblastic leukemia) by imatinib and its derivatives. [23, 24]

In Ewing sarcoma, the EWS-ETS fusion proteins would be ideal candidates for a targeted therapy: They are found in all tumor cells (the presence of one of the ETS-EWS transcription factor variants is required to make the diagnosis of Ewing sarcoma), are only expressed in Ewing sarcoma cells (so targeting them might leave normal cells unaffected), and are highly oncogenic (suggesting their inhibition would drastically reduce the proliferation of malignant cells). However, EWS-ETS proteins are transcription factors, which are inherently difficult to drug due to their disordered structure. Efforts to develop inhibitors for EWS-ETS transcription factors that might be used in patients have been largely unsuccessful. [2, 25, 26] As EWS-ETS transcription factors have proven to be hard to drug, other proteins and pathways need to be investigated.

In adult cancers, oncogenic gene mutations frequently give rise to aberrant molecules that are feasible drug targets. In pediatric cancers however, frequencies of DNA mutations are often low, resulting in a paucity of druggable targets such as mutated kinases or overexpressed transmembrane receptors. This is also true for Ewing sarcoma. Genomic landscape studies revealed that Ewing sarcoma tumors have very quiet genomes except for the highly recurrent EWS-ETS fusion transcription factors, and not directly therapeutically actionable mutations in *TP53* and *STAG2* and deletions of *CDKN2A*. [16-18] As the sequencing of Ewing sarcoma tumor genomes has not led to the identification of molecular vulnerabilities, other approaches to developing targeted therapies need to be employed.

6.4 - CRISPR-Cas9 as a tool for the identification of molecular vulnerabilities

CRISPR (clustered regularly interspaced short palindromic repeats) are DNA sequences expressed by a number of prokaryotes as a defense mechanism against viruses. Paired with endonuclease

Cas9 (CRISPR associated protein 9) and enveloped in a viral vector, it becomes a DNA editing tool that can induce double-strand breaks in any genomic region to disrupt gene function, and allows for the study of loss of function of genes. The CRISPR-Cas9 system is used in oncology to nominate and evaluate therapeutic targets. [27-32]

CRISPR-Cas9 can be adapted to high-throughput, genome-scale assays. With these systematic approaches, many genes (and even the whole genome) can be perturbed concurrently in a pool of cells. This allows for interpretation of potential molecular vulnerabilities in their phenotypic (e.g., cancer type) and genotypic (e.g., mutational status) context. Therefore, high-throughput screening methods have gained importance for finding molecular vulnerabilities in cancer cells. [33-38]

6.5 - Genomic and chemical screening methods

In this dissertation, two screening methods are used to identify new therapeutic targets in Ewing sarcoma. One method is a genomic knockout screen using CRISPR-Cas9, the other a chemical screen of a panel of cancer cell lines with a novel inhibitor. The approaches demonstrate two complementary ways to discover new therapeutic strategies for cancer by using screening methods.

In genome-scale CRISPR-Cas9 screens, a library of CRISPR sgRNA constructs is designed to cover every gene in the genome with several probes. The constructs are each tagged with unique DNA sequence barcodes. The library is packaged in viral vectors via transfection of host cells and following an incubation period, recombinant virus is harvested and stored. After engineering the target cells to express Cas9, proliferation rate, transduction dynamics, and doubling times of the cells of interest are standardized. Then, cells are transduced with the viral vectors containing the CRISPR library at a multiplicity of infection of 1, meaning each target cell is infected with one CRISPR plasmid. After a predefined amount of proliferation in cell culture, the target cell DNA is extracted. By sequencing the barcode DNA, the abundance and depletion of each construct in the pool of cells is determined. The computational analysis of this data allows for the identification of

genes that are essential to the proliferation of a particular cell type, which informs the search for new targets for drug therapy. [33, 38]

Chemical screenings of cancer cell lines can effectively complement genomic screening data. In a chemical screen of a novel inhibitor, the genes/proteins of interest are known (as defined by the target of the tested inhibitor), and the cancer types in which they are relevant is to be determined. To do so, a panel of cancer cell lines are treated at defined concentrations and cell viability is assessed. Cancer cell types that are highly sensitive to an inhibitor are then evaluated in secondary assays. [39]

6.6 - Reactivation of p53 as a molecular vulnerability

The publication by Stolte et al. included in this dissertation revolves around p53 regulation in Ewing sarcoma.

The *TP53* gene and the corresponding p53 protein are among the most heavily studied entities in oncology. Its major influence on many cellular processes make p53 a central player in oncogenesis. Cancer cells benefit from *TP53* loss-of-function mutations by evading its powerful cell death-inducing capabilities, and p53 is one of the most frequently mutated genes in cancer overall. [40] Many pediatric neoplastic diseases including Ewing sarcoma, however, retain a functional p53 protein. This leaves the path to therapeutically activating the protein open for exploration. [16-18, 40-47]

In previous studies, inhibition of the p53 regulator MDM2 has been explored. [48] However, systematic approaches to finding p53-dependant molecular vulnerabilities have not been made previously.

In this dissertation, a systemic approach via a CRISPR-Cas9 knockout screen to identify p53-dependent molecular vulnerabilities in Ewing sarcoma is described, and the study of these targets is demonstrated.

6.7 - Transcriptional regulation as a molecular vulnerability

The publication by Balboni Iniguez et al. that is part of this dissertation investigates the therapeutic strategy of inhibiting factors involved in transcription in Ewing sarcoma.

Many cancers show specific patterns of gene expression and targeting this oncogenic transcriptional activity is a promising angle for therapy. To advance this approach, new transcriptional inhibitors are being developed. [49-53]

Previous studies have shown that in Ewing sarcoma cells, EWS-ETS transcription factors induce a number of target genes that contribute to malignant behavior. The cells' survival and proliferation rely on this specific gene expression signature maintained by the EWS-ETS transcription factors, and disturbing this system might reduce the proliferation capabilities of the cells. The study of factors contributing to the execution of transcription might identify molecular vulnerabilities amendable to targeted therapy. [54-60]

One new class of transcriptional inhibitors is molecules inhibiting cyclin-dependent kinases (CDKs) that are involved in transcription. THZ1, a first-in-class covalent inhibitor of primarily CDK7, has been shown to have anti-proliferative activity in T-cell acute lymphoblastic leukemia [50], *MYCN*-amplified Neuroblastoma [61], and small-cell lung cancer [62]. Given that Ewing sarcoma is a cancer with altered transcription, the investigation of CDK inhibitors in the disease is of interest.

The publication explores the use of THZ1 and its derivatives as a new therapeutic strategy for Ewing sarcoma and explores their mechanisms of action.

7 - Contributions by the author

7.1 - Publication I

Björn Stolte was the project leader for this study. He designed, planned and executed the vast majority of experiments. Reagents used in this project were acquired, tested and stored by him. Cloning of utilized plasmids was performed by Björn Stolte. He analyzed the resulting data, kept

records of performed experiments and archived obtained results. Computational analysis of the screen was performed by Björn Stolte using software provided by the Broad Institute including the depmap portal data explorer software.

All experimental *in vivo* work was performed by Björn Stolte with assistance in feeding animals, changing beddings and monitoring of animal health by Dana-Farber Cancer Institute mouse core facility staff.

The initial manuscript was written, revised after receiving comments from the co-authors, and submitted to the scientific journal by Björn Stolte. After comments from the reviewers were received, he designed, planned and executed the required experiments. He wrote the revised manuscript and re-submitted it to the scientific journal. All figure panels of the initial and the revised manuscript were created by him.

Björn Stolte presented the data during regularly scheduled meetings with Dr. Stegmaier, meetings of the whole laboratory, meetings with collaborators, and in form of poster presentations at the 2017 Dana-Farber Cancer Institute Pediatric Oncology summer retreat meeting as well as the 2017 American Association for Cancer Research (AACR) Pediatric Oncology conference.

The other authors made contributions to the following aspects of the publication:

Design of experiments: A. Balboni Iniguez, N.V. Dharia, A.M. Morgan, G.H. Bird, A. Tsherniak, F. Vazquez, N.J. Schauer, X. Liu, S.J. Buhrlage, L.D. Walensky, and K. Stegmaier

Acquisition of data: A.M. Morgan, A.L. Robichaud, and A. Conway Saur

Statistical analysis, biostatistics, and computational analysis: N.V. Dharia, G. Alexe

Writing and revising the manuscript: A. Balboni Iniguez, N.V. Dharia, A.L. Robichaud, A. Saur Conway, A.M. Morgan, G. Alexe, G.H. Bird, A. Tsherniak, F. Vazquez, N.J. Schauer, X. Liu, S.J. Buhrlage, L.D. Walensky, and K. Stegmaier

Supervision of the study: K. Stegmaier and L.D. Walensky

7.2 - Publication II

Björn Stolte and Amanda Balboni Iniguez led this research study and closely collaborated in designing, planning of the experiments of this project. A separate set of reagents and a separate lab notebook were maintained by Björn Stolte who worked independently on his contribution to

the publication. He analyzed the resulting data, kept records of performed experiments and archived obtained results.
Björn Stolte assisted in the experimental *in vivo* work including by measuring tumor engraftment and tumor size development over time in mice implanted with Ewing sarcoma cells.
Björn Stolte contributed sections to the initial as well as to the revised manuscript text and to the creation of figure panels for this study.
During regularly scheduled meetings with Dr. Stegmaier and Amanda Balboni Iniguez, Björn Stolte presented his data and outlined his interpretation. He also presented his data during laboratory meetings on the project and during meetings with collaborators.

The other authors made contributions to the following aspects of the publication:
Conceptualization: A. Balboni Iniguez, K. Stegmaier, N.S. Gray, R.A. Young, D. Chowdhury, and C.H. Benes
Formal Analysis: G. Alexe, B.J. Abraham, and N.V. Dharia
Investigation: A. Balboni Iniguez, E.J. Wang, A. Saur Conway, A. Leggett, P. Kalev, and C.H. Benes
Resources: N. Kwiatkowski, T. Zhang, and J. Mora
Writing – Original Draft: A. Balboni Iniguez and K. Stegmaier
Writing – Review & Editing: A. Balboni Iniguez, K. Stegmaier, N. Kwiatkowski, and B.J. Abraham
Funding Acquisition: K. Stegmaier and R.A. Young

8 - Summary of the publications

This dissertation explores new treatment strategies for Ewing sarcoma in two publications, both of which are informed by characteristics of Ewing sarcoma biology and demonstrate the power of screening methods to discover therapeutically-actionable molecular vulnerabilities. The projects follow a similar itinerary: the starting points are screening efforts (genomic for one, chemical and genomic for the other), leading to the identification of potential targets which are tested using genetic tools and chemical probes. Combination therapies are then evaluated to find feasible drug combination to enhance the efficacy of the inhibition of the new targets. Finally, the *in vitro* evaluation is followed by *in vivo* experiments in mouse models.

In “Genome-scale CRISPR-Cas9 screen identifies druggable dependencies in *TP53* wild-type Ewing sarcoma” by Stolte et al., the hypothesis is explored that the absence of *TP53* mutations in the majority of Ewing sarcoma tumors enables therapies aiming at the reactivation of p53 protein, and the identification and evaluation of several p53 regulators as drug targets in the disease is described.

In “EWS/FLI Confers Tumor Cell Synthetic Lethality to CDK12 Inhibition in Ewing Sarcoma” by Balboni Iniguez et al., the hypothesis is tested that the downstream oncogenic transcriptional programs of the EWS-ETS fusion transcription factors might be feasible drug targets. The study includes the use of novel transcriptional cyclin-dependent kinase inhibitors, their mechanism of action in the disease, and evaluation as therapeutic strategies in several models.

8.1 - Publication I - Genome-scale CRISPR-Cas9 screen identifies druggable dependencies in *TP53* wild-type Ewing sarcoma

Tumor protein 53 is a major player in the biology of cancer, and mutations in the gene are some of the most common occurrences in cancer as a whole. [40] In Ewing sarcoma tumors, however, mutations in *TP53* are exceedingly rare. Only about 10% of investigated tumors exhibit alterations in the gene. [16-18] Remarkably, this ratio seems inverted in Ewing sarcoma cell lines, of which the majority lose functional p53 protein. This could either be the result of single cells having acquired a *TP53* mutation after prolonged periods of tissue culture (which can be hypothesized to select for proliferation enhancing alterations such as loss-of-function mutations in *TP53*), or because mutated *TP53* facilitates the generation of a cell line. With patient-derived xenografts of Ewing sarcoma tumors having been established only recently, decades of Ewing sarcoma research have relied heavily on cell lines. [63] The overrepresentation of *TP53* mutations in these models is a misrepresentation of the disease, a bias that might have obliterated feasible drug targets in previous studies. To address this possibility, this research effort aims at studying *TP53* wild type models of Ewing sarcoma. [16-18, 40-47]

A genome-wide CRISPR-Cas9 screen previously published included diverse cancer types, among them nine Ewing sarcoma cell lines. [38] This screen was analyzed with the specific question of genetic dependencies (i.e., genes whose loss-of-function reduces proliferation of cells) in *TP53* wild type Ewing sarcoma cell lines. The analysis nominated four genes (*MDM2*, *MDM4*, *PPM1D, and USP7*) whose gene products are druggable with compounds in preclinical or clinical evaluation. All four proteins are known to have roles in p53 regulation.

Low-throughput validation confirmed the screening data and showed strictly p53-dependent dependencies on *MDM2*, *MDM4*, *PPM1D*, and *USP7*. The stapled-peptide dual inhibitor of MDM2 and MDM4 ATSP7041 proved efficacious in decreasing Ewing sarcoma cell proliferation *in vitro* and *in vivo* with little to no effect on Ewing sarcoma models with mutated *TP53*, suggesting few off-target events. The USP7 inhibitor P5091 and the Wip1 (the gene product of *PPM1D*) inhibitor GSK2830371 decreased viability of Ewing sarcoma cells *in vitro*, but did not show a strictly p53-dependent response.

Combination treatment studies demonstrated the feasibility of combining inhibitors of p53 regulators to synergistic effects. Additive to synergistic effects were seen with combinations of ATSP7041 with chemotherapeutic agents, suggesting a possible benefit of adding a derivative of the drug to current chemotherapy regiments.

Finally, *TP53* knockout Ewing sarcoma cell lines were generated to further test the requirement of functional p53 for response to genetic or chemical inhibition of the target genes. Loss of p53 fully rescued the effects of ATSP7041 on Ewing sarcoma cell lines, while only partial rescue was seen for treatments with P5091 and GSK2830371. To distinguish whether the incomplete rescue was due to possible off-target effects of the chemical compounds or additional non-p53-dependant functions of USP7 and Wip1 in Ewing sarcoma, double-knockout experiments were performed. The assays confirm that loss of p53 indeed renders cells more resistant to loss of either *USP7* or *PPM1D*, which is strong evidence that the initial finding of the screen and previously performed experiments in the study are true. Further support is provided by testing of

new generation USP7 inhibitor XL-188 whose viability effects are fully rescued by p53 loss in two Ewing sarcoma cell lines.

In conclusion, this study presents a systematic approach to identifying p53-dependent molecular vulnerabilities in Ewing sarcoma, and investigates several new targets, inhibitors, and combination treatments. A derivative of the MDM2 and MDM4 dual inhibitor ATSP7041 is since being evaluated in clinical trials in pediatric cancers (ClinicalTrials.gov Identifier: NCT03654716), underlining the potential of clinical translation of the therapeutic strategies described here.

8.2 - Publication II - EWS/FLI Confers Tumor Cell Synthetic Lethality to CDK12 Inhibition in Ewing Sarcoma

Ewing sarcoma is defined by oncogenic EWS-ETS transcription factors. EWS-FLI and other, rarer variants initiate and maintain the transcription of target genes, which drive the malignant behavior of the cells. [12, 54-60]

As Ewing sarcoma cells rely on transcription of these target genes, a possible strategy for treating the disease is the inhibition of transcription. Targeting transcription is known to be effective in cancer therapy, including by use of transcriptional inhibitor Actinomycin D that has been in use for many decades. Previous studies with newer inhibitors have shown that cancers with high rates of transcription show response to transcriptional modulators, including to inhibitors of transcriptional cyclin-dependent kinases (CDKs). THZ1, an inhibitor of CDK7, CDK12, and CDK13, has shown promise in previous studies in preclinical models of a number of cancers. [50, 61, 62]

In a chemical screen with a large panel of cancer cell lines, Ewing sarcoma cell lines were highly sensitive to THZ1. In low-throughput experiments, it was confirmed that THZ1 decreases proliferation of Ewing sarcoma cell lines, induces apoptosis (as shown by Annexin V assays and probing for the cleavage of PARP), and acts on-target (i.e. decreases phosphorylation of RNA polymerase II at the predicted Serine residues). *In vivo*, THZ1 reduced tumor progression and prolonged survival in mice bearing Ewing sarcoma tumors.

Mining genomic screening data, Ewing sarcoma cells seemed to be sensitive to *CDK12* loss but not loss of *CDK13*. Also, loss of *CDK7* presented as a pan-lethal in the cancer cell lines. This raises the suspicion that all human cells might rely on CDK7, which might suggest a small therapeutic window for its inhibition. Therefore, CDK12 was pursued as a molecular vulnerability in Ewing sarcoma.

THZ531, a derivative of THZ1, is a selective CDK12/13 inhibitor. Ewing sarcoma cells were found to be highly sensitive to THZ531 and on-target mechanism of action was shown by confirming the interruption cyclin K with CDK12 after THZ531 treatment in immunoprecipitation experiments. Genetic knockout (via CRISPR-Cas9) and knockdown (via small hairpins RNAs) of the genes confirmed that loss of *CDK12*, and not *CDK13*, reduces proliferation.

To study the effects of THZ531 in Ewing sarcoma, gene expression profiling was performed. Intriguingly, the data does not support the hypothesis that the anti-proliferative effect of THZ531 is due to preferential down-regulation of EWS-ETS target genes. While an overall decrease in transcription was observed, EWS-ETS target genes were not among the most down-regulated genes. Instead, it was the transcription of DNA damage repair-related genes, including genes of homologous repair and DNA damage checkpoint control, which were greatly affected by inhibition of the CDKs. This suppression of DNA damage related genes by THZ531 was confirmed in low-throughput.

The sensitivity of Ewing sarcoma cells to CDK12 inhibition appeared to be EWS-ETS transcription factor-dependent, as cells with repressed EWS-FLI were found to be more resistant to THZ531. Furthermore, EWS-FLI is a biomarker for sensitivity to DNA damaging agents in publicly available chemical screening data, further supporting a link between EWS-ETS transcription factors and DNA damage and DNA damage repair.

As monotherapies rarely cure a patient with cancer of the disease, possible combination treatments of THZ531 were investigated. Given the suggested link between THZ531 and DNA damage, combination treatments of THZ531 with various agents causing DNA damage and/or

affecting DNA damage repair were performed. THZ531 showed synergistic effects with DNA damaging agents. In particular, strong synergy was observed for its combination with PARP inhibitors, which have previously been reported to be active in Ewing sarcoma in preclinical studies. Mechanistic studies revealed that THZ531 and PARP inhibitors synergistically induce gamma-H2AX foci (a marker of double-stranded DNA breaks), while at the same time RAD51 foci (a marker of homologous repair of double-stranded DNA breaks) are decreased. This suggests that THZ531 might perturb homologous repair capabilities. Encouragingly, it was found that loss of CDK12 makes Ewing sarcoma cells more sensitive to PARP inhibitors, while loss of EWS-FLI makes them more resistant. This data is further support for a possible connection between EWS-FLI, CDK12, and DNA damaging agents in general and PARP inhibitors in particular.

In vivo evaluation of THZ531 in combination with PARP inhibitor olaparib consistently showed greater effect on tumor size and survival of the two agents than with either compound alone. Importantly, the combination treatment was overall well tolerated by the mice.

In summary, this study presents the testing of first-in-class CDK inhibitors in Ewing sarcoma, demonstrating their efficacy and providing insights into their mechanism of action. Further studies on the effect of EWS-ETS transcription factors and DNA damage are needed to explore this element of Ewing sarcoma biology. The promising preclinical evaluation supports further development of CDK12 inhibitors for treatment of patients with Ewing sarcoma in the clinic.

9 - Zusammenfassung der Publikationen (Summary of the publications in German)

In dieser Dissertation wird in zwei Publikationen die Erforschung neuer Behandlungsstrategien für das Ewing Sarkom beschrieben. In beiden Publikationen werden durch Screening Methoden die biologischen Besonderheiten dieser Krebserkrankung ausgenutzt um molekulare Schwachstellen zu entdecken. Dabei kommt folgender Ansatz zur Anwendung: Zu Beginn stehen Screening Experimente (in der ersten Publikation ein genomischer Screen, in der zweiten Publikation sowohl ein chemischer als auch ein genomischer Screen), die zur Identifikation von potentiellen molekularen Schwachstellen führen. Diesem ersten Schritt folgt die Testung der

potentiellen Schwachstellen in Folgeexperimenten mit genetischen und chemischen Werkzeugen. Anschließend werden Kombinationen mit anderen Wirkstoffen untersucht. Zuletzt erfolgt die Erprobung der beschriebenen Strategien *in vivo* mit Experimenten an Mausmodellen.

In der Publikation „Genome-scale CRISPR-Cas9 screen identifies druggable dependencies in *TP53* wild-type Ewing sarcoma" von Stolte et al., wird die Hypothese getestet, dass das Fehlen von *TP53* Mutationen in der überwältigenden Mehrzahl von Ewing Sarkom Tumoren Therapieansätze ermöglicht, die auf die Aktivierung des p53 Proteins abzielen. Mehrere p53 Regulatorproteine werden identifiziert und deren Evaluierung als therapeutische Ziele beschrieben.

Die Publikation „EWS/FLI Confers Tumor Cell Synthetic Lethality to CDK12 Inhibition in Ewing Sarcoma" von Balboni Iniguez et al., testet die Hypothese, dass von EWS-ETS Fusionstranskriptionsfaktoren codierte maligne Transkriptionsprogramme therapeutische Ziele sein können. Es werden neuartige Inhibitoren von cyclin-dependant Kinasen untersucht, die auf Transkription wirken, ihr Mechanismus beschrieben und die Evaluation ihres Einsatzes als Therapeutika in mehreren Modellen des Ewing Sarkoms demonstriert.

9.1 - Publikation I - Genome-scale CRISPR-Cas9 screen identifies druggable dependencies in *TP53* wild-type Ewing sarcoma

Tumor Protein 53 spielt eine große Rolle in der Krebsbiologie. Mutationen dieses Gens, die zum Verlust seiner Aktivität führen, sind eine der häufigsten Vorkommnisse in Krebszellen. [40] Im Ewing Sarkom Tumoren sind *TP53* Mutationen allerdings selten. Nur 10% von in aktuellen Studien untersuchten Tumoren zeigten Änderungen im *TP53* Gen. [16-18] Bemerkenswerterweise gilt in Ewing Sarkom Zelllinien das Gegenteil. Die Mehrheit der Zelllinien haben kein funktionales p53 Protein. Dies kann entweder daran liegen, dass einzelne Zellen nach längerer Zeit in Zellkultur (was für Proliferation-verstärkende Mutation wie die in *TP53* selektiert) *TP53* Mutationen entwickeln, oder daran, dass das Vorhandensein einer *TP53* Mutation die Etablierung einer Zelllinie vereinfacht. Da patient-derived xenografts (PDXs) von Ewing Sarkom Tumoren erst seit kurzer Zeit verfügbar sind, wurden Jahrzehnte in der Ewing Sarkom Forschung vor allem anhand eben dieser Zelllinien durchgeführt. [63] Die Überrepräsentation von *TP53* Mutationen in den

Zelllinien ist somit eine verzerrte Darstellung der Erkrankung und könnte mögliche therapeutische Ziele verborgen haben. Daher werden in diesem Projekt nicht-*TP53*-mutierte Modelle des Ewing Sarkoms untersucht. [16-18, 40-47]

In einem kürzlich publizierten CRISPR-Cas9 Screen wurde eine Vielzahl an Krebsarten untersucht, darunter neun Ewing Sarkom Zelllinien. [38] Eine Analyse dieses Screens mit dem Ziel genetische Schwachstellen (also Gene, ohne die eine Krebszelle nicht leben kann) in *TP53* wild type Ewing Sarkom zu identifizieren, nominierte vier Gene (*MDM2*, *MDM4*, *PPM1D* und *USP7*). Die Genprodukte dieser vier Gene (MDM2, MDM4, Wip1, USP7) können mit Molekülen, die sich aktuell in präklinischer oder klinischer Entwicklung befinden, inhibiert werden. Allen vier zugehörigen Proteinen werden p53 Regulationsfunktionen zugeschrieben.

Die Evaluierung der nominierten Proteine bestätigte die Daten des Screens und zeigte einen obligat p53-abhängigen Mechanismus von MDM2, MDM4, Wip1 und USP7. Der stapled-peptide MDM2 und MDM4 Inhibitor ATSP7041 minderte die Proliferation von Ewing Sarkom Zellen sowohl *in vitro* als auch *in vivo*, und zeigte dabei wenig bis keine Wirkung auf Zelllinien mit mutiertem *TP53*, was auf geringe off-target Wirkung schließen lässt. USP7 Inhibitor P5091 und Wip1 (das Genprodukt von *PPM1D*) Inhibitor GSK2830371 minderten die Proliferation von Ewing Sarkom Zellen *in vitro*, hatten dabei allerdings keine streng p53-abhängige Wirkung.

In Kombinationsstudien zeigte sich, dass die gleichzeitige Inhibition mehrerer p53 Regulatoren eine synergistische Wirkung hat. Außerdem zeigte die Kombination von ATSP7041 mit mehreren Chemotherapeutika eine additive Wirkung, was einen möglichen Nutzen vom Zusatz eines Derivats dieses Moleküls zu chemotherapeutischen Behandlungsplänen suggeriert.

Abschließend wurden *TP53* knockout Ewing Sarkom Zelllinien generiert, um zu testen, ob und in welchem Ausmaß funktionales p53 Protein für ein Ansprechen der Zellen auf Inhibition der nominierten Proteine nötig ist. Verlust von funktionalem p53 hob den Effekt von ATSP7041 nahezu vollständig auf, während die Effekte von P5091 und GSK2830371 nur unvollständig vermindert wurden. Um zu erforschen, ob der unvollständige Effekt an off-target Wirkung der

Moleküle, oder an nicht-p53-abhängigen Funktionen von USP7 und Wip1 im Ewing Sarkom liegt, wurden double-knockout Experimente durchgeführt. Diese Experimente bestätigten, dass Verlust von p53 die Zellen tatsächlich resistent gegen den Verlust von *USP7* und *PPM1D* macht, was deutlich dafürspricht, dass die Ergebnisse des Screens und der vorhergehend durchgeführten Experimente zutreffen. Weitere Unterstützung für diese Hypothese liefert die Testung des neuen, spezifischeren USP7 Inhibitors XL-188, dessen Effekte auf Ewing Sarkom Zellen vollständig durch p53 Verlust aufgehoben werden konnten.

Zusammenfassend wird in dieser Studie ein systematischer Ansatz zur Identifikation von p53-abhängigen molekularen Schwachstellen im Ewing Sarkom aufgezeigt und die Studie dieser Schwachstellen sowie die Testung von Inhibitoren und Kombinationstherapien beschrieben. Ein Abkömmling des MDM2 und MDM4 Dualinhibitors ATSP7041 wird aktuell in einer klinischen Studie an Patienten und Patientinnen mit Kinderkrebserkrankungen erforscht (ClinicalTrials.gov Identifier: NCT03654716), wodurch die klinische Relevanz der hier präsentierten Arbeit unterstrichen wird.

9.2 - Publikation II – EWS/FLI Confers Tumor Cell Synthetic Lethality to CDK12 Inhibition in Ewing Sarcoma

Ewing Sarkom Zellen exprimieren onkogene EWS-ETS Transkriptionsfaktoren wie EWS-FLI. EWS-FLI (und andere, seltenere EWS-ETS Varianten) initiieren die Transkription von spezifischen Zielgenen, was zum malignen Verhalten der Zellen führt. [12, 54-60]

Da Ewing Sarkom Zellen von der Transkription dieser Zielgene abhängen, ist die Inhibition von Transkriptionsprozessen ein denkbarer Ansatz für die Behandlung der Erkrankung. Die Inhibition von Transkriptionsprozessen ist als Krebsbehandlungsstrategie seit längerer Zeit anerkannt, unter anderem durch den Einsatz des Transkriptionsinhibitors Actinomycin D, der seit vielen Jahren therapeutisch genutzt wird. Vorausgegangene Studien haben gezeigt, dass Krebsarten mit hohen Transkriptionsraten auf transkriptionale Modulatoren, wie z.B. Inhibitoren von transkriptional-aktiven cyclin-dependant kinases (CDKs), deutlich ansprechen. THZ1 ist ein Inhibitor von CDK7

(und im gewissen Maße ebenso von CDK12 und CDK13), der in vorherigen Studien vielversprechende Ergebnisse zeigte. [50, 61, 62]

In einem chemischen Screen, der eine große Anzahl von verschiedenen Krebsarten untersuchte, zeigten Ewing Sarkom Zelllinien ein sehr starkes Ansprechen auf THZ1. In Folgeexperimenten bestätigte sich, dass THZ1 die Proliferation von Ewing Sarkom Zellen mindert, Apoptose induziert, veranschaulicht durch Experimente, die die erhöhtes Annexin V und die Spaltung von PARP zeigten. On-target Aktivität konnte durch den Nachweis von verminderter Phosphorylierung von RNA polymerase II an bestimmten Serin Gruppen in Zellen nach Behandlung mit THZ1 gezeigt werden. In *in vivo* Experimenten reduzierte die Gabe von THZ1 das Wachstum von Tumoren und verlängerte die Überlebenszeit von Mäusen mit Ewing Sarkom Tumoren.

Durch Analyse eines genomischen Screens zeigte sich, dass Ewing Sarkom Zellen stark auf den Verlust von *CDK12* ansprechen, der Verlust von *CDK13* allerdings keinen und nur äußerst geringen Effekt hat. Der Verlust von *CDK7* hingegen verminderte Proliferation von allen Zelllinien. Dies lässt unter Umständen darauf schließen, dass alle menschlichen Zellen CDK7 für ihr Überleben benötigen, was ein kleines therapeutisches Fenster für die Inhibition von CDK7 bedeuten könnte. Daher wurde CDK12 (und nicht CDK7 oder CDK13) als molekulare Schwachstelle im Ewing Sarkom weiterverfolgt.

THZ531, ein Abkömmling von THZ1, ist ein selektiver CDK12/13 Inhibitor. Ewing Sarkom Zellen sprachen sehr stark auf THZ531 an und on-target Effekte konnten in Immunoprezipitation Experimenten gezeigt werden, in denen nach THZ531 Gabe die Bindung von CDK12 an Cyclin K an CDK12 vermindert war. Weiterhin, bestätigte genetischer Knockout (durch CRISPR-Cas9) und knockdown (durch small hairpin RNAs), dass der Verlust von CDK12 und nicht CDK13 die Proliferation von Ewing Sarkom Zellen mindert.

Um die Effekte von THZ531 im Ewing Sarkom zu untersuchen, wurden Gen Expressionsexperimente durchgeführt. Interessanterweise widerlegten die Ergebnisse die Hypothese, dass die anti-proliferativen Effekte von THZ531 durch die Herunterregulation von

EWS-ETS Zielgenen verursacht werden. Zwar wurde insgesamt eine Minderung von Transkription beobachtet, von EWS-ETS regulierte Gene waren allerdings nicht unter den davon am stärksten betroffenen Genen. Stattdessen waren es an DNA Reparatur beteiligte Gene, inklusive verschiedener Gene, die der homologen DNA Reparatur und DNA damage checkpoint Kontrolle zugeordnet werden, deren Expression durch THZ531 am stärksten vermindert wurden. Diese Minderung von spezifischen DNA Reparatur Genen durch THZ531 konnte in Folgeexperimenten bestätigt werden.

Als besonders bemerkenswert zeigte sich, dass das Ansprechen von Ewing Sarkom Zellen auf Inhibition von CDK12 EWS-ETS Transkriptionsfaktoren abhängig ist, da Zellen, in denen die EWS-FLI Expression durch small hairpin RNA vermindert wurde, resistenter gegenüber THZ531 werden. Weiterhin zeigt die Analyse von chemischen Screening Daten, dass EWS-FLI ein Biomarker für das Ansprechen auf Medikamente und DNA schädigende Moleküle ist, was eine weitere Verbindung zwischen EWS-ETS Transkriptionsfaktoren und DNA Schaden und Reparatur herstellt.

Da Krebspatienten selten durch Monotherapien mit einem einzigen Medikament geheilt werden können, wurden mögliche Kombinationstherapien mit THZ531 erforscht. Aufgrund der Verbindung zwischen THZ531 und DNA Schäden und Reparatur aus den vorhergehenden Experimenten, erfolgte die Erprobung von Kombinationen von THZ531 mit verschiedenen Medikamenten und Molekülen, die DNA Schäden hervorrufen und/oder DNA Reparatur beeinflussen. THZ531 zeigte synergistische Effekte in diesen Experimenten. Im Besonderen war die Kombination mit PARP Inhibitoren besonders effektiv. Vorherige Studien zeigten, dass PARP Inhibitoren wirkungsvoll im Ewing Sarkom sind. Mechanistische Studien zeigten, dass THZ531 und PARP Inhibitoren synergistisch gamma-H2AX Foci (ein Marker für Doppelstrang DNA Brüche) hervorrufen, während gleichzeitig RAD51 Foci (ein Marker für die Reperatur von Doppelstrang DNA Brüchen) vermindert wurden. Dies könnte bedeuten, dass THZ531 die Fähigkeit zur Doppelstrang DNA Bruch Reparatur stört. Weiterhin zeigte sich, dass das Ansprechen von Ewing Sarkom Zellen auf PARP Inhibitoren nach Verlust von CDK12 verstärkt ist, während der Verlust von EWS-FLI die Zellen resistenter gegenüber PARP Inhibitoren macht. Diese Daten stützen die

Hypothese, dass es einen Zusammenhang zwischen EWS-FLI, CDK12 und DNA Schäden und vor allem der Inhibition von PARP gibt.

In vivo Evaluation von THZ531 in Kombination mit PARP Inhibitor Olaparib ergaben, dass die Kombination beider Wirkstoffe einen größeren Effekt auf die Entwicklung von Tumorgröße und Überleben der Mäuse hat, als je einer der Wirkstoffe allein. Von klinischer Relevanz war hierbei, dass diese Behandlung von den Mäusen gut vertragen wurde.

Zusammengefasst zeigt diese Studie erstmals die Testung von CDK Inhibitoren im Ewing Sarkom, demonstriert ihre Effektivität und gibt Einsicht in den Mechanismus der CDK12 Inhibition in dieser Krebserkrankung. Weitere Studien sind nötig um den Zusammenhang von EWS-ETS Transkriptionsfaktoren und DNA Schäden im Ewing Sarkom weiter zu erforschen. Die vielversprechende präklinische Evaluation unterstützt die weitere Entwicklung von CDK12 Inhibitoren für die Behandlung dieser Krebserkrankung.

Published Online: 25 July, 2018 | Supp Info: http://doi.org/10.1084/jem.20171066

JEM Journal of Experimental Medicine

ARTICLE

Genome-scale CRISPR-Cas9 screen identifies druggable dependencies in *TP53* wild-type Ewing sarcoma

Björn Stolte[1,2,3], Amanda Balboni Iniguez[1,3], Neekesh V. Dharia[1,3], Amanda L. Robichaud[1], Amy Saur Conway[1], Ann M. Morgan[4], Gabriela Alexe[1,3,5], Nathan J. Schauer[6,7], Xiaoxi Liu[6,7], Gregory H. Bird[4], Aviad Tsherniak[3], Francisca Vazquez[3], Sara J. Buhrlage[6,7], Loren D. Walensky[4], and Kimberly Stegmaier[1,3]

Ewing sarcoma is a pediatric cancer driven by EWS-ETS transcription factor fusion oncoproteins in an otherwise stable genomic background. The majority of tumors express wild-type *TP53*, and thus, therapies targeting the p53 pathway would benefit most patients. To discover targets specific for *TP53* wild-type Ewing sarcoma, we used a genome-scale CRISPR-Cas9 screening approach and identified and validated *MDM2*, *MDM4*, *USP7*, and *PPM1D* as druggable dependencies. The stapled peptide inhibitor of MDM2 and MDM4, ATSP-7041, showed anti-tumor efficacy in vitro and in multiple mouse models. The USP7 inhibitor, P5091, and the Wip1/*PPM1D* inhibitor, GSK2830371, decreased the viability of Ewing sarcoma cells. The combination of ATSP-7041 with P5091, GSK2830371, and chemotherapeutic agents showed synergistic action on the p53 pathway. The effects of the inhibitors, including the specific USP7 inhibitor XL-188, were rescued by concurrent *TP53* knockout, highlighting the essentiality of intact p53 for the observed cytotoxic activities.

Introduction

Ewing sarcoma is a pediatric small round blue cell tumor that is treated with a combination of interval compressed chemotherapy, radiation, and surgery. While outcomes have improved over the last several decades for patients with localized disease, little progress has been made in the treatment of patients with newly diagnosed metastatic or relapsed disease. Moreover, treatment-related toxicity is significant, and currently, there are no targeted therapies for Ewing sarcoma that are approved by the United States Food and Drug Administration (Balamuth and Womer, 2010; Gaspar et al., 2015).

The defining event in Ewing sarcoma is a somatic chromosomal translocation, most commonly between chromosomes 11 and 22, causing a fusion between the *EWSR1* (Ewing sarcoma breakpoint region 1) gene and an ETS family gene *FLI1* (Friend leukemia virus integration 1). The resulting fusion protein, EWS/FLI, is an aberrant oncogenic transcription factor (Riggi et al., 2008). Efforts to directly inhibit EWS/FLI have largely been unsuccessful (Gaspar et al., 2015). Several recent massively parallel sequencing efforts revealed that Ewing sarcoma tumors possess remarkably quiet genomes, with few recurrent genetic events and no immediately druggable mutated kinases (Brohl et al., 2014; Crompton et al., 2014; Tirode et al., 2014). While the paucity of genetic events is a challenge for the development of precision medicine approaches using kinase inhibitors, the genomic simplicity may enable other treatment strategies. Indeed, up to 90% of Ewing sarcoma tumors present with wild-type *TP53* (Tumor protein 53), allowing for new therapeutic strategies involving p53 activation.

Although the majority of patient tumors retain wild-type *TP53*, there has been a historic bias against studying p53 dependent genes in this disease. The vast majority of Ewing sarcoma cell lines harbor *TP53* mutations (Brohl et al., 2014; Crompton et al., 2014; Tirode et al., 2014), and patient-derived Ewing sarcoma xenografts have only recently been established (Ordóñez et al., 2015). Consequently, models with *TP53* mutations have been overrepresented in Ewing sarcoma studies in the past. Therefore, we sought to identify druggable dependencies in *TP53* wild-type Ewing sarcoma models, which better recapitulate the more common disease biology.

[1]Department of Pediatric Oncology, Dana-Farber Cancer Institute and Boston Children's Hospital, Harvard Medical School, Boston, MA; [2]Dr. von Hauner Children's Hospital, Department of Pediatrics, University Hospital, LMU Munich, Munich, Germany; [3]The Broad Institute of MIT and Harvard, Cambridge, MA; [4]Department of Pediatric Oncology and the Linde Program in Cancer Chemical Biology, Dana-Farber Cancer Institute, Boston, MA; [5]Bioinformatics Graduate Program, Boston University, Boston, MA; [6]Department of Cancer Biology, Dana-Farber Cancer Institute, Boston, MA; [7]Department of Biological Chemistry and Molecular Pharmacology, Harvard Medical School, Boston, MA.

Correspondence to Kimberly Stegmaier: kimberly_stegmaier@dfci.harvard.edu; Loren D. Walensky: loren_walensky@dfci.harvard.edu.

The use of clustered regularly interspaced short palindromic repeats (CRISPR) paired with the CRISPR-associated nuclease 9 (Cas9) has emerged as a tool to study the biology of mammalian cells (Cong et al., 2013; Mali et al., 2013). Genome-scale CRISPR-Cas9 screening provides a powerful new strategy to identify cancer dependencies (Shalem et al., 2014). Using this approach, we report genetic dependencies specific for *TP53* wild-type tumors, including Ewing sarcoma, from analysis of a previously published dataset (Aguirre et al., 2016). We hypothesized that deletion of *TP53* by single guide RNA (sgRNA)–guided CRISPR-Cas9 constructs would give a proliferative advantage exclusively in *TP53* wild-type cell lines and, therefore, leveraged the data to identify genetic dependencies anti-correlated with *TP53* dependency scores. The p53 regulators murine double minute 2 (*MDM2*), murine double minute 4 (*MDM4*), ubiquitin specific peptidase 7 (*USP7*), and protein phosphatase, Mg^{2+}/Mn^{2+}-dependent 1D (*PPM1D*) were among the top druggable dependencies with strong anti-correlation to *TP53* dependency scores. All four were validated in secondary assays to be essential for proliferation of *TP53* wild-type Ewing sarcoma cells. Moreover, chemical inhibitors of these targets, including a stapled peptide dual inhibitor of MDM2 and MDM4 (ATSP-7041), an USP7 inhibitor (P5091), and a wild-type p53-induced phosphatase 1 (Wip1; encoded by the *PPM1D* gene) inhibitor (GSK2830371) reduced the viability of Ewing sarcoma cell lines as single agents. ATSP-7041 showed anti-tumor efficacy in vivo in several Ewing sarcoma models. Consistent with all four targets being highly correlated dependencies in the screening data, combinatorial targeting with these pharmacologic inhibitors showed synergistic activity. Furthermore, ATSP-7041 synergized with some standard-of-care Ewing sarcoma chemotherapeutic agents. To prove that these treatment strategies depend on functional p53, *TP53* knockout cell lines were generated. *TP53* knockout rescued the cytotoxic effects of CRISPR-Cas9–mediated suppression or pharmacologic inhibition of all four targets. Collectively, these data highlight the therapeutic relevance of the intact p53 regulatory network in Ewing sarcoma tumors and provide preclinical evidence to support the testing of p53 modulators in patients with *TP53* wild-type Ewing sarcoma.

Results

Genome-scale CRISPR-Cas9 screening distinguishes between *TP53* wild-type and *TP53* mutant cell lines

To identify new therapeutic targets for *TP53* wild-type Ewing sarcoma, we analyzed the data from our genome-scale CRISPR-Cas9 screen of 33 cancer cell lines, including nine Ewing sarcoma cell lines (Aguirre et al., 2016). We determined that targeting *TP53* in this genome-scale screen provided a proliferative advantage in wild-type *TP53* cell lines (indicated by positive scores) and very little to no effect in mutant *TP53* cell lines (Fig. 1 A). p53 mutation status was assigned by mining published data from several large studies (Barretina et al., 2012; Cancer Cell Line Encyclopedia Consortium; Genomics of Drug Sensitivity in Cancer Consortium, 2015; Klijn et al., 2015), a curated list of mutations (Edlund et al., 2012), and a literature search for cell lines for which no information was available from other sources (Table S1). The response to *TP53* disruption was consistent with the annotated mutation status in 97% of cell lines, including all of the Ewing sarcoma cell lines in this screen.

Regulators of p53 are anti-correlated with *TP53* dependency scores

To identify targets in *TP53* wild-type cell lines, we hypothesized that cell lines with the greatest proliferative advantage upon *TP53* suppression (presumably due to the presence of a functional p53 pathway) would also be dependent on negative regulators of *TP53.* The top eight variable genetic dependencies that were anti-correlated to *TP53* dependency scores in all 33 cancer cell lines in the screen included *MDM2, MDM4, USP7,* and *PPM1D,* as well as other genes with known roles in p53 regulation (Fig. 1 B) and with p53 interaction in the Search Tool for the Retrieval of Interacting Genes/Proteins (STRING) database (Fig. 1 C; Szklarczyk et al., 2015). Prioritizing translatable targets, we focused on the druggable dependencies *MDM2, MDM4, USP7,* and *PPM1D,* which have inhibitors in preclinical or clinical evaluation. In Ewing sarcoma, *MDM2, MDM4, USP7,* and *PPM1D* were preferential dependencies in the *TP53* wild-type cell lines (Fig. 1 D and Fig. S1, A and B).

MDM2 is an E3 ubiquitin ligase that marks p53 for degradation by the proteasome (Wade et al., 2013). MDM4, a structural homologue of MDM2, inhibits p53 by binding to and sequestering its transactivation domain (Wade et al., 2013). USP7 has been implicated in several cellular processes, including deubiquitination of MDM2, which leads to a decrease in p53 (Nicholson and Suresh Kumar, 2011). *PPM1D* encodes for the serine-phosphatase Wip1 that dephosphorylates and inactivates p53 and other proteins involved in cell stress and DNA damage (Zhu and Bulavin, 2012).

With an eye toward clinical translation, we first focused on MDM2 and MDM4, both of which can be targeted simultaneously with a dual inhibitor currently in clinical trials for adults with *TP53* wild-type cancers (Chang et al., 2013; Meric-Bernstam et al., 2017).

Genetic disruption of *MDM2* and *MDM4* has a selective cytotoxic effect in *TP53* wild-type Ewing sarcoma cell lines

We sought to validate the dependencies on *MDM2* and *MDM4* by CRISPR-Cas9 in two *TP53* wild-type cell lines (TC32 and TC138) and two *TP53* mutant cell lines (A673 and EWS502).

To genetically disrupt *MDM2,* we infected the Ewing sarcoma cell lines with *MDM2* sgRNAs and then treated with the MDM2 inhibitor RG7388, which causes an up-regulation of MDM2 through a negative feedback mechanism in response to elevated p53 levels (Ding et al., 2013). *TP53* wild-type cells infected with sgRNAs targeting *MDM2* exhibited a weaker increase in MDM2 protein levels compared with cells infected with the control sgRNA, consistent with *MDM2* knockout in a population of cells in the pool (Fig. 2 A). Given the disrupted p53–MDM2 axis in the *TP53* mutant lines, there was no increase in MDM2 protein following RG7388 treatment of A673 and EWS502 cells, irrespective of infection with *MDM2* or control sgRNAs (Fig. 2 A). To further validate the on-target activity of the sgRNAs, we infected the os-

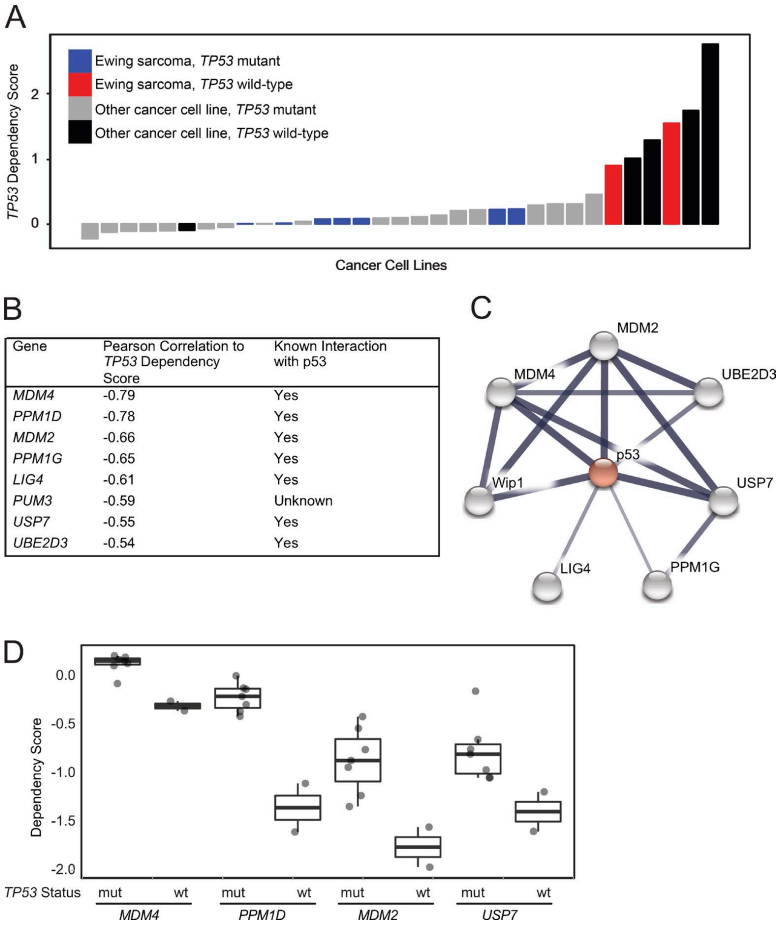

Gene	Pearson Correlation to *TP53* Dependency Score	Known Interaction with p53
MDM4	-0.79	Yes
PPM1D	-0.78	Yes
MDM2	-0.66	Yes
PPM1G	-0.65	Yes
LIG4	-0.61	Yes
PUM3	-0.59	Unknown
USP7	-0.55	Yes
UBE2D3	-0.54	Yes

Figure 1. **Genome-scale CRISPR-Cas9 screen of 33 cancer cell lines identifies genetic vulnerabilities negatively correlated with *TP53* dependency in *TP53* wild-type lines. (A)** Waterfall plot of *TP53* dependency in 33 cancer cell lines shows positive dependency score in known *TP53* wild-type cell lines consistent with the hypothesis that disruption of *TP53* in these lines would lead to a proliferation advantage. Based on these data, 6 of 33 lines likely have a functional p53 pathway. A single cell line for which there is no documented *TP53* mutation, PANC08.13, behaves like a *TP53* mutant line, suggesting it has a nonfunctional p53 pathway. **(B)** Top eight anti-correlated genetic dependencies to *TP53* dependency. **(C)** Seven of the top eight anti-correlated genes are connected to *TP53* in the STRING database indicating putative protein–protein interactions. The widths of the edges correspond to the level of confidence in interactions (medium confidence STRING score of 0.4; high confidence STRING score of 0.7; highest confidence STRING score of 0.9). **(D)** *MDM4*, *PPM1D*, *MDM2*, and *USP7* dependency scores in Ewing sarcoma cell lines in the CRISPR-Cas9 screen stratified by *TP53* mutational status (mut, mutant; wt, wild-type).

teosarcoma cell line, SJSA-X, engineered to overexpress *MDM4* in the context of endogenously elevated MDM2 levels (Wade et al., 2008), with sgRNAs targeting *MDM2*. Knockout was confirmed by Western blot (Fig. 2 B) and selectively impaired the viability of *TP53* wild-type Ewing sarcoma and SJSA-X cells, with little to no effect on the *TP53* mutant cell lines (Fig. 2 C), consistent with the CRISPR-Cas9 screening results.

Similarly, we next disrupted *MDM4* by CRISPR-Cas9 in Ewing sarcoma cell lines (Fig. 2 D) and demonstrated *MDM4* knockout in two *TP53* mutant cell lines and SJSA-X cells (Fig. 2 E). As predicted by the screen, and consistent with our MDM2 findings (Fig. 2 C), loss of MDM4 impaired the viability of *TP53* wild-type Ewing sarcoma cell lines in a strikingly selective fashion, while SJSA-X, a cell line engineered to overexpress *MDM4*, does not depend on the gene as previously reported (Wade et al., 2008; Fig. 2 F).

Chemical inhibition of MDM2/MDM4 reduces viability of *TP53* wild-type Ewing sarcoma

ATSP-7041 is a stapled peptide, dual inhibitor of MDM2 and MDM4 (Chang et al., 2013). Modeled after the p53 transactivation α-helix, stapled p53 peptides engage the p53 binding domain of

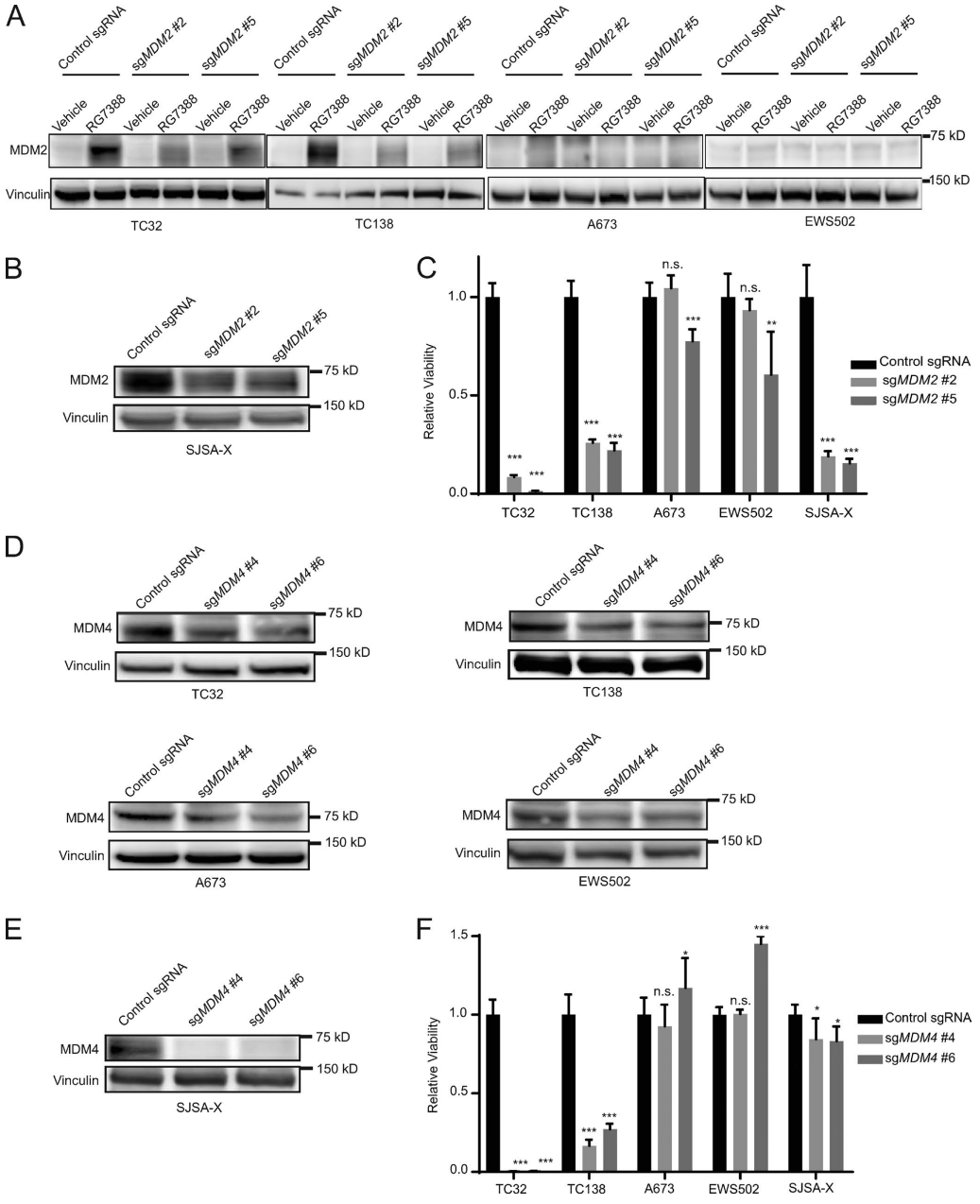

Figure 2. **Validation of MDM2 and MDM4 as dependencies in *TP53* wild-type Ewing sarcoma. (A)** Western blots demonstrate abrogation of the observed increase in MDM2 protein levels upon RG7388 treatment (1 µM; 4 h) in *TP53* wild-type cell lines TC32 and TC138 cells infected with sgRNAs targeting *MDM2* compared with a nontargeting control sgRNA and no response to RG7388 treatment in *TP53* mutated cell lines A673 and EWS502. **(B)** Western blot demonstrating decreased protein levels of MDM2 with sgRNAs targeting *MDM2* compared with a control guide in the SJSA-X cell line. **(C)** Relative viability of Ewing sarcoma and SJSA-X cells infected with sgRNAs targeting *MDM2* compared with control sgRNAs 14 d after infection. Each data point shows the mean of eight

MDM2 and MDM4 with high affinity and respectively block the degradation and sequestration of p53 (Bernal et al., 2010).

We observed concentration-dependent increases in MDM2, p53, and p21 protein levels after ATSP-7041 treatment of *TP53* wild-type Ewing sarcoma cell lines (Fig. 3 A). To verify the mechanism of action of ATSP-7041 in Ewing sarcoma, we performed immunoprecipitation experiments. TC32 cells were pretreated with the MDM2 inhibitor RG7388 to increase p53 protein levels and then cell lysates were treated with vehicle, ATSP-7041 or RG7388, followed by MDM4 immunoprecipitation and p53 and MDM4 Western blot analysis. Whereas RG7388 was unable to dissociate the inhibitory p53–MDM4 complexes formed in response to selective inhibition of MDM2 in Ewing sarcoma cells, ATSP-7041 exposure decreased the level of p53–MDM4 interaction (Fig. 3 B), consistent with the mechanism reported for other cancer cell lines (Bernal et al., 2010; Chang et al., 2013).

ATSP-7041 selectively reduced the viability of five *TP53* wild-type Ewing sarcoma cell lines at low micromolar concentrations (Fig. 3 C), whereas *TP53* mutated Ewing sarcoma cell lines were resistant, mirroring the results of our genetic perturbation studies. ATSP-7342, a negative control stapled peptide that bears an inactivating F19A point mutation and thus exhibits impaired MDM2/MDM4 binding activity (Chang et al., 2013), was essentially ineffective at these concentrations (Fig. 3 D). Annexin V staining likewise demonstrated induction of cell death at the corresponding concentrations of ATSP-7041 in *TP53* wild-type Ewing sarcoma cell lines (Fig. 3 E).

To study a genetic model of ATSP-7041 that allows for the comparison of MDM2/4 dual inhibition to MDM2 inhibition alone, we performed dual-knockout experiments with CRISPR-Cas9 constructs targeting *MDM2* and *MDM4*. TC32 cells were infected with CRISPR-Cas9 constructs either targeting *MDM2* alone, *MDM4* alone, or one construct each for targeting *MDM2* and *MDM4* simultaneously. Overall, knockout of both *MDM2* and *MDM4* decreased viability more effectively than loss of either alone at this time point (Fig. 3 F), validating the potential therapeutic benefit of dual inhibition of MDM2 and MDM4 over inhibiting MDM2 alone.

ATSP-7041 reactivates the p53 transcriptional pathway and suppresses Ewing sarcoma growth in vivo

We next sought to evaluate the activity of ATSP-7041 Ewing sarcoma in vivo. TC32 Ewing sarcoma cells were implanted subcutaneously in nude mice. Following tumor engraftment with tumor volumes of >100 mm^3, mice were dosed with 30 mg/kg IV ATSP-7041 or vehicle every other day for 6 d. 8 h after the last dose, mice were sacrificed and tumors were collected for comparative analysis of p53 pathway reactivation. We found that ATSP-7041 treatment led to both an increase in MDM2, p53, and p21 protein levels (Fig. 4 A) and MDM2 and p21 mRNA levels (Fig. 4, B and C) in tumor tissue. After validating the on-mechanism activity of ATSP-7041 in vivo, we next sought to assess anti-tumor efficacy. Treatment of TC32 Ewing sarcoma xenografted mice with 30 mg/kg ATSP-7041 or vehicle IV every other day for 20 d significantly suppressed tumor growth, sustaining a reduction in tumor progression throughout the 22-d evaluation period (Fig. 4 D).

To test ATSP-7041 in a model that more closely recapitulates patient tumors, we studied a patient-derived xenograft (PDX) model of Ewing sarcoma (HSJD-ES-002), which was derived from a tumor resected from the fibula of a 12-yr-old patient at diagnosis (Ordóñez et al., 2015). In vivo treatment of mice bearing HSJD-ES-002 tumors with ATSP-7041 increased intratumoral p53 and p21 protein levels (Fig. 4 E) and increased MDM2 and p21 mRNA levels (Fig. 4, F and G). Tumor growth was slowed significantly after 10 doses of ATSP-7041 (Fig. 4 H). The survival of ATSP-7041–treated mice was significantly extended, and remarkably, one mouse was cured of disease, showing complete tumor regression without recurrence over the observed time frame of 227 d (Fig. 4 I).

Genetic disruption of *USP7* and *PPM1D* is selectively cytotoxic to Ewing sarcoma lines bearing wild-type *TP53*

After validating *MDM2* and *MDM4* as gene dependencies in *TP53* wild-type Ewing sarcoma, we next evaluated *USP7* and *PPM1D*. We disrupted *USP7* by CRISPR-Cas9 in TC32, TC138, A673, and EWS502 cells (Fig. 5 A) and observed reduced viability of *TP53* wild-type compared with mutant Ewing sarcoma cell lines (Fig. 5 B).

Similarly, the disruption of *PPM1D* by CRISPR-Cas9 in TC32, TC138, A673, and EWS502 led to reduced protein levels of Wip1 (Fig. 5 C) and a decrease in viability of the *TP53* wild-type compared with the *TP53* mutant Ewing sarcoma cell lines (Fig. 5 D).

Chemical inhibition of USP7 and Wip1 impairs the viability of *TP53* wild-type Ewing sarcoma cells

Given the selective effects of genetic disruption of *USP7* and *PPM1D* on the viability of wild-type *TP53* Ewing sarcoma, we tested the pharmacologic activities of their respective small inhibitors, P5091 (Chauhan et al., 2012) and GSK2830371 (Gilmartin et al., 2014). P5091 increased p53 and p21 protein levels in a time-dependent fashion in the wild-type *TP53* cells, TC32 and TC138 (Fig. 6 A). The inhibitor appeared to be relatively more cytotoxic to a subset of *TP53* wild-type Ewing sarcoma lines compared with *TP53* mutant cells (Fig. 6 B). Annexin V staining likewise demonstrated P5091-induced cell death in *TP53* wild-type Ewing sarcoma cell lines (Fig. 6 C).

GSK2830371 reduced the protein levels of Wip1 in a time-dependent manner and triggered a surge in phosphorylation of Serine 15 of p53, the primary p53 dephosphorylation target site of

replicates, and data are plotted as mean values ± standard deviation. The experiment was performed twice and data points of one representative experiment are shown. **(D)** Western blots showing decreased protein levels of MDM4 after infection with sgRNAs targeting *MDM4* compared with control sgRNAs. **(E)** Western blot demonstrating decreased protein levels of MDM4 with sgRNAs targeting *MDM4* compared with control guides in the SJSA-X cell line. **(F)** Relative viability of Ewing sarcoma and SJSA-X cells infected with sgRNAs targeting *MDM4* or control sgRNAs 14 d after infection. Each data point shows the mean of eight replicates, and data are plotted as mean values ± standard deviation. The experiment was performed twice and data points of one representative experiment are shown. Significance was calculated by paired, two-tailed *t* test: n.s., not significant for $P > 0.05$; *, $P \le 0.05$; **, for $P \le 0.01$; ***, $P \le 0.001$).

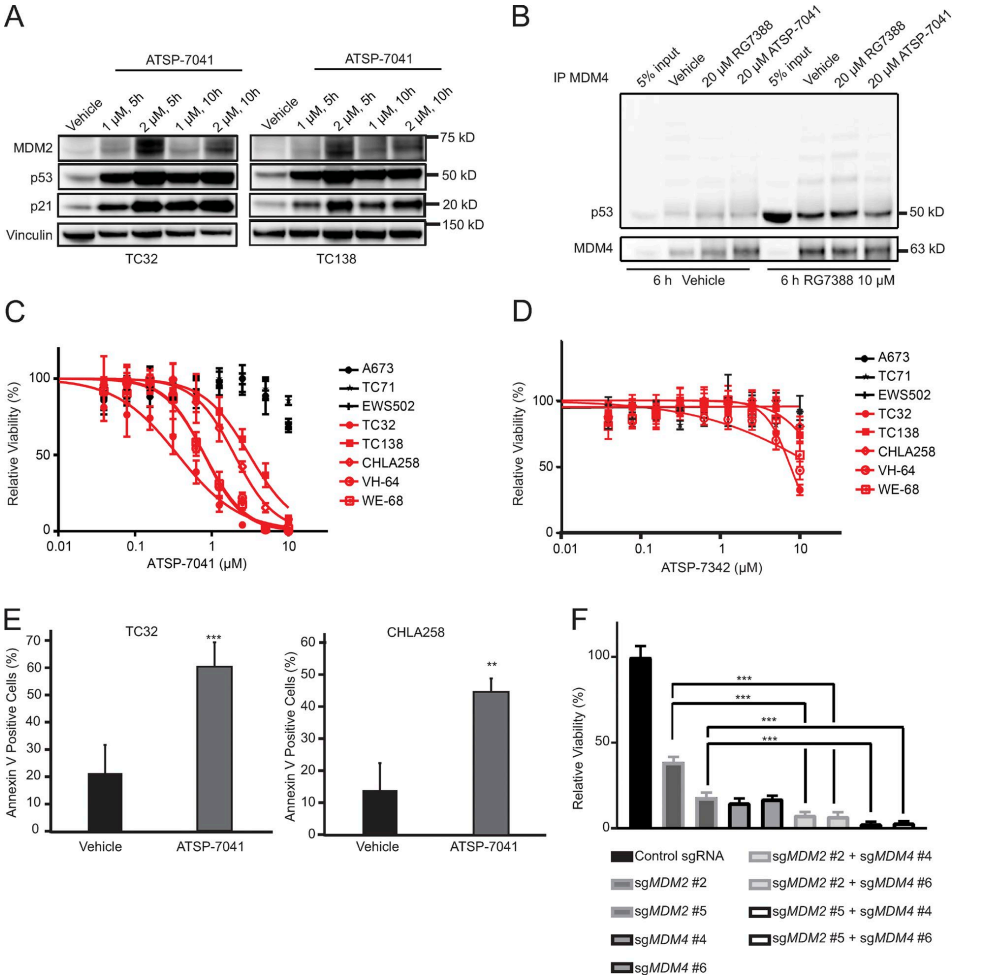

Figure 3. **ATSP-7041 reactivates the p53 pathway to induce cell death in *TP53* wild-type Ewing sarcoma cell lines. (A)** Western blots showing increased protein levels of MDM2, p53, and p21 after ATSP-7041 treatment at the indicated time and concentrations in *TP53* wild-type Ewing sarcoma cell lines. **(B).** Immunoprecipitation experiments show partial disruption of p53–MDM4 complex after treating cellular lysates with ATSP-7041, while RG7388 does not interrupt binding. TC32 cells were treated with RG7388 (last four lanes) to increase p53 protein levels. **(C)** Ewing sarcoma cells were treated with ATSP-7041 for 3 d. *TP53* wild-type Ewing sarcoma cell lines are shown in red. *TP53* mutated Ewing sarcoma cell lines are shown in black. Values are normalized to vehicle control. Each data point shows the mean of eight replicates; error bars are mean values ± standard deviation. The experiment was performed twice and data points of one representative experiment are shown. **(D)** Ewing sarcoma cells were treated with negative control peptide ATSP-7342 for 3 d. *TP53* wild-type Ewing sarcoma cell lines are shown in red. *TP53* mutant Ewing sarcoma cell lines are shown in black. Values are normalized to vehicle control. Each data point shows the mean of eight replicates; error bars are mean values ± standard deviation. The experiment was performed twice and data points of one representative experiment are shown. **(E)** 2-d treatment with ATSP-7041 triggers cell death in TC32 (treated with 2 µM) and CHLA258 (treated with 4 µM) cell lines, as measured by Annexin V staining. Data points represent the mean of five replicates of two experiments and error bars are mean ± standard deviation. **(F)** Viability effect of dual CRISPR-Cas9 knockout of *MDM2* and *MDM4* in TC32 cells. Cells were infected with sgRNAs targeting *MDM2* and selected with puromycin and sgRNAs targeting *MDM4* and selected with blasticidin. Relative viability of eight replicates is shown 11 d post-infection. The experiment was performed twice and data points of one representative experiment are shown. Significance was calculated by paired, two-tailed *t* test: **, P ≤ 0.01; ***, P ≤ 0.001.

Wip1 (Fig. 6 D). There was a notable increase in susceptibility of *TP53* wild-type Ewing sarcoma cell lines to micromolar concentrations of GSK2830371, as compared with the *TP53* mutated cell lines (Fig. 6 E). GSK2830371-induced cell death in *TP53* wild-type Ewing sarcoma cell lines was likewise observed by Annexin V staining (Fig. 6 F).

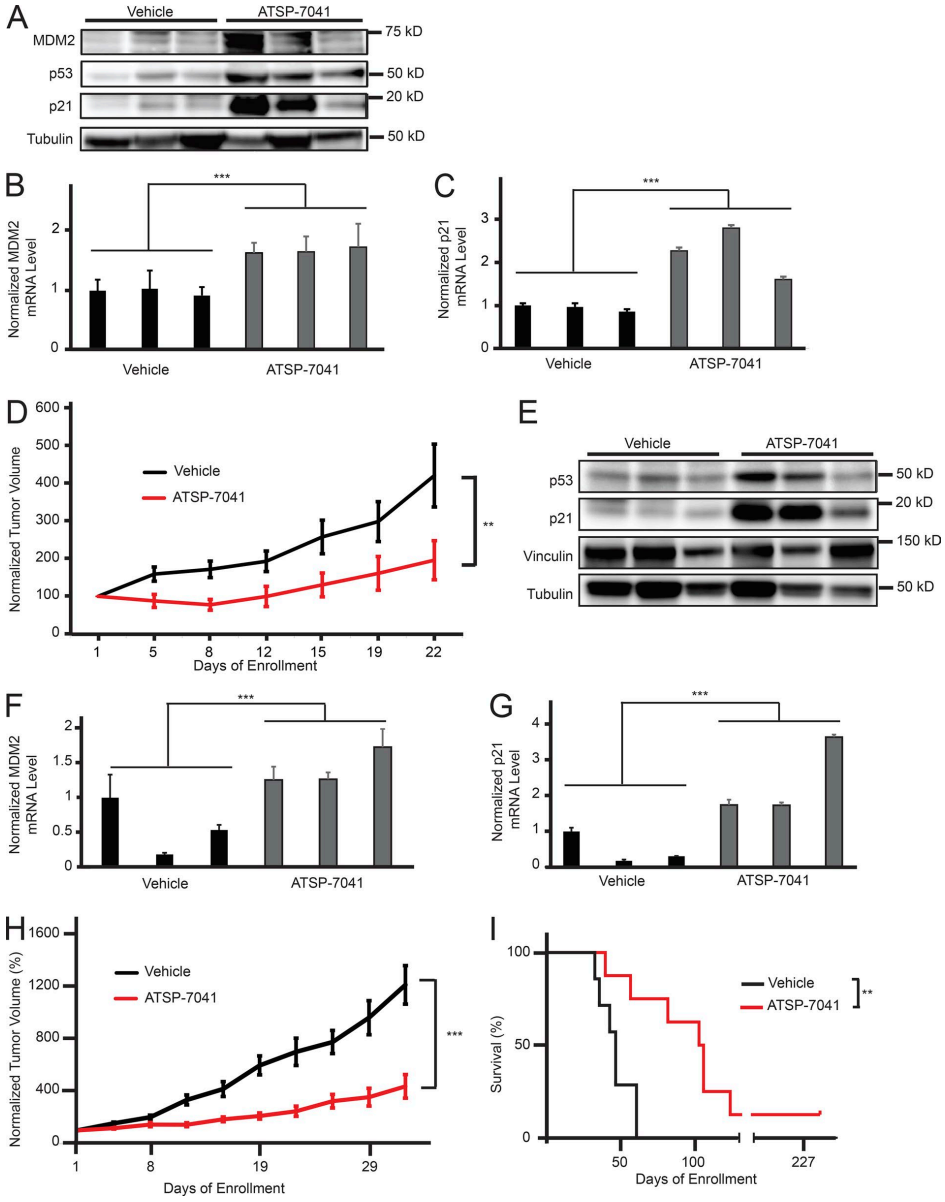

Figure 4. **ATSP-7041 shows anti-tumor efficacy in Ewing sarcoma models in vivo. (A)** Western blot showing an increase of MDM2, p53, and p21 protein levels in TC32 xenograft tumor tissues after ATSP-7041 treatment in vivo. After tumor engraftment, mice were treated with three doses of 30 mg/kg q.o.d. ATSP-7041 or vehicle and sacrificed 8 h after the last dose. Each lane represents an individual mouse tumor. **(B)** Quantitative PCR showing comparative MDM2 mRNA levels with vehicle (black) or ATSP-7041 (gray) treatment of TC32 xenograft cells in vivo. Values were normalized to the first vehicle-treated sample. Each bar represents an individual mouse tumor; error bars represent standard deviation of three technical replicates. Significance was calculated by paired, two-tailed *t* test: ***, $P \leq 0.001$. **(C)** Quantitative PCR showing comparative p21 mRNA levels with vehicle (black) or ATSP-7041 (gray) treatment of TC32 xenograft cells in vivo. Values were normalized to the first vehicle-treated sample. Each bar represents an individual mouse tumor; error bars represent standard deviation of three technical replicates. Significance was calculated by paired, two-tailed *t* test: ***, $P \leq 0.001$. **(D)** Normalized average tumor volume from mice bearing TC32 xenograft tumors treated with 30 mg/kg ATSP-7041 q.o.d. (red, $n = 8$), or vehicle q.o.d. (black, $n = 7$). Mice were treated with 10 doses. Tumor volume from each

ATSP-7041 synergizes with chemical inhibition of USP7 and Wip1

Given the promising single-agent activity of GSK2830371 and P5091 in reactivating the p53 pathway, we next evaluated the therapeutic potential of combining these molecules with ATSP-7041. Because *MDM2*, *MDM4*, *USP7*, and *PPM1D* all scored as top dependencies in *TP53* wild-type Ewing sarcoma, we reasoned that chemically inhibiting these proteins in combination could provide the most effective mechanism to trigger p53-mediated cell death in Ewing sarcoma. Indeed, we found that the combination of ATSP-7041 with P5091 exhibited synergy in TC32 and TC138 and additivity in CHLA258 cells, as assessed by the Chou-Talalay combination index for Loewe additivity model (Fig. 7 A; Chou, 2006, 2010). We hypothesized that the heightened therapeutic response could be due to synergistic action on the p53 axis. Western blot analysis revealed that P5091 decreased the level of MDM2 protein that is otherwise induced by ATSP-7041 as a result of the surge in p53 and counter–up-regulation of MDM2 (Fig. 7 B). These data suggest that pharmacologic blockade of USP7 may counteract the natural up-regulation of MDM2 in response to elevated p53 levels, thereby maximizing the p53 response to ATSP-7041.

The combination of ATSP-7041 with GSK2830371 exhibited strong synergy across a broad concentration range in TC32, TC138, and CHLA258 cells (Fig. 7 C). Western blot assays revealed that the combination of ATSP-7041 and GSK2830371 increased the phosphorylation of p53 at Serine 15 in two Ewing sarcoma cell lines (Fig. 7 D). These data suggest that phosphorylation of p53 may underlie the synergism of these two drugs and provides mechanistic evidence that Wip1 acts as a phosphatase of p53 in Ewing sarcoma.

After identifying *MDM2*, *MDM4*, *USP7*, and *PPM1D* as co-dependencies in the CRISPR-Cas9 screen, we tested the combination of pharmacologic inhibitors targeting these proteins. We observed synergistic cytotoxicity, suggesting that a subset of correlated genetic dependencies may indeed predict the synergy of inhibitor combinations.

ATSP-7041 synergizes with standard of care chemotherapeutics in Ewing sarcoma

Since an MDM2/4 dual inhibitor stapled peptide is currently in Phase 1 and Phase 2 testing in adult cancers bearing wild-type *TP53*, we sought to test for synergistic activity of ATSP-7041 with approved treatment regimens for Ewing sarcoma. Thus, we combined ATSP-7041 with doxorubicin, etoposide, or vincristine, three drugs used clinically in the treatment of Ewing sarcoma (Gaspar et al., 2015). All drug combinations demonstrated additivity or synergy at several concentrations, as assessed by the Chou-Talalay combination index for Loewe additivity model (Fig. 8, A–C).

As cytotoxic chemotherapeutic agents are well known to induce pro-apoptotic signals in cancer cells, we investigated the effect of combining ATSP-7041 and chemotherapy agents on p53 protein levels. Combination treatments of ATSP-7041 with etoposide, doxorubicin, or vincristine greatly increased p53 protein levels in Ewing sarcoma cells, suggesting that the observed synergy is due to combinatorial action on the p53 signaling axis (Fig. 8, D–F).

These data support further consideration of adding a stapled peptide dual inhibitor of MDM2/MDM4 to standard chemotherapy regimens in patients with *TP53* wild-type Ewing sarcoma.

Loss of *TP53* rescues the effects of *MDM2*, *MDM4*, *PPM1D*, and *USP7* inhibition

While these data suggest that *TP53* wild-type Ewing sarcoma cancer cell lines are more sensitive to loss of *MDM2*, *MDM4*, *PPM1D*, and *USP7* than *TP53* mutated ones, we next generated isogenic cell lines with *TP53* loss to more definitively support this hypothesis. Three *TP53* wild-type cell lines were infected with CRISPR-Cas9 constructs targeting *TP53*, and loss of *TP53* was demonstrated by diminished increases of p53 protein levels in response to etoposide treatment (Fig. 9 A). Treatment of *TP53* knockout cells revealed that loss of *TP53* fully rescues the cytotoxic effect of ATSP-7041, indicating on-target activity of the drug (Fig. 9 B) and dependency on intact p53 for the response to MDM2/MDM4 inhibition. Similarly, the Wip1 inhibitor GSK2830371 was less effective in *TP53* knockout cells than control cells, which indicates on-target activity of GSK2830371 (Fig. 9 C).

TP53 knockout, however, did not rescue cells from the effects of P5091, suggestive of either a p53 independent mechanism or the possibility of an off-target effect(s) of the molecule (Fig. 9 D). To address this question, we undertook both genetic and chemical analyses. First, we infected *TP53* knockout cells with CRISPR-Cas9 constructs targeting *USP7*. The concurrent loss of *TP53* effectively rescued the cytotoxic effect of *USP7* knockout, as also observed for *PPM1D* knockout (Fig. 9, E–G).

Several new USP7 inhibitors have been described in recent publications. We chose the highly selective XL-188 molecule (Lamberto et al., 2017) to examine the effect of a more refined USP7 inhibitor on Ewing sarcoma susceptibility. XL-188 reduced

mouse was normalized to the tumor volume at the day of enrollment. Error bars represent standard deviation. Significance was calculated by two-way ANOVA analysis: **, P ≤ 0.01. **(E)** Western blot showing an increase of MDM2, p53, and p21 protein levels in PDX tumor tissues after ATSP-7041 treatment in vivo. After tumor engraftment, mice were treated with three doses of 30 mg/kg q.o.d. ATSP-7041 or vehicle and sacrificed 8 h after the last dose. Each lane represents an individual mouse tumor. **(F)** Quantitative PCR showing comparative MDM2 mRNA levels with vehicle (black) or ATSP-7041 (gray) treatment of PDX cells in vivo. Values were normalized to the first vehicle-treated sample. Each bar represents an individual mouse tumor; error bars represent standard deviation of three technical replicates. Significance was calculated by paired, two-tailed *t* test: ***, P ≤ 0.001. **(G)** Quantitative PCR showing comparative p21 mRNA levels with vehicle (black) or ATSP-7041 (gray) treatment of PDX cells in vivo. Values were normalized to the first vehicle-treated sample. Each bar represents an individual mouse tumor; error bars represent standard deviation of three technical replicates. Significance was calculated by paired, two-tailed *t* test: ***, P ≤ 0.001. **(H)** Normalized average tumor volume from mice bearing PDX tumors treated with 30 mg/kg ATSP-7041 q.o.d. (red, *n* = 8), or vehicle q.o.d. (black, *n* = 7). Mice were treated with 10 doses. Tumor volume for each mouse was normalized to the tumor volume at the day of enrollment. Error bars represent standard deviation. Significance was calculated by two-way ANOVA analysis: ***, P ≤ 0.001. **(I)** Survival of mice bearing PDX tumors. One mouse treated with ATSP-7041 had complete tumor regression without recurrence over the observed time frame. Significance was calculated by Log-rank (Mantel-Cox) test: **, P ≤ 0.01.

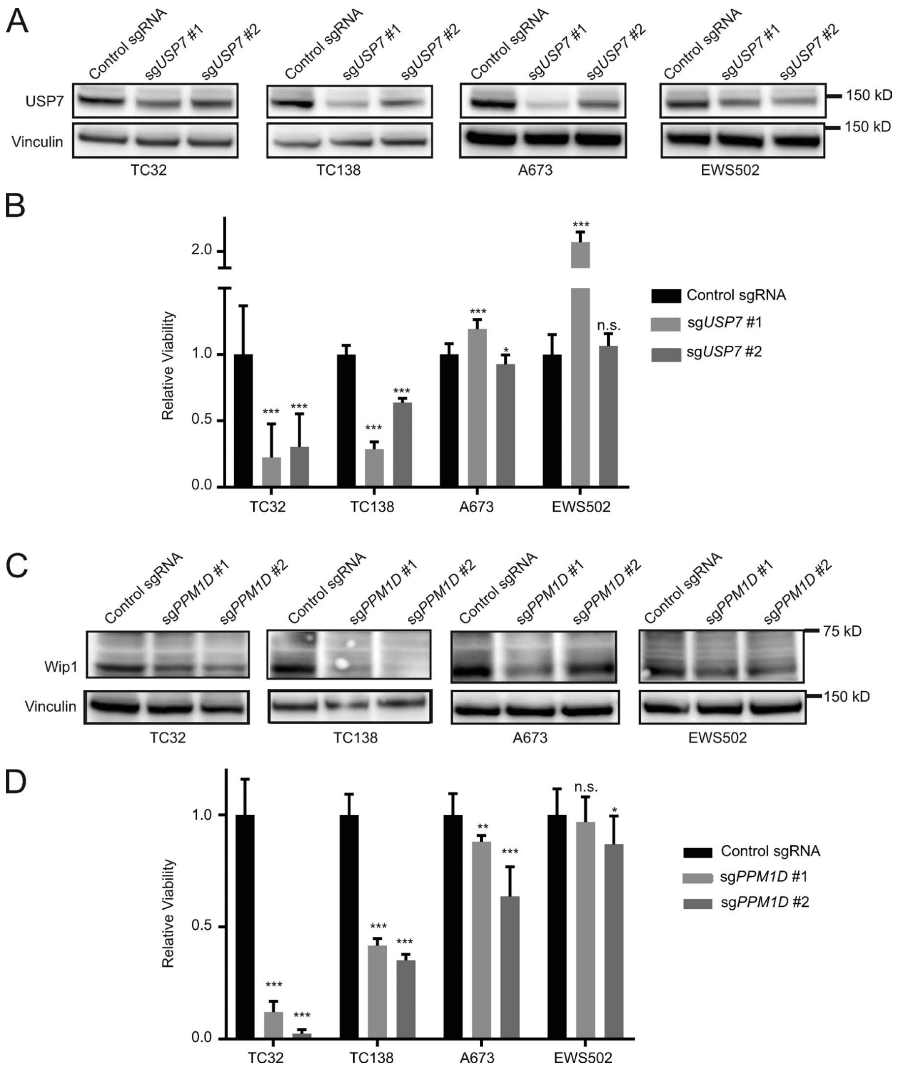

Figure 5. **Validation of *PPM1D* and *USP7* as dependencies in *TP53* wild-type Ewing sarcoma. (A)** Western blots showing decreased protein levels of USP7 after infection with sgRNAs targeting *USP7* compared with control sgRNAs. **(B)** Relative viability of Ewing sarcoma cells infected with sgRNAs targeting *USP7* or control sgRNAs 14 d after infection. Each data point shows the mean of eight replicates; data are plotted as mean values ± standard deviation. The experiment was performed twice and data points of one representative experiment are shown. **(C)** Western blots showing decreased protein levels of Wip1 after infection with sgRNAs targeting *PPM1D* compared with control sgRNAs. **(D)** Relative viability of Ewing sarcoma cells infected with sgRNAs targeting *PPM1D* or control sgRNAs 14 d after infection. Each data point shows the mean of eight replicates, and data are plotted as mean values ± standard deviation. The experiment was performed twice and data points of one representative experiment are shown. Significance was calculated by paired, two-tailed *t* test: not significant (n.s.) for $P > 0.05$; *, $P \le 0.05$; **, $P \le 0.01$; ***, $P \le 0.001$.

viability predominantly in *TP53* wild-type Ewing sarcoma cell lines, with an especially robust effect observed in TC32 cells (Fig. 9 H). Strikingly, *TP53* knockout completely reversed the cytotoxic effect of XL-188 (Fig. 9 I), supporting the requirement of functional p53 for the observed response to USP7 inhibition in Ewing sarcoma. Collectively, these data validate the hypothesis that in Ewing sarcoma, *MDM2*, *MDM4*, *PPM1D*, and *USP7* dependencies are mediated by functional p53 and exert their cytotoxic effects, singly and in combination, by reactivating the p53 tumor suppressor pathway.

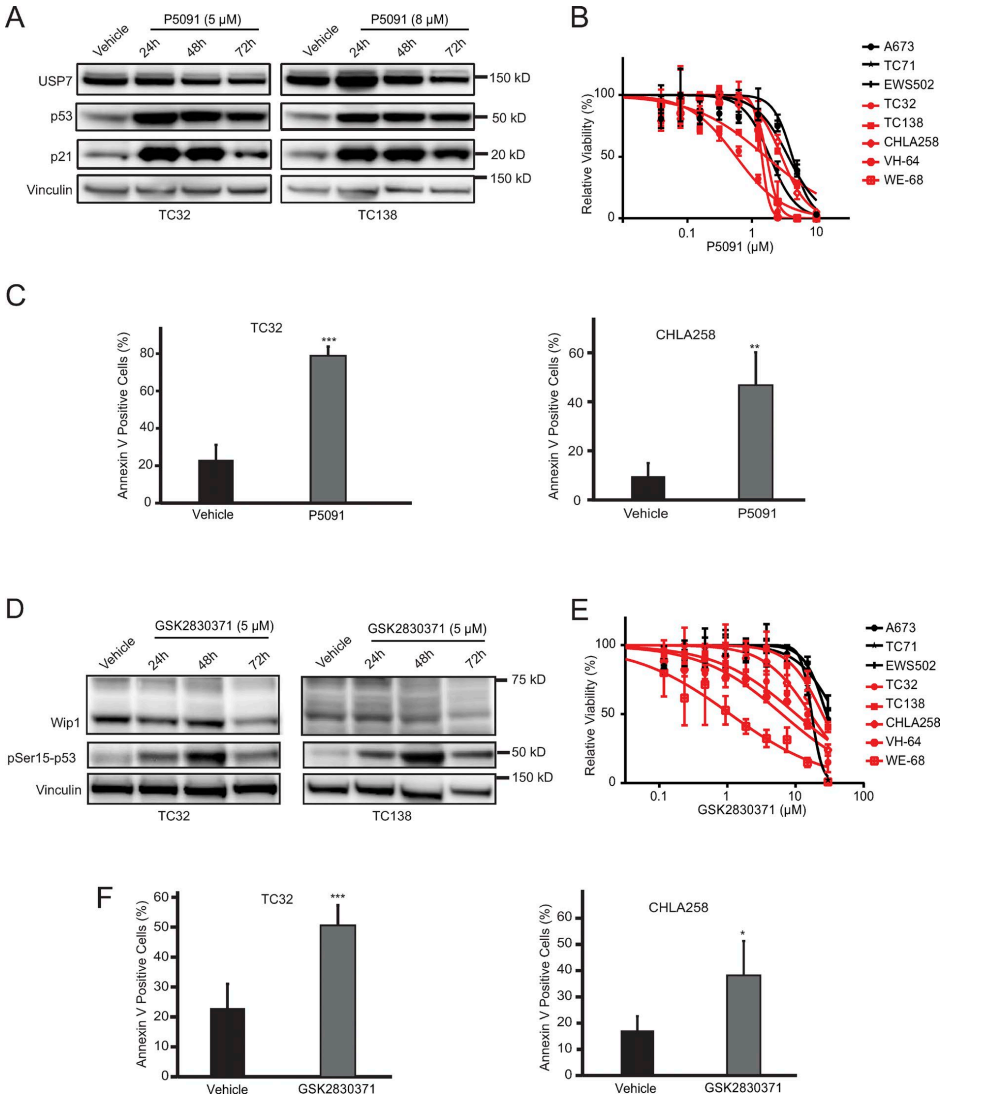

Figure 6. **GSK2830371 and P5091 reduce viability and induce cell death in *TP53* wild-type Ewing sarcoma cell lines. (A)** Western blots showing increase in p53 and p21 protein levels with P5091 treatment in *TP53* wild-type Ewing sarcoma cell lines. **(B)** Ewing sarcoma cells were treated with P5091 for 3 d. *TP53* wild-type Ewing sarcoma cell lines are shown in red; *TP53* mutant Ewing sarcoma cell lines are shown in black. Values were normalized to vehicle controls. Each data point shows the mean of eight replicates; error bars are mean values ± standard deviation. The experiment was performed twice and data points of one representative experiment are shown. **(C)** 2-d treatment with P5091 triggers cell death in TC32 (treated with 6.5 μM) and CHLA258 cells (treated with 8 μM) as measured by Annexin V staining. Data points represent the mean of five replicates of two experiments, and error bars are mean ± standard deviation. **(D)** Western blots showing decreased protein levels of Wip1 and increased pSer15-p53 upon GSK2830371 treatment at the indicated time and concentration. **(E)** Ewing sarcoma cells were treated with GSK2830371 for 3 d. *TP53* wild-type Ewing sarcoma cell lines are shown in red. *TP53* mutated Ewing sarcoma cell lines are shown in black. Values were normalized to vehicle controls. Each data point shows the mean of eight replicates; error bars are mean values ± standard deviation. The experiment was performed twice, and data points of one representative experiment are shown. **(F)** 3-d treatment with GSK2830371 triggers cell death in TC32 and CHLA258 (both treated with 15 μM) cell lines, as measured by Annexin V staining. Data points represent the mean of five replicates of two experiments, and error bars are mean values ± standard deviation. Significance was calculated by paired, two-tailed *t* test: *, P ≤ 0.05; **, P ≤ 0.01; ***, P ≤ 0.001.

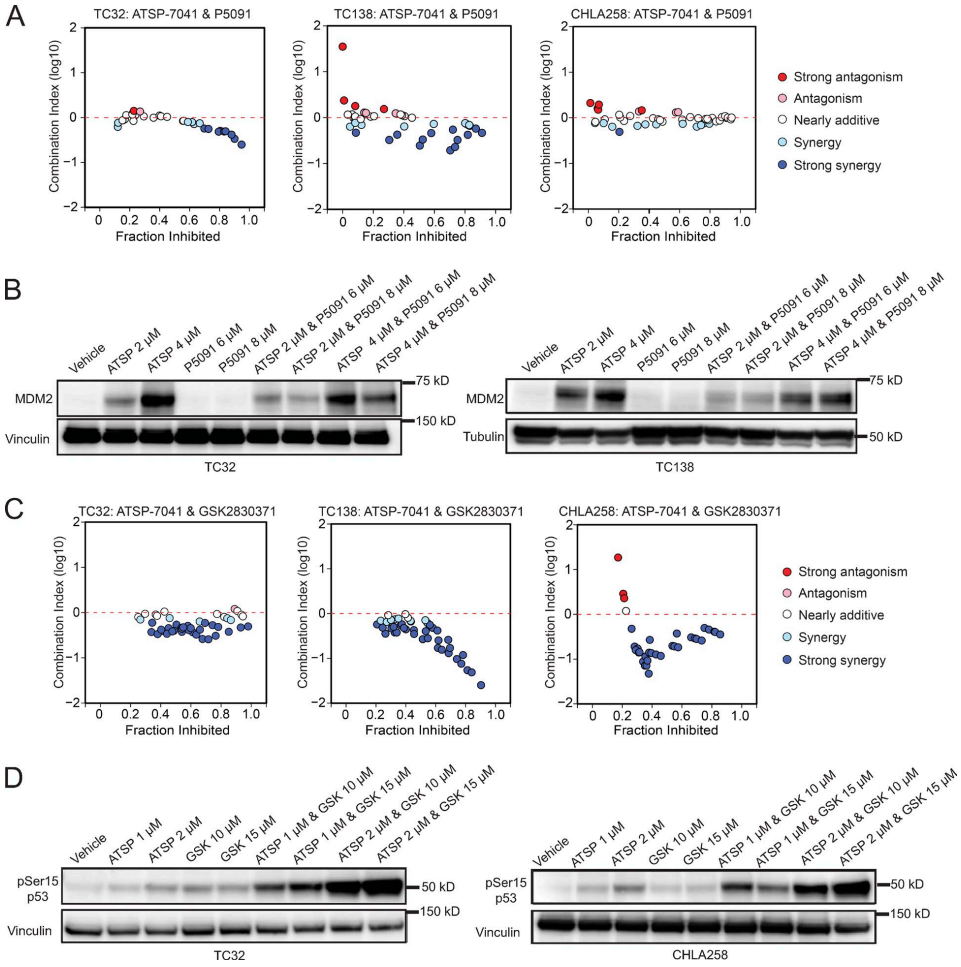

Figure 7. **ATSP-7041 synergizes with GSK2830371 and P5091. (A)** CI plots for the combination of ATSP-7041 with P5091 in TC32, TC138, and CHLA258 cells after 5 d of treatment. **(B)** Western blots showing decreased MDM2 protein levels in TC32 and TC138 cells treated with a combination of ATSP-7041 and P5091 compared with ATSP-7041 treatment alone. Cells were treated at the indicated concentrations for 2 d (ATSP, ATSP-7041). **(C)** CI plots for the combination of ATSP-7041 with GSK2830371 in TC32, TC138, and CHLA258 cells after 3 d of treatment. **(D)** Western blots showing increased phospho-Serine15-p53 protein levels with combination treatment of ATSP-7041 and GSK2830371 in TC32 and CHLA258 cells. Cells were treated at the indicated concentrations for 2 d (ATSP, ATSP-7041; GSK, GSK2830371).

Discussion

TP53 is a potent tumor suppressor gene critical to cellular homeostasis (Lane, 1992). Loss of p53, either by genetic deletion, mutation, or protein interaction–based suppression, is a key oncogenic event in tumorigenesis (Hanahan and Weinberg, 2011). Whereas *TP53* is mutated in ∼50% of human tumors (Leroy et al., 2014), a large subset of pediatric cancers exhibit a low frequency of *TP53* mutations (Malkin et al., 1994; Kato et al., 1996; Hendy et al., 2009; Hof et al., 2011; Ognjanovic et al., 2012), implicating negative regulation of p53 through protein interactions as a pathogenic mechanism. Indeed, several recent studies indicate that the *TP53* mutation rate in Ewing sarcoma is very low (Brohl et al., 2014; Crompton et al., 2014; Tirode et al., 2014). Given the urgent need for new therapeutic approaches to treat Ewing sarcoma, we sought to identify drug targets in the context of *TP53* wild-type disease.

To discover druggable candidates in *TP53* wild-type Ewing sarcoma, we mined the data of a previously published CRISPR-Cas9 screen (Aguirre et al., 2016). The large number of heterogeneous cell lines with diverse molecular features allows for analysis of disease-specific dependencies or dependencies correlated with specific gene mutations. Here, we analyzed the

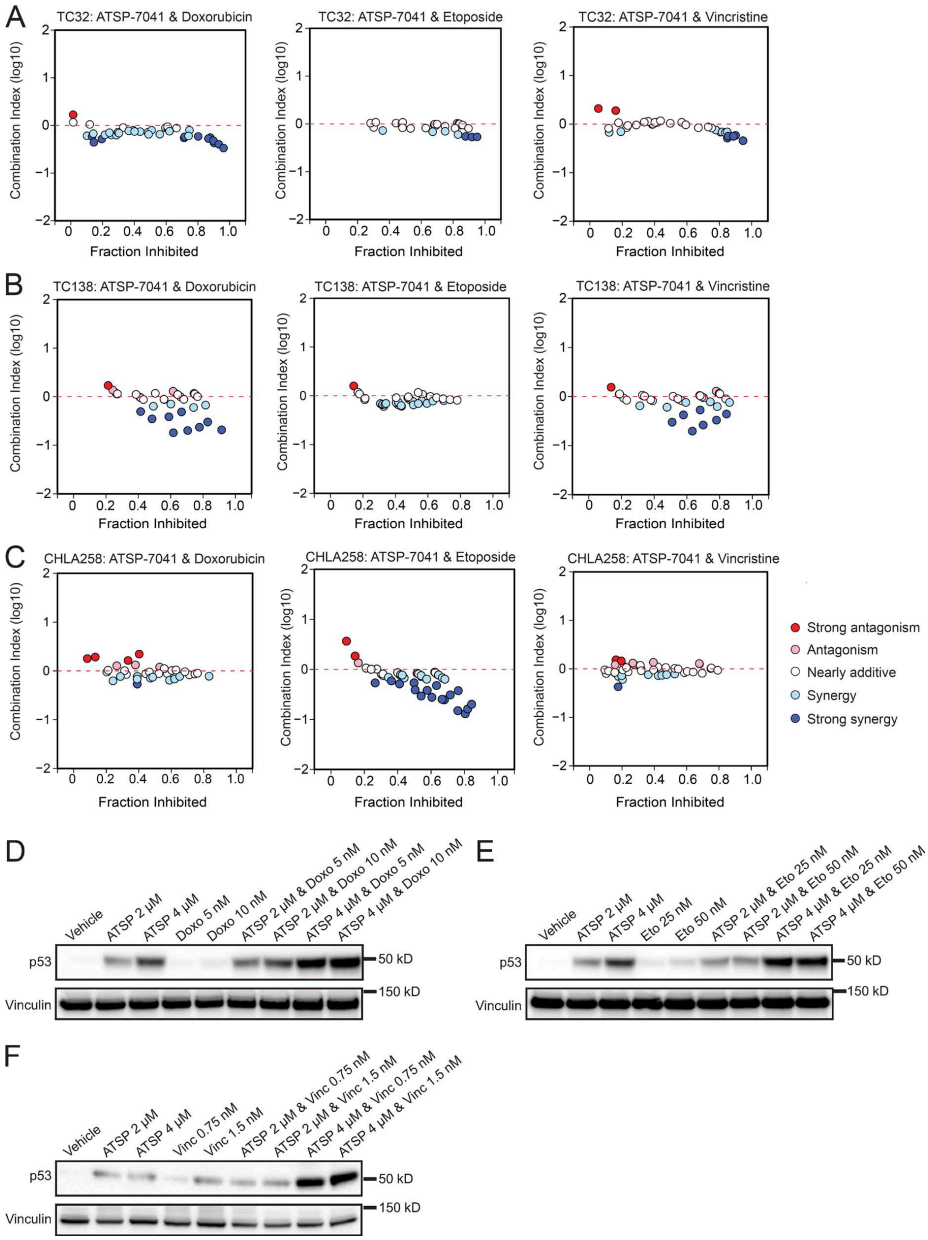

Figure 8. **ATSP-7041 synergizes with chemotherapy agents. (A–C)** CI plots for the combination of ATSP-7041 with doxorubicin, etoposide, and vincristine after 3-d treatment of (A) TC32, (B) TC138, and (C) CHLA258 cells. **(D)** Western blots showing increased p53 protein levels in TC32 cells treat with combinations of ATSP-7041 and doxorubicin. Cells were treated at indicated concentrations for 2 d (ATSP, ATSP-7041; Doxo, doxorubicin). **(E)** Western blots showing increased p53 protein levels in TC32 cells treated with combinations of ATSP-7041 and etoposide. Cells were treated at the indicated concentrations for 2 d (ATSP, ATSP-7041; Eto, etoposide). **(F)** Western blots showing increased p53 protein levels in TC32 cells treated with combinations of ATSP-7041 and vincristine. Cells were treated at the indicated concentrations for 2 d (ATSP, ATSP-7041; Vinc, vincristine).

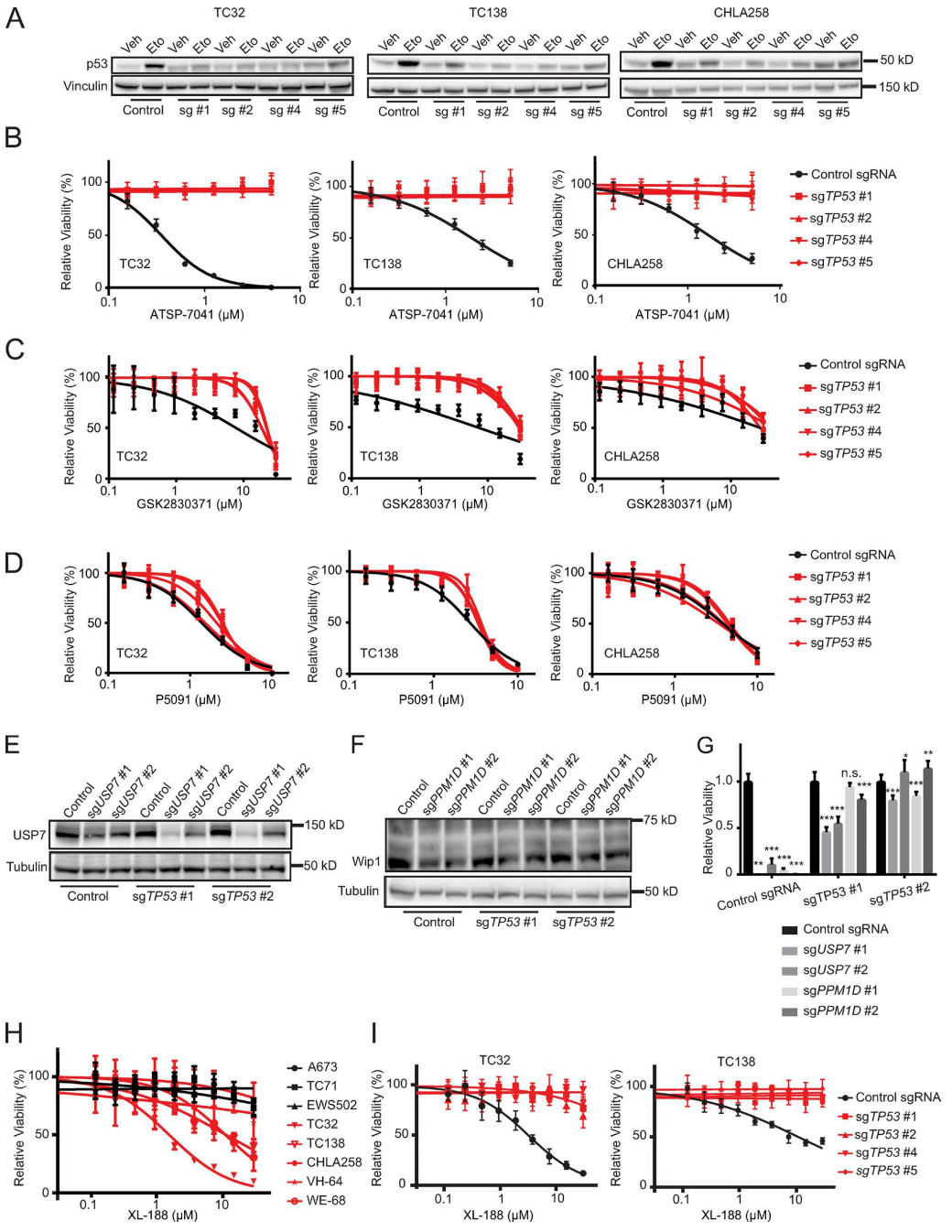
A
TC32
TC138
CHLA258
Veh
Eto
p53
Vinculin
50 kD
150 kD
Control
sg #1
sg #2
sg #4
sg #5
B
Relative Viability (%)
TC32
TC138
CHLA258
ATSP-7041 (μM)
Control sgRNA
sgTP53 #1
sgTP53 #2
sgTP53 #4
sgTP53 #5
C
GSK2830371 (μM)
D
P5091 (μM)
E
USP7
Tubulin
150 kD
50 kD
sgUSP7 #1
sgUSP7 #2
F
Wip1
75 kD
sgPPM1D #1
sgPPM1D #2
G
Relative Viability
n.s.
Control sgRNA
sgTP53 #1
sgTP53 #2
sgUSP7 #1
sgUSP7 #2
sgPPM1D #1
sgPPM1D #2
H
XL-188 (μM)
A673
TC71
EWS502
TC32
TC138
CHLA258
VH-64
WE-68
I

dataset to study the differences between *TP53* wild-type and *TP53* mutated cell lines. As expected, cell lines with functional p53 proliferate faster upon *TP53* knockout (leading to a positive dependency score), while cell lines with mutated *TP53* show little to no effect. We leveraged data from 33 cancer cell lines and identified *MDM2*, *MDM4*, *PPM1D*, and *USP7* as anti-correlated with *TP53* dependency scores in Ewing sarcoma and across all cancer cell lines in the dataset. A similar approach was recently used in the context of acute myeloid leukemia (Wang et al., 2017).

Each of the proteins, MDM2, MDM4, Wip1, and USP7, has been implicated in p53 regulation. MDM2 is an E3 ubiquitin ligase that targets p53 for degradation and is induced by p53 in a negative feedback loop. *MDM2*-deficient murine embryos are nonviable, a phenotype that can be rescued by concurrent *TP53* loss (Wade et al., 2013). In cancer, *MDM2* can act as an oncogene whose overexpression promotes malignancy by inhibiting the tumor suppressor function of p53 (Wade et al., 2013). Indeed, *MDM2* was found to be amplified in Ewing sarcoma patient samples, highlighting the importance of the gene in this disease (Ladanyi et al., 1995). MDM4 is a structural homologue of MDM2 that inhibits p53 by binding and blocking its transactivation domain. Similar to MDM2, MDM4 deficiency is embryonic lethal in mice and can be rescued by *TP53* loss (Wade et al., 2013). The *MDM4* gene is located on chromosome 1q, which is found to have copy number gains in a subset of Ewing sarcoma patient samples (Crompton et al., 2014). One study reported that 50% of Ewing sarcoma tumors contained greater than threefold amplification of *MDM4* (Ito et al., 2011). *PPM1D* encodes the phosphatase wild-type p53–induced phosphatase 1 (Wip1) that has several functions as an anti-apoptotic regulator, including dephosphorylation of p53 at serine 15 and deactivation. Wip1 has also been suggested to target ataxia telangiectasia mutated (ATM), ataxia telangiectasia and Rad3 related (ATR), checkpoint kinase 1 (CHK1), and checkpoint kinase 2 (CHK2), as well as MDM2 and MDM4 (Lu et al., 2007; Zhu and Bulavin, 2012). High Wip1 levels or *PPM1D* amplification have been found to correlate with poor prognosis in a variety of cancer types (Saito-Ohara et al., 2003; Castellino et al., 2008; Tan et al., 2009; Lambros et al., 2010; Ma et al., 2014; Peng et al., 2014; Xu et al., 2016; Zhao et al., 2016). USP7 is a deubiquitinating enzyme involved in a variety of cellular processes and is implicated in the regulation of MDM2, MDM4, and p53, as well as several other targets (Nicholson and Suresh Kumar, 2011).

Prior studies have targeted MDM2 in Ewing sarcoma and found anti-tumor efficacy in vitro and in vivo (Pishas et al., 2011; Sonnemann et al., 2011; Carol et al., 2013). MDM2 inhibition by RG7112 and RG7388 is being investigated in clinical trials as single agents or combination treatments for several malignancies. While early clinical trials testing RG7112 in patients with leukemia (Andreeff et al., 2016) and advanced solid tumors (Patnaik et al., 2015) have shown promise, coexpression of MDM4 can cause resistance (Hu et al., 2006; Patton et al., 2006; Wade et al., 2008; Chapeau et al., 2017). In addition, our finding that alternative negative regulators can coexist to thwart wild-type *TP53* signaling suggests that inhibitory strategies beyond selective MDM2 targeting may be required to achieve maximal reactivation of p53. The notion of dual targeting of MDM2 and MDM4 is further supported by dual-knockout experiments of *MDM2* and *MDM4* presented here, where we demonstrate that loss of both MDM2 and MDM4 decreases viability of Ewing sarcoma cells more effectively than loss of either target alone. Of note, these latter experiments must be interpreted within the technical limitations of dual knockout of two strong dependencies, where we were unable to obtain adequate protein for confirmation of equivalent knockout across these conditions because of the rapid onset of cell death.

Because *MDM4* overexpression has been established as a mechanism of resistance to MDM2 inhibitors, the development of MDM4 inhibitors has been of special interest (Bernal et al., 2010). Whereas a putative small molecule MDM4 inhibitor, XI-006, has been reported previously (Wang et al., 2011), *TP53* mutational status was not a biomarker for XI-006 sensitivity in Ewing sarcoma and breast cancer models (Pishas et al., 2015), suggesting potential off-target effects. ATSP-7041 is a mechanistically validated stapled peptide inhibitor of both MDM2 and MDM4 (Chang et al., 2013; Wachter et al., 2017). The ATSP-7041 derivative, ALRN-6924, is the first clinical grade stapled peptide to target intracellular protein interactions in human cancer, prompting its advancement to clinical testing. ALRN-6924 is currently in phase 1/2 evaluation for *TP53* wild-type solid tumors and lymphomas in adults (NCT02264613) and in phase 1 evaluation for acute myeloid leukemia and for myelodysplastic syndrome (NCT02909972). Thus,

Figure 9. **Loss of *PPM1D* and *USP7* is rescued by concurrent *TP53* loss. (A)** Western blots showing attenuated increase of p53 protein levels in TC32, TC138, and CHLA258 cells infected with sgRNAs targeting *TP53* after etoposide treatment (Control, control sgRNA; sg #1, sg*TP53* #1; sg #2, sg*TP53* #2; sg #4, sg*TP53* #4; sg #5, sg*TP53* #5). Cells were treated with vehicle or 50 µM etoposide for one hour (Veh, vehicle; Eto, etoposide). **(B)** *TP53* knockout cells were treated with ATSP-7041 for 3 d. Values were normalized to vehicle controls. Each data point shows the mean of eight replicates; error bars are mean values ± standard deviation. The experiment was performed twice and data points of one representative experiment are shown. **(C)** *TP53* knockout cells were treated with GSK2830371 for 3 d. Values were normalized to vehicle controls. Each data point shows the mean of eight replicates; error bars are mean values ± standard deviation. The experiment was performed twice, and data points of one representative experiment are shown. **(D)** *TP53* knockout cells were treated with P5091 for 3 d. Values were normalized to vehicle controls. Each data point shows the mean of eight replicates; error bars are mean values ± standard deviation. The experiment was performed twice, and data points of one representative experiment are shown. **(E)** Western blots showing decreased protein levels of USP7 after infection with sgRNAs targeting *USP7* in TC32 *TP53* knockout cells. **(F)** Western blots showing decreased protein levels of Wip1 after infection with sgRNAs targeting *PPM1D* in TC32 *TP53* knockout cells. **(G)** Relative viability of TC32 *TP53* knockout cells infected with sgRNAs targeting *USP7 or PPM1D* or control sgRNAs 14 d after infection. Each data point shows the mean of eight replicates, and data are plotted as mean values ± standard deviation. The experiment was performed twice and data points of one representative experiment are shown. Significance was calculated by paired, two-tailed *t* test: not significant (n.s.) for $P > 0.05$; *, $P \le 0.05$; **, $P \le 0.01$; ***, $P \le 0.001$. **(H)** Ewing sarcoma cells were treated with XL-188 for 3 d. *TP53* wild-type Ewing sarcoma cell lines are shown in red. *TP53* mutated Ewing sarcoma cell lines are shown in black. Values were normalized to vehicle controls. Each data point shows the mean of eight replicates; error bars are mean values ± standard deviation. The experiment was performed twice, and data points of one representative experiment are shown. **(I)** *TP53* knockout cells were treated with XL-188 for 3 d. Values were normalized to vehicle controls. Each data point shows the mean of eight replicates; error bars are mean values ± standard deviation. The experiment was performed twice and data points of one representative experiment are shown.

stapled p53 peptides offer the unique opportunity to target two of the highest scoring dependencies in *TP53* wild-type Ewing sarcoma cell lines simultaneously. We have shown that both *MDM2* and *MDM4* are strong dependencies in Ewing sarcoma. The therapeutic potential of ATSP-7041 is shown by its ability to decrease tumor growth in two different Ewing sarcoma models, including a study with an aggressive PDX model, where tumor progression was slowed in all mice, and one of eight mice achieved complete and sustained remission of disease. Therefore, we consider a dual MDM2/MDM4 inhibitor strategy to potentially be the most effective and rapidly translatable approach to reactivate p53 in patients with Ewing sarcoma.

Since single agent therapies rarely cure cancer, we sought to identify agents that could be used in combination with ATSP-7041. To evaluate the most readily translatable combinations, we combined ATSP-7041 with standard-of-care Ewing sarcoma cytotoxic chemotherapeutics and observed additivity or synergy with doxorubicin, etoposide, and vincristine. We have shown that the combination of ATSP-7041 with chemotherapeutic agents induces a stronger p53 response than these agents achieve individually. These mechanistic data support the addition of ATSP-7041 or other p53 reactivating agents to chemotherapy regimens. The synergistic induction of pro-apoptotic signals in cancer cells might allow for reduced doses of chemotherapy, thereby decreasing adverse effects. Our preclinical data support this notion and provide a compelling rationale for additional testing of ATSP-7041 with cytotoxic chemotherapy regimens in *TP53* wild-type Ewing sarcoma models. Such studies will help prioritize combinations for testing in clinical trials.

Furthermore, the combination of ATSP-7041 with the Wip1 inhibitor GSK2830371, and the USP7 inhibitor P5091, strongly synergizes in *TP53* wild-type Ewing sarcoma cell lines. These results support the hypothesis that inhibiting several members of the p53 regulatory network could be therapeutically beneficial (Pechackova et al., 2016; Sriraman et al., 2016). For example, in the case of ATSP-7041 and P5091 treatment, the addition of P5091 suppresses the counter up-regulation of MDM2. The combination of ATSP-7041 with GSK2830371 increases the level of pSer15 p53 more than with either molecule alone. Future studies will evaluate the efficacy of these combination treatments in vivo.

This study highlights the potential of genetic screening approaches to predict synergistic drug combinations, as *MDM2*, *MDM4*, *PPM1D*, and *USP7* were highly correlated dependencies in our analysis of the CRISPR-Cas9 screen. Based on our findings that inhibitors of these targets have synergistic anti-cancer activity, we suggest that systematic analysis of correlated dependencies in genetic screens can inform new, effective, and potentially rapidly translatable drug combinations. Additionally, these results suggest that analysis of genetic screens for biomarker-specific dependencies (in this case *TP53* status) can reveal proteins involved in the homeostasis of that biomarker (in this case MDM2, MDM4, Wip1, and USP7). This methodology may be applicable to a wide variety of clinical contexts.

USP7 has received increasing attention as a target in cancer and recent publications report new, selective inhibitors of the enzyme (Kategaya et al., 2017; Lamberto et al., 2017; Turnbull et al., 2017; Gavory et al., 2018). A series of p53-independent molecular targets and functions of USP7 have been proposed in different cancer types, such as the regulation of RAD18 in DNA damage response in hematologic malignancies (Agathanggelou et al., 2017), regulation of wingless-type MMTV integration site (Wnt) family signaling in colorectal cancer (An et al., 2017), Geminin deregulation in breast cancer (Hernández-Pérez et al., 2017), regulation of the Sonic Hedgehog pathway in medulloblastomas (Zhan et al., 2017), and stabilization of MYCN in neuroblastoma (Tavana et al., 2016). Here, we show that in Ewing sarcoma a key target of USP7 is the p53 pathway, as demonstrated by *TP53* knockout experiments and the notable synergism of ATSP-7041 and P5091. The identified role of USP7 in Ewing sarcoma is distinct from that reported in other cancer types and warrants further exploration in this disease. Given the superior selectivity of the small-molecule inhibitor XL-188, as compared with previous generation molecules such as P5091, the clinical translation of our USP7 findings may be achievable.

Our results also indicate a p53 dependent mechanism for Wip1 in Ewing sarcoma. While the phosphatase has been shown to target a variety of proteins in different disease contexts, it appears to act through p53 in Ewing sarcoma, as indicated by *TP53* knockout experiments and the synergistic elevation of phosphorylated p53 at serine 15 when GSK2830371 was combined with ATSP-7041. This finding advances our understanding of Wip1 activity in Ewing sarcoma and warrants further evaluation of Wip1 as a drug target in this disease.

In summary, we used CRISPR-Cas9 screening data to identify dependencies specific for *TP53* wild-type cancers, including Ewing sarcoma, and discovered the four p53 regulators *MDM2*, *MDM4*, *PPM1D*, and *USP7* as top hits. Validation of these targets using genetic and pharmacologic approaches confirmed their dependencies in Ewing sarcoma via a p53-dependent mechanism of action. We further demonstrated the in vivo activity of ATSP-7041 in two mouse models of Ewing sarcoma and highlight potential synergistic combinations for clinical translation using standard cytotoxic drugs and small molecule inhibitors of Wip1 and USP7, which warrant further development.

Materials and methods

CRISPR-Cas9 screening

The CRISPR-Cas9 screen was performed using the Broad Institute's GeCKO library (Sanjana et al., 2014; Aguirre et al., 2016). 33 cancer cell lines (including nine Ewing sarcoma lines) were screened with the GeCKO library, containing ∼95,000 guides and an average of six guides per gene (Sanjana et al., 2014; Aguirre et al., 2016). The library contains ∼1,000 negative control guides that do not target any location in the reference genome. The library also included guides with more than one perfect match in the reference genome allowing us to computationally correct for the previously described cutting toxicity associated with multiple Cas9 cuts in the genome (Aguirre et al., 2016).

Cancer cell lines were transduced with Cas9 using a lentiviral system (Aguirre et al., 2016). Cell lines that met quality control criteria, including Cas9 activity measured using a GFP reporter, and other parameters, were then screened with the CRISPR library. A pool of guides was transduced into a population of cells. The cells were cultured for ∼21 d in vitro, and at the end of the

assay, barcodes for each guide were sequenced for each cell line in replicate. Reads per kilobase were calculated for each replicate and then the log2 fold change compared with the initial plasmid pool was calculated for each guide. Samples with poor replicate reproducibility, as well as guides that have low representation in the initial plasmid pool, were removed from the analysis. Next, the guides from multiple replicates for each sample were used to collapse the data into gene scores using the CERES algorithm (Meyers et al., 2017), which models the cutting effect of each guide correcting for multiple cuts in the genome to produce a score that reflects the effect of disruption of the gene. After the dependency scores were calculated using the CERES algorithm, the scores for each cell line were scaled so that mean of negative controls was 0 and the mean of a subset of positive controls was −1.

For all of our analysis, the data were filtered and only the set of genetic dependencies with variable dependency scores that had standard deviations two sigma above the mean standard deviation across all genes were used. This resulted in 705 dependencies. Pearson correlations were then computed between the dependency gene score for *TP53* and all other variable dependencies in the screen. The top eight anti-correlated genes were used for subsequent analysis.

Cell lines and chemical compounds

Cell lines were obtained from the American Type Culture Collection (ATCC), except for VH-64 and WE-68, which were provided by J. Sonnemann (Universitätsklinikum Jena, Jena, Germany); TC138 and CHLA258, which were purchased from the COG Cell Line and Xenograft Repository; and SJSA-X, which was provided by G. Wahl (The Salk Institute for Biological Studies, La Jolla, CA). Cell line identity was confirmed by Short Tandem Repeat (STR) profiling. ATSP-7041 and ATSP-7342 were synthesized according to established methods (Bird et al., 2011; Chang et al., 2013). XL-188 was synthesized according to established methods (Lamberto et al., 2017). RG7388 (ApexBio Technology), GSK2830371 (Selleck Chemicals), P5091 (Sigma-Aldrich), doxorubicin (Cell Signaling), etoposide (Selleck Chemicals), and vincristine (Selleck Chemicals) were solubilized in DMSO.

Lentivirus production and transduction

Lentivirus was produced by transfecting HEK-293T cells with the pLentiV2 vector (Addgene plasmid 52961) and the packaging plasmids pCMV8.9 and pCMV-VSVG according to the FuGENE 6 (Roche) protocol. For lentiviral transduction, Ewing sarcoma cells were incubated with 2 ml of virus and 8 µg/ml of polybrene (Sigma-Aldrich). Cells were selected in puromycin (Sigma-Aldrich) 48 h after infection for single knockout experiments. For dual knockout experiments *PPM1D*, *USP7*, and *MDM4* sgRNA sequences were cloned into a LentiV2 vector with a blasticidin selection marker (Addgene plasmid 83480).

sgRNA sequences

sgRNAs were designed using the Broad Institute's sgRNA designer tool. The following sequences were used as control or to target the respective genes: control sgRNA, 5′-GTAGCGAACGTGTCCGGCGT-3′; sg*MDM2* 2: 5′-AGTTACTGTGTATCAGGCAG-3′; sg*MDM2* 5: 5′-AGACACTTATACTATGAAAG-3′; sg*MDM4* 4: 5′-AGATGTTGAACACTGAGCAG-3′; sgMDM4 6: 5′-AAGAATTCCACTGAGTTGCA-3′; sg*USP7* 1: 5′-AGATGTATGATCCCAAAACG-3′; sg*USP7* 2: 5′-ACCATACCCAAATTATTCCG-3′; sg*PPM1D* 1: 5′-CTGAAGAAAAGCCCTCGCCG-3′; sg*PPM1D* 2: 5′-CAGGTGATTTGTGGAGCTAT-3′; sg*TP53* 1: 5′-GCTTGTAGATGGCCATGGCG-3′; sg*TP53* 2: 5′-TCCTCAGCATCTTATCCGAG-3′; sg*TP53* 4: 5′-GCAGTCACAGCACATGACGG-3′; and sg*TP53* 5: 5′-GTAGTGGTAATCTACTGGGA-3′.

Protein extraction and immunoblotting

Whole-cell lysates were extracted in cell lysis buffer (Cell Signaling) supplemented with EDTA-free protease inhibitors and PhosSTOP phosphatase inhibitors (Roche). Western immunoblotting was performed using standard techniques. Primary antibodies used included anti-MDM2 (ab178938; Abcam), anti-MDM2 (86934; Cell Signaling), anti-MDM4 (A300-287A; Bethyl Laboratories), anti-p53 (2527S; Cell Signaling), anti-p21 (2946S; Cell Signaling), anti-Vinculin (18058; Abcam), anti-Wip1 (A300-664A; Bethyl Laboratories), anti-pSer15-p53 (9284; Cell Signaling), anti-USP7 (A300-033A; Bethyl Laboratories), and anti-Tubulin (cp06; CalBiochem).

Cell viability assays

Cell viability was assessed using the CellTiter-Glo Luminescent Cell Viability Assay (Promega). Viability assays were performed after Ewing sarcoma cell lines were infected with sgRNAs targeting *TP53*, *MDM2*, *MDM4*, *PPM1D*, or *USP7* or treated with ATSP-7041, ATSP-7342, GSK2830371, P5091, XL-188, or vehicle control.

Immunoprecipitation experiments

Five million TC32 cells were treated with either 10 µM RG7388 or vehicle control for 4 h. Cells were lysed in buffer A (150 mM NaCl, 50 mM Tris, and 0.5% NP-40, pH 7.4) and combined with anti-MDM4 antibody (A300-287A; Bethyl Laboratories) in the presence of 20 µM RG7388, ATSP-7041, or vehicle control in a total volume of 1 ml, rotating at 4°C for 16 h. Subsequently, 50 µl washed Protein AG beads (sc-2003; Santa Cruz) were added and the mixture was incubated for 1 h rotating at 4°C. Beads were washed three times in buffer A, and protein complexes were eluted by boiling in NuPage LDS Sample Buffer (NP0007; Invitrogen) supplemented with DTT. Samples were analyzed by Western blot with antibodies against p53 DO-1 (sc-126; Santa Cruz) and MDM4 (A300-287A; Bethyl Laboratories).

Annexin V staining

Ewing sarcoma cells lines were assessed for induction of cell death after 2 d of treatment with ATSP-7041 or P5091, or after 3 d of treatment with GSK2830371. Cell death was measured using flow cytometric analysis of Annexin V staining according to the manufacturer's instructions (eBioscience). Data analysis was completed using Flowjo 7.6 software (Treestar).

Quantitative PCR

RNA was extracted from cells with the RNeasy kit and on-column DNA digestion (Qiagen). cDNA was prepared using M-MLV reverse transcription (ThermoFisher Scientific). TaqMan Gene Expression Master Mix (Applied Biosystems) was used per the manufacturer's protocol. TaqMan probes included *RPL13A* (Hs04194366_g1;

ThermoFisher Scientific), *CDKN1A* (Hs00355782_m1; Thermo Fisher Scientific), and *MDM2* (Hs01066930_m1; ThermoFisher Scientific). Data were collected in triplicate and analyzed using the ΔΔCT method.

Ewing sarcoma xenograft studies

For anti-tumor efficacy studies, tumor xenografts were established in 15 nude female mice by implanting three million TC32 cells into the right flank. Animals were randomized to either 20 d of treatment with 30 mg/kg q.o.d. IV ATSP-7041 (n = 8) or vehicle (n = 7) for a total of 10 doses. Treatment was started when tumors reached 100–200 mm^3. Tumor volumes were measured with calipers twice a week. For PDX studies, tumor fragments were implanted into the right flank of nude female mice by minor surgery. After tumor engraftment, studies were performed as described for TC32 xenograft studies.

For pharmacodynamics studies, tumor xenografts were established in six nude female mice by implanting three million TC32 cells or PDX tumor fragments into the right flank. Animals were randomized to either ATSP-7041 (n = 3) or vehicle treatment (n = 3). Mice were treated with 30 mg/kg ATSP-7041 IV or vehicle every other day for three total doses and were sacrificed 8 h after the third dose. Tumor tissue was flash frozen for protein or RNA extraction using standard methods.

For in vivo studies, ATSP-7041 was prepared using the following protocol: mPEG-DSPE (Nanocs) was dissolved in chloroform and dried by a rotary evaporator. ATSP-7041 was dissolved in 1 M NaOH and diluted 100-fold in 10 mM histidine-buffered saline to a final concentration of 3 mg/ml. This mixture was added to the dried lipid film to a final mPEG-DSPE concentration of 50 mg/ml and final pH of 7. The film was rehydrated by brief sonication and heating in a 50°C water bath. The mixture was then subjected to five freeze-thaw cycles in liquid nitrogen and 40°C water, respectively, and the solution passed 10 times through an Avanti Mini-Extruder Set (Avanti Polar Lipids) equipped with a 800-nm filter (Whatman).

All animal studies were conducted under the auspices of protocols approved by the Dana-Farber Cancer Institute Animal Care and Use Committee.

Drug synergy analysis Chou-Talalay combination index for Loewe additivity

Loewe Additivity is a dose-effect approach that estimates the effect of combining two drugs based on the concentration of each individual drug that produces the same quantitative effect (Goldoni and Johansson, 2007). Chou and Talalay (Chou, 2006, 2010) showed that Loewe equations are valid for enzyme inhibitors with similar mechanisms of action, either competitive or noncompetitive toward the substrate. They introduced the combination index (CI) scores to estimate the interaction between the two drugs. If CI < 1, the drugs have a synergistic effect, and if CI > 1, the drugs have an antagonistic effect. CI = 1 means the drugs have an additive effect.

Online supplemental material

Supplemental material includes two items providing additional information on the CRISPR-Cas9 screen: *TP53* mutation annotations of cancer cell lines (Table S1) and correlation of *TP53* dependency with top scoring genes (Fig. S1).

Acknowledgments

The authors thank Jaume Mora for providing the PDX model HSJD-ES-002. The authors thank Jürgen Sonnemann for providing VH-64 and WE-68 Ewing sarcoma cell lines and Geoff Wahl for SJSA-X cells. The authors thank Franziska Wachter for insightful discussions.

B. Stolte was supported by a DAAD (Deutscher Akademischer Austauschdienst) fellowship in the thematic network "Research for Rare Diseases and Personalized Medicine." A. Balboni Iniguez is a Damon Runyon-Sohn Pediatric Fellow supported by the Damon Runyon Cancer Research Foundation (grant DRSG-12-15). N.V. Dharia is supported by the National Institutes of Health (NIH) training grant T32 CA136432. A.M. Morgan is supported by the NIH grant F30 CA221087, with prior support from NIH training grants T32 GM007753 and T32 GM008313. G.H. Bird is supported by NIH grant R50 CA211399. S.J. Buhrlage was supported by NIH grant R01 CA211681. This work was supported by a Quantum Award from Hyundai Hope on Wheels and a REACH grant from the Alex's Lemonade Stand Foundation to L.D. Walensky and K. Stegmaier, Leukemia and Lymphoma Society Scholar Awards to L.D. Walensky and K. Stegmaier, and by the Brian MacIsaac Sarcoma Foundation, St. Baldrick's Foundation Robert J. Arceci Innovation Award and National Cancer Institute grant R35 CA210030 to K. Stegmaier. This work was also supported by a generous gift from the family of Ivo Coll and the Cubans Curing Children's Cancers (4C's Fund).

L.D. Walensky is a scientific advisory board member and consultant for Aileron Therapeutics. The authors declare no further competing financial interests.

B. Stolte, A. Balboni Iniguez, N.V. Dharia, A.M. Morgan, G.H. Bird, A. Tsherniak, F. Vazquez, N.J. Schauer, X. Liu, S.J. Buhrlage, L.D. Walensky, and K. Stegmaier designed the experiments. B. Stolte, A.M. Morgan, A.L. Robichaud, and A. Conway Saur acquired the data. N.V. Dharia, G. Alexe, and B. Stolte performed statistical analysis, biostatistics, and computational analysis. B. Stolte, A. Balboni Iniguez, N.V. Dharia, A.L. Robichaud, A. Saur Conway, A.M. Morgan, G. Alexe, G.H. Bird, A. Tsherniak, F. Vazquez, N.J. Schauer, X. Liu, S.J. Buhrlage, L.D. Walensky, and K. Stegmaier wrote and revised the manuscript. K. Stegmaier and L.D. Walensky supervised the study.

Submitted: 12 June 2017
Revised: 16 March 2018
Accepted: 27 June 2018

References

Agathanggelou, A., E. Smith, N.J. Davies, M. Kwok, A. Zlatanou, C.E. Oldreive, J. Mao, D. Da Costa, S. Yadollahi, T. Perry, et al. 2017. USP7 inhibition alters homologous recombination repair and targets CLL cells independently of ATM/p53 functional status. *Blood.* 130:156–166. https://doi.org/10.1182/blood-2016-12-758219

Aguirre, A.J., R.M. Meyers, B.A. Weir, F. Vazquez, C.Z. Zhang, U. Ben-David, A. Cook, G. Ha, W.F. Harrington, M.B. Doshi, et al. 2016. Genomic Copy

Number Dictates a Gene-Independent Cell Response to CRISPR/Cas9 Targeting. *Cancer Discov.* 6:914–929. https://doi.org/10.1158/2159-8290.CD-16-0154

An, T., Y. Gong, X. Li, L. Kong, P. Ma, L. Gong, H. Zhu, C. Yu, J. Liu, H. Zhou, et al. 2017. USP7 inhibitor P5091 inhibits Wnt signaling and colorectal tumor growth. *Biochem. Pharmacol.* 131:29–39. https://doi.org/10.1016/j.bcp.2017.02.011

Andreeff, M., K.R. Kelly, K. Yee, S. Assouline, R. Strair, L. Popplewell, D. Bowen, G. Martinelli, M.W. Drummond, P. Vyas, et al. 2016. Results of the Phase I Trial of RG7112, a Small-Molecule MDM2 Antagonist in Leukemia. *Clin. Cancer Res.* 22:868–876. https://doi.org/10.1158/1078-0432.CCR-15-0481

Balamuth, N.J., and R.B. Womer. 2010. Ewing's sarcoma. *Lancet Oncol.* 11:184–192. https://doi.org/10.1016/S1470-2045(09)70286-4

Barretina, J., G. Caponigro, N. Stransky, K. Venkatesan, A.A. Margolin, S. Kim, C.J. Wilson, J. Lehár, G.V. Kryukov, D. Sonkin, et al. 2012. The Cancer Cell Line Encyclopedia enables predictive modelling of anticancer drug sensitivity. *Nature.* 483:603–607. https://doi.org/10.1038/nature11003

Bernal, F., M. Wade, M. Godes, T.N. Davis, D.G. Whitehead, A.L. Kung, G.M. Wahl, and L.D. Walensky. 2010. A stapled p53 helix overcomes HDMX-mediated suppression of p53. *Cancer Cell.* 18:411–422. https://doi.org/10.1016/j.ccr.2010.10.024

Bird, G.H., W.C. Crannell, and L.D. Walensky. 2011. Chemical synthesis of hydrocarbon-stapled peptides for protein interaction research and therapeutic targeting. *Curr. Protoc. Chem. Biol.* 3:99–117.

Brohl, A.S., D.A. Solomon, W. Chang, J. Wang, Y. Song, S. Sindiri, R. Patidar, L. Hurd, L. Chen, J.F. Shern, et al. 2014. The genomic landscape of the Ewing Sarcoma family of tumors reveals recurrent STAG2 mutation. *PLoS Genet.* 10:e1004475. https://doi.org/10.1371/journal.pgen.1004475

Cancer Cell Line Encyclopedia Consortium. Genomics of Drug Sensitivity in Cancer Consortium. 2015. Pharmacogenomic agreement between two cancer cell line data sets. *Nature.* 528:84–87.

Carol, H., C.P. Reynolds, M.H. Kang, S.T. Keir, J.M. Maris, R. Gorlick, E.A. Kolb, C.A. Billups, B. Geier, R.T. Kurmasheva, et al. 2013. Initial testing of the MDM2 inhibitor RG7112 by the Pediatric Preclinical Testing Program. *Pediatr. Blood Cancer.* 60:633–641. https://doi.org/10.1002/pbc.24235

Castellino, R.C., M. De Bortoli, X. Lu, S.H. Moon, T.A. Nguyen, M.A. Shepard, P.H. Rao, L.A. Donehower, and J.Y. Kim. 2008. Medulloblastomas overexpress the p53-inactivating oncogene WIP1/PPM1D. *J. Neurooncol.* 86:245–256. https://doi.org/10.1007/s11060-007-9470-8

Chang, Y.S., B. Graves, V. Guerlavais, C. Tovar, K. Packman, K.H. To, K.A. Olson, K. Kesavan, P. Gangurde, A. Mukherjee, et al. 2013. Stapled α-helical peptide drug development: a potent dual inhibitor of MDM2 and MDMX for p53-dependent cancer therapy. *Proc. Natl. Acad. Sci. USA.* 110:E3445–E3454. https://doi.org/10.1073/pnas.1303002110

Chapeau, E.A., A. Gembarska, E.Y. Durand, E. Mandon, C. Estadieu, V. Romanet, M. Wiesmann, R. Tiedt, J. Lehar, A. de Weck, et al. 2017. Resistance mechanisms to TP53-MDM2 inhibition identified by in vivo piggyBac transposon mutagenesis screen in an $Arf^{-/-}$ mouse model. *Proc. Natl. Acad. Sci. USA.* 114:3151–3156. https://doi.org/10.1073/pnas.1620262114

Chauhan, D., Z. Tian, B. Nicholson, K.G. Kumar, B. Zhou, R. Carrasco, J.L. McDermott, C.A. Leach, M. Fulcinniti, M.P. Kodrasov, et al. 2012. A small molecule inhibitor of ubiquitin-specific protease-7 induces apoptosis in multiple myeloma cells and overcomes bortezomib resistance. *Cancer Cell.* 22:345–358. https://doi.org/10.1016/j.ccr.2012.08.007

Chou, T.C. 2006. Theoretical basis, experimental design, and computerized simulation of synergism and antagonism in drug combination studies. *Pharmacol. Rev.* 58:621–681. https://doi.org/10.1124/pr.58.3.10

Chou, T.C. 2010. Drug combination studies and their synergy quantification using the Chou-Talalay method. *Cancer Res.* 70:440–446. https://doi.org/10.1158/0008-5472.CAN-09-1947

Cong, L., F.A. Ran, D. Cox, S. Lin, R. Barretto, N. Habib, P.D. Hsu, X. Wu, W. Jiang, L.A. Marraffini, and F. Zhang. 2013. Multiplex genome engineering using CRISPR/Cas systems. *Science.* 339:819–823. https://doi.org/10.1126/science.1231143

Crompton, B.D., C. Stewart, A. Taylor-Weiner, G. Alexe, K.C. Kurek, M.L. Calicchio, A. Kiezun, S.L. Carter, S.A. Shukla, S.S. Mehta, et al. 2014. The genomic landscape of pediatric Ewing sarcoma. *Cancer Discov.* 4:1326–1341. https://doi.org/10.1158/2159-8290.CD-13-1037

Ding, Q., Z. Zhang, J.J. Liu, N. Jiang, J. Zhang, T.M. Ross, X.J. Chu, D. Bartkovitz, F. Podlaski, C. Janson, et al. 2013. Discovery of RG7388, a potent and selective p53-MDM2 inhibitor in clinical development. *J. Med. Chem.* 56:5979–5983. https://doi.org/10.1021/jm400487c

Edlund, K., O. Larsson, A. Ameur, I. Bunikis, U. Gyllensten, B. Leroy, M. Sundström, P. Micke, J. Botling, and T. Soussi. 2012. Data-driven unbiased curation of the TP53 tumor suppressor gene mutation database and validation by ultradeep sequencing of human tumors. *Proc. Natl. Acad. Sci. USA.* 109:9551–9556. https://doi.org/10.1073/pnas.1200019109

Gaspar, N., D.S. Hawkins, U. Dirksen, I.J. Lewis, S. Ferrari, M.C. Le Deley, H. Kovar, R. Grimer, J. Whelan, L. Claude, et al. 2015. Ewing Sarcoma: Current Management and Future Approaches Through Collaboration. *J. Clin. Oncol.* 33:3036–3046. https://doi.org/10.1200/JCO.2014.59.5256

Gavory, G., C.R. O'Dowd, M.D. Helm, J. Flasz, E. Arkoudis, A. Dossang, C. Hughes, E. Cassidy, K. McClelland, E. Odrzywol, et al. 2018. Discovery and characterization of highly potent and selective allosteric USP7 inhibitors. *Nat. Chem. Biol.* 14:118–125. https://doi.org/10.1038/nchembio.2528

Gilmartin, A.G., T.H. Faitg, M. Richter, A. Groy, M.A. Seefeld, M.G. Darcy, X. Peng, K. Federowicz, J. Yang, S.Y. Zhang, et al. 2014. Allosteric Wip1 phosphatase inhibition through flap-subdomain interaction. *Nat. Chem. Biol.* 10:181–187. https://doi.org/10.1038/nchembio.1427

Goldoni, M., and C. Johansson. 2007. A mathematical approach to study combined effects of toxicants in vitro: evaluation of the Bliss independence criterion and the Loewe additivity model. *Toxicol. In Vitro.* 21:759–769. https://doi.org/10.1016/j.tiv.2007.03.003

Hanahan, D., and R.A. Weinberg. 2011. Hallmarks of cancer: the next generation. *Cell.* 144:646–674. https://doi.org/10.1016/j.cell.2011.02.013

Hendy, O.M., D.M. Elghannam, J.A. El-Sharnouby, E.F. Goda, R. El-Ashry, and Y. Al-Tonbary. 2009. Frequency and prognostic significance of murine double minute protein-2 overexpression and p53 gene mutations in childhood acute lymphoblastic leukemia. *Hematology.* 14:335–340. https://doi.org/10.1179/102453309X12473408860389

Hernández-Pérez, S., E. Cabrera, E. Salido, M. Lim, L. Reid, S.R. Lakhani, K.K. Khanna, J.M. Saunus, and R. Freire. 2017. DUB3 and USP7 de-ubiquitinating enzymes control replication inhibitor Geminin: molecular characterization and associations with breast cancer. *Oncogene.* 36:4802–4809. https://doi.org/10.1038/onc.2017.21

Hof, J., S. Krentz, C. van Schewick, G. Körner, S. Shalapour, P. Rhein, L. Karawajew, W.D. Ludwig, K. Seeger, G. Henze, et al. 2011. Mutations and deletions of the TP53 gene predict nonresponse to treatment and poor outcome in first relapse of childhood acute lymphoblastic leukemia. *J. Clin. Oncol.* 29:3185–3193. https://doi.org/10.1200/JCO.2011.34.8144

Hu, B., D.M. Gilkes, B. Farooqi, S.M. Sebti, and J. Chen. 2006. MDMX overexpression prevents p53 activation by the MDM2 inhibitor Nutlin. *J. Biol. Chem.* 281:33030–33035. https://doi.org/10.1074/jbc.C600147200

Ito, M., L. Barys, T. O'Reilly, S. Young, B. Gorbatcheva, J. Monahan, S. Zumstein-Mecker, P.F. Choong, I. Dickinson, P. Crowe, et al. 2011. Comprehensive mapping of p53 pathway alterations reveals an apparent role for both SNP309 and MDM2 amplification in sarcomagenesis. *Clin. Cancer Res.* 17:416–426. https://doi.org/10.1158/1078-0432.CCR-10-2050

Kategaya, L., P. Di Lello, L. Rougé, R. Pastor, K.R. Clark, J. Drummond, T. Kleinheinz, E. Lin, J.P. Upton, S. Prakash, et al. 2017. USP7 small-molecule inhibitors interfere with ubiquitin binding. *Nature.* 550:534–538. https://doi.org/10.1038/nature24006

Kato, M.V., T. Shimizu, K. Ishizaki, A. Kaneko, D.W. Yandell, J. Toguchida, and M.S. Sasaki. 1996. Loss of heterozygosity on chromosome 17 and mutation of the p53 gene in retinoblastoma. *Cancer Lett.* 106:75–82. https://doi.org/10.1016/0304-3835(96)04305-4

Klijn, C., S. Durinck, E.W. Stawiski, P.M. Haverty, Z. Jiang, H. Liu, J. Degenhardt, O. Mayba, F. Gnad, J. Liu, et al. 2015. A comprehensive transcriptional portrait of human cancer cell lines. *Nat. Biotechnol.* 33:306–312. https://doi.org/10.1038/nbt.3080

Ladanyi, M., R. Lewis, S.C. Jhanwar, W. Gerald, A.G. Huvos, and J.H. Healey. 1995. MDM2 and CDK4 gene amplification in Ewing's sarcoma. *J. Pathol.* 175:211–217. https://doi.org/10.1002/path.1711750209

Lamberto, I., X. Liu, H.S. Seo, N.J. Schauer, R.E. Iacob, W. Hu, D. Das, T. Mikhailova, E.L. Weisberg, J.R. Engen, et al. 2017. Structure-Guided Development of a Potent and Selective Non-covalent Active-Site Inhibitor of USP7. *Cell Chem. Biol.* 24:1490–1500.e11. https://doi.org/10.1016/j.chembiol.2017.09.003

Lambros, M.B., R. Natrajan, F.C. Geyer, M.A. Lopez-Garcia, K.J. Dedes, K. Savage, M. Lacroix-Triki, R.L. Jones, C.J. Lord, S. Linardopoulos, et al. 2010. PPM1D gene amplification and overexpression in breast cancer: a qRT-PCR and chromogenic in situ hybridization study. *Mod. Pathol.* 23:1334–1345. https://doi.org/10.1038/modpathol.2010.121

Lane, D.P. 1992. p53, guardian of the genome. *Nature.* 358:15–16. https://doi.org/10.1038/358015a0

Leroy, B., M. Anderson, and T. Soussi. 2014. TP53 mutations in human cancer: database reassessment and prospects for the next decade. *Hum. Mutat.* 35:672–688. https://doi.org/10.1002/humu.22552

Lu, X., O. Ma, T.A. Nguyen, S.N. Jones, M. Oren, and L.A. Donehower. 2007. The Wip1 Phosphatase acts as a gatekeeper in the p53-Mdm2 autoregulatory loop. *Cancer Cell.* 12:342–354. https://doi.org/10.1016/j.ccr.2007.08.033

Ma, D., C.J. Zhang, Z.L. Chen, and H. Yang. 2014. Prognostic value of PPM1D in 800 gastric cancer patients. *Mol. Med. Rep.* 10:191–194. https://doi.org/10.3892/mmr.2014.2165

Mali, P., L. Yang, K.M. Esvelt, J. Aach, M. Guell, J.E. DiCarlo, J.E. Norville, and G.M. Church. 2013. RNA-guided human genome engineering via Cas9. *Science.* 339:823–826. https://doi.org/10.1126/science.1232033

Malkin, D., E. Sexsmith, H. Yeger, B.R. Williams, and M.J. Coppes. 1994. Mutations of the p53 tumor suppressor gene occur infrequently in Wilms' tumor. *Cancer Res.* 54:2077–2079.

Meric-Bernstam, F., M.N. Saleh, J.R. Infante, S. Goel, G.S. Falchook, G. Shapiro, K.Y. Chung, R.M. Conry, D.S. Hong, J.S.-Z. Wang, et al. 2017. Phase I trial of a novel stapled peptide ALRN-6924 disrupting MDMX- and MDM2-mediated inhibition of WT p53 in patients with solid tumors and lymphomas. *J. Clin. Oncol.* 35:2505–2505.

Meyers, R.M., J.G. Bryan, J.M. McFarland, B.A. Weir, A.E. Sizemore, H. Xu, N.V. Dharia, P.G. Montgomery, G.S. Cowley, S. Pantel, et al. 2017. Computational correction of copy number effect improves specificity of CRISPR-Cas9 essentiality screens in cancer cells. *Nat. Genet.* 49:1779–1784. https://doi.org/10.1038/ng.3984

Nicholson, B., and K.G. Suresh Kumar. 2011. The multifaceted roles of USP7: new therapeutic opportunities. *Cell Biochem. Biophys.* 60:61–68. https://doi.org/10.1007/s12013-011-9185-5

Ognjanovic, S., G. Martel, C. Manivel, M. Olivier, E. Langer, and P. Hainaut. 2012. Low Prevalence of TP53 Mutations and MDM2 Amplifications in Pediatric Rhabdomyosarcoma. *Sarcoma.* 2012:492086. https://doi.org/10.1155/2012/492086

Ordóñez, J.L., A.T. Amaral, A.M. Carcaboso, D. Herrero-Martín, M. del Carmen García-Macías, V. Sevillano, D. Alonso, G. Pascual-Pasto, L. San-Segundo, M. Vila-Ubach, et al. 2015. The PARP inhibitor olaparib enhances the sensitivity of Ewing sarcoma to trabectedin. *Oncotarget.* 6:18875–18890. https://doi.org/10.18632/oncotarget.4303

Patnaik, A., A. Tolcher, M. Beeram, J. Nemunaitis, G.J. Weiss, K. Bhalla, M. Agrawal, G. Nichols, S. Middleton, A. Beryozkina, et al. 2015. Clinical pharmacology characterization of RG7112, an MDM2 antagonist, in patients with advanced solid tumors. *Cancer Chemother. Pharmacol.* 76:587–595. https://doi.org/10.1007/s00280-015-2830-8

Patton, J.T., L.D. Mayo, A.D. Singhi, A.V. Gudkov, G.R. Stark, and M.W. Jackson. 2006. Levels of HdmX expression dictate the sensitivity of normal and transformed cells to Nutlin-3. *Cancer Res.* 66:3169–3176. https://doi.org/10.1158/0008-5472.CAN-05-3832

Pechackova, S., K. Burdova, J. Benada, P. Kleiblova, G. Jenikova, and L. Macurek. 2016. Inhibition of WIP1 phosphatase sensitizes breast cancer cells to genotoxic stress and to MDM2 antagonist nutlin-3. *Oncotarget.* 7:14458–14475. https://doi.org/10.18632/oncotarget.7363

Peng, T.S., Y.H. He, T. Nie, X.D. Hu, H.Y. Lu, J. Yi, Y.F. Shuai, and M. Luo. 2014. PPM1D is a prognostic marker and therapeutic target in colorectal cancer. *Exp. Ther. Med.* 8:430–434. https://doi.org/10.3892/etm.2014.1762

Pishas, K.I., F. Al-Ejeh, I. Zinonos, R. Kumar, A. Evdokiou, M.P. Brown, D.F. Callen, and P.M. Neilsen. 2011. Nutlin-3a is a potential therapeutic for ewing sarcoma. *Clin. Cancer Res.* 17:494–504. https://doi.org/10.1158/1078-0432.CCR-10-1587

Pishas, K.I., A. Adwal, S.J. Neuhaus, M.T. Clayer, G. Farshid, A.H. Staudacher, and D.F. Callen. 2015. XI-006 induces potent p53-independent apoptosis in Ewing sarcoma. *Sci. Rep.* 5:11465. https://doi.org/10.1038/srep11465

Riggi, N., M.L. Suvà, D. Suvà, L. Cironi, P. Provero, S. Tercier, J.M. Joseph, J.C. Stehle, K. Baumer, V. Kindler, and I. Stamenkovic. 2008. EWS-FLI-1 expression triggers a Ewing's sarcoma initiation program in primary human mesenchymal stem cells. *Cancer Res.* 68:2176–2185. https://doi.org/10.1158/0008-5472.CAN-07-1761

Saito-Ohara, F., I. Imoto, J. Inoue, H. Hosoi, A. Nakagawara, T. Sugimoto, and J. Inazawa. 2003. PPM1D is a potential target for 17q gain in neuroblastoma. *Cancer Res.* 63:1876–1883.

Sanjana, N.E., O. Shalem, and F. Zhang. 2014. Improved vectors and genome-wide libraries for CRISPR screening. *Nat. Methods.* 11:783–784. https://doi.org/10.1038/nmeth.3047

Shalem, O., N.E. Sanjana, E. Hartenian, X. Shi, D.A. Scott, T. Mikkelson, D. Heckl, B.L. Ebert, D.E. Root, J.G. Doench, and F. Zhang. 2014. Genome-scale CRISPR-Cas9 knockout screening in human cells. *Science.* 343:84–87. https://doi.org/10.1126/science.1247005

Sonnemann, J., C.D. Palani, S. Wittig, S. Becker, F. Eichhorn, A. Voigt, and J.F. Beck. 2011. Anticancer effects of the p53 activator nutlin-3 in Ewing's sarcoma cells. *Eur. J. Cancer.* 47:1432–1441. https://doi.org/10.1016/j.ejca.2011.01.015

Sriraman, A., M. Radovanovic, M. Wienken, Z. Najafova, Y. Li, and M. Dobbelstein. 2016. Cooperation of Nutlin-3a and a Wip1 inhibitor to induce p53 activity. *Oncotarget.* 7:31623–31638. https://doi.org/10.18632/oncotarget.9302

Szklarczyk, D., A. Franceschini, S. Wyder, K. Forslund, D. Heller, J. Huerta-Cepas, M. Simonovic, A. Roth, A. Santos, K.P. Tsafou, et al. 2015. STRING v10: protein-protein interaction networks, integrated over the tree of life. *Nucleic Acids Res.* 43(D1):D447–D452. https://doi.org/10.1093/nar/gku1003

Tan, D.S., M.B. Lambros, S. Rayter, R. Natrajan, R. Vatcheva, Q. Gao, C. Marchiò, F.C. Geyer, K. Savage, S. Parry, et al. 2009. PPM1D is a potential therapeutic target in ovarian clear cell carcinomas. *Clin. Cancer Res.* 15:2269–2280. https://doi.org/10.1158/1078-0432.CCR-08-2403

Tavana, O., D. Li, C. Dai, G. Lopez, D. Banerjee, N. Kon, C. Chen, A. Califano, D.J. Yamashiro, H. Sun, and W. Gu. 2016. HAUSP deubiquitinates and stabilizes N-Myc in neuroblastoma. *Nat. Med.* 22:1180–1186. https://doi.org/10.1038/nm.4180

Tirode, F., D. Surdez, X. Ma, M. Parker, M.C. Le Deley, A. Bahrami, Z. Zhang, E. Lapouble, S. Grossetête-Lalami, M. Rusch, et al. St. Jude Children's Research Hospital–Washington University Pediatric Cancer Genome Project and the International Cancer Genome Consortium. 2014. Genomic landscape of Ewing sarcoma defines an aggressive subtype with co-association of STAG2 and TP53 mutations. *Cancer Discov.* 4:1342–1353. https://doi.org/10.1158/2159-8290.CD-14-0622

Turnbull, A.P., S. Ioannidis, W.W. Krajewski, A. Pinto-Fernandez, C. Heride, A.C.L. Martin, L.M. Tonkin, E.C. Townsend, S.M. Buker, D.R. Lancia, et al. 2017. Molecular basis of USP7 inhibition by selective small-molecule inhibitors. *Nature.* 550:481–486. https://doi.org/10.1038/nature24451

Wachter, F., A.M. Morgan, M. Godes, R. Mourtada, G.H. Bird, and L.D. Walensky. 2017. Mechanistic validation of a clinical lead stapled peptide that reactivates p53 by dual HDM2 and HDMX targeting. *Oncogene.* 36:2184–2190. https://doi.org/10.1038/onc.2016.361

Wade, M., L.W. Rodewald, J.M. Espinosa, and G.M. Wahl. 2008. BH3 activation blocks Hdmx suppression of apoptosis and cooperates with Nutlin to induce cell death. *Cell Cycle.* 7:1973–1982. https://doi.org/10.4161/cc.7.13.6072

Wade, M., Y.C. Li, and G.M. Wahl. 2013. MDM2, MDMX and p53 in oncogenesis and cancer therapy. *Nat. Rev. Cancer.* 13:83–96. https://doi.org/10.1038/nrc3430

Wang, H., X. Ma, S. Ren, J.K. Buolamwini, and C. Yan. 2011. A small-molecule inhibitor of MDMX activates p53 and induces apoptosis. *Mol. Cancer Ther.* 10:69–79. https://doi.org/10.1158/1535-7163.MCT-10-0581

Wang, T., H. Yu, N.W. Hughes, B. Liu, A. Kendirli, K. Klein, W.W. Chen, E.S. Lander, and D.M. Sabatini. 2017. Gene Essentiality Profiling Reveals Gene Networks and Synthetic Lethal Interactions with Oncogenic Ras. *Cell.* 168:890–903.e15. https://doi.org/10.1016/j.cell.2017.01.013

Xu, Z., C. Cao, H. Xia, S. Shi, L. Hong, X. Wei, D. Gu, J. Bian, Z. Liu, W. Huang, et al. 2016. Protein phosphatase magnesium-dependent 1δ is a novel tumor marker and target in hepatocellular carcinoma. *Front. Med.* 10:52–60. https://doi.org/10.1007/s11684-016-0433-3

Zhan, M., X. Sun, J. Liu, Y. Li, Y. Li, X. He, Z. Zhou, and L. Lu. 2017. Usp7 promotes medulloblastoma cell survival and metastasis by activating Shh pathway. *Biochem. Biophys. Res. Commun.* 484:429–434. https://doi.org/10.1016/j.bbrc.2017.01.144

Zhao, M., H. Zhang, G. Zhu, J. Liang, N. Chen, Y. Yang, X. Liang, H. Cai, and W. Liu. 2016. Association between overexpression of Wip1 and prognosis of patients with non-small cell lung cancer. *Oncol. Lett.* 11:2365–2370. https://doi.org/10.3892/ol.2016.4245

Zhu, Y.H., and D.V. Bulavin. 2012. Wip1-dependent signaling pathways in health and diseases. *Prog. Mol. Biol. Transl. Sci.* 106:307–325. https://doi.org/10.1016/B978-0-12-396456-4.00001-8

Article

Cancer Cell

EWS/FLI Confers Tumor Cell Synthetic Lethality to CDK12 Inhibition in Ewing Sarcoma

Graphical Abstract

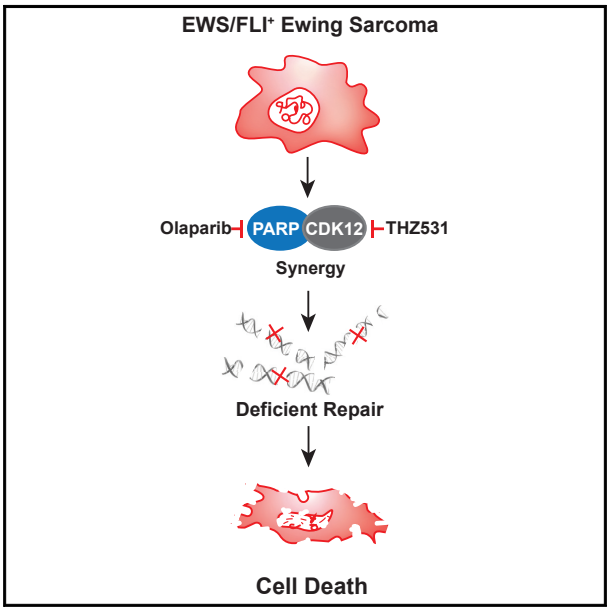

Authors

Amanda Balboni Iniguez, Björn Stolte, Emily Jue Wang, ..., Richard A. Young, Nathanael S. Gray, Kimberly Stegmaier

Correspondence

kimberly_stegmaier@dfci.harvard.edu

In Brief

Iniguez et al. find that inhibition of CDK12 is synthetic lethal with EWS/FLI expression. CDK12/13 inhibitors impair DNA damage repair in cells expressing EWS/FLI, and the combination of CDK12/13 and PARP inhibitors synergistically reduces tumor growth and extends survival in Ewing sarcoma mouse models.

Highlights

- Ewing sarcoma cells are highly sensitive to CDK7/12/13 inhibitors
- Tumor-specific EWS/FLI expression is synthetic lethal with suppression of CDK12
- CDK12/13 inhibitors impair DNA damage repair in fusion-positive Ewing sarcoma
- CDK12/13 and PARP inhibitors are highly synergistic in Ewing sarcoma

Iniguez et al., 2018, Cancer Cell *33*, 202–216
February 12, 2018
https://doi.org/10.1016/j.ccell.2017.12.009

CellPress

CellPress

Cancer Cell
Article

EWS/FLI Confers Tumor Cell Synthetic Lethality to CDK12 Inhibition in Ewing Sarcoma

Amanda Balboni Iniguez,[1,2] Björn Stolte,[1,3] Emily Jue Wang,[1,2] Amy Saur Conway,[1] Gabriela Alexe,[1,2,4] Neekesh V. Dharia,[1,2] Nicholas Kwiatkowski,[5,6,7] Tinghu Zhang,[6,7] Brian J. Abraham,[5] Jaume Mora,[8] Peter Kalev,[9] Alan Leggett,[6,7] Dipanjan Chowdhury,[9] Cyril H. Benes,[10] Richard A. Young,[5,11] Nathanael S. Gray,[6,7] and Kimberly Stegmaier[1,2,12,*]

[1]Department of Pediatric Oncology, Dana-Farber Cancer Institute and Boston Children's Hospital, Harvard Medical School, 450 Brookline Avenue, Boston, MA 02215, USA
[2]The Broad Institute of MIT and Harvard, Cambridge, MA 02142, USA
[3]Ludwig Maximilians University of Munich, Munich 80539, Germany
[4]Bioinformatics Graduate Program, Boston University, Boston, MA 02215, USA
[5]The Whitehead Institute for Biomedical Research, Cambridge, MA 02142, USA
[6]Department of Cancer Biology, Dana-Farber Cancer Institute, Boston, MA 02215, USA
[7]Department of Biological Chemistry and Molecular Pharmacology, Harvard Medical School, Boston, MA 02115, USA
[8]Development Tumor Biology Laboratory and Department of Pediatric Oncology and Hematology, Hospital Sant Joan de Déu Barcelona, Barcelona 08950, Spain
[9]Department of Radiation Oncology, Dana-Farber Cancer Institute, Harvard Medical School, Boston, MA 02215, USA
[10]Massachusetts General Hospital, Center for Cancer Research, Boston, MA 02114, USA
[11]Department of Biology, Massachusetts Institute of Technology, Cambridge, MA 02139, USA
[12]Lead Contact
*Correspondence: kimberly_stegmaier@dfci.harvard.edu
https://doi.org/10.1016/j.ccell.2017.12.009

SUMMARY

Many cancer types are driven by oncogenic transcription factors that have been difficult to drug. Transcriptional inhibitors, however, may offer inroads into targeting these cancers. Through chemical genomics screening, we identified that Ewing sarcoma is a disease with preferential sensitivity to THZ1, a covalent small-molecule CDK7/12/13 inhibitor. The selective CDK12/13 inhibitor, THZ531, impairs DNA damage repair in an EWS/FLI-dependent manner, supporting a synthetic lethal relationship between response to THZ1/THZ531 and EWS/FLI expression. The combination of these molecules with PARP inhibitors showed striking synergy in cell viability and DNA damage assays *in vitro* and in multiple models of Ewing sarcoma, including a PDX, *in vivo* without hematopoietic toxicity.

INTRODUCTION

A therapeutic challenge in oncology is the paucity of readily "druggable" genetic events in many malignancies, particularly childhood cancers. These tumors are frequently defined by sentinel abnormalities involving transcription factors in an otherwise quiet genomic landscape. Ewing sarcoma, the second most common cancer involving bone in children, is characterized by a chromosomal rearrangement that fuses the strong transactivation domain of the RNA binding protein, EWS, with the DNA binding domain of an ETS protein, most commonly FLI1. EWS/FLI acts as both a transcriptional activator and a transcriptional repressor via distinct chromatin binding mechanisms (Riggi et al., 2014), and numerous studies have demonstrated a strict dependency on EWS/FLI in Ewing sarcoma cells, supporting the targeting of this fusion protein or its transcriptional output

Significance

Here we report that Ewing sarcoma is a disease with exquisite sensitivity to the covalent small-molecule CDK7/12/13 inhibitors, THZ1 and THZ531. These compounds act, in part, through inhibition of CDK12 and the subsequent suppression of genes involved in DNA damage repair. The preferential sensitivity of Ewing sarcoma cells to THZ1/THZ531 is imparted by the tumor-specific expression of the fusion oncoprotein EWS/FLI. The combination of these molecules with PARP inhibitors showed prominent synergy in multiple models of Ewing sarcoma without apparent toxicity. With this class of compounds moving toward the clinic, this study has promising translational potential for patients with Ewing sarcoma and important translational relevance to other tumors that are sensitive to PARP inhibitors.

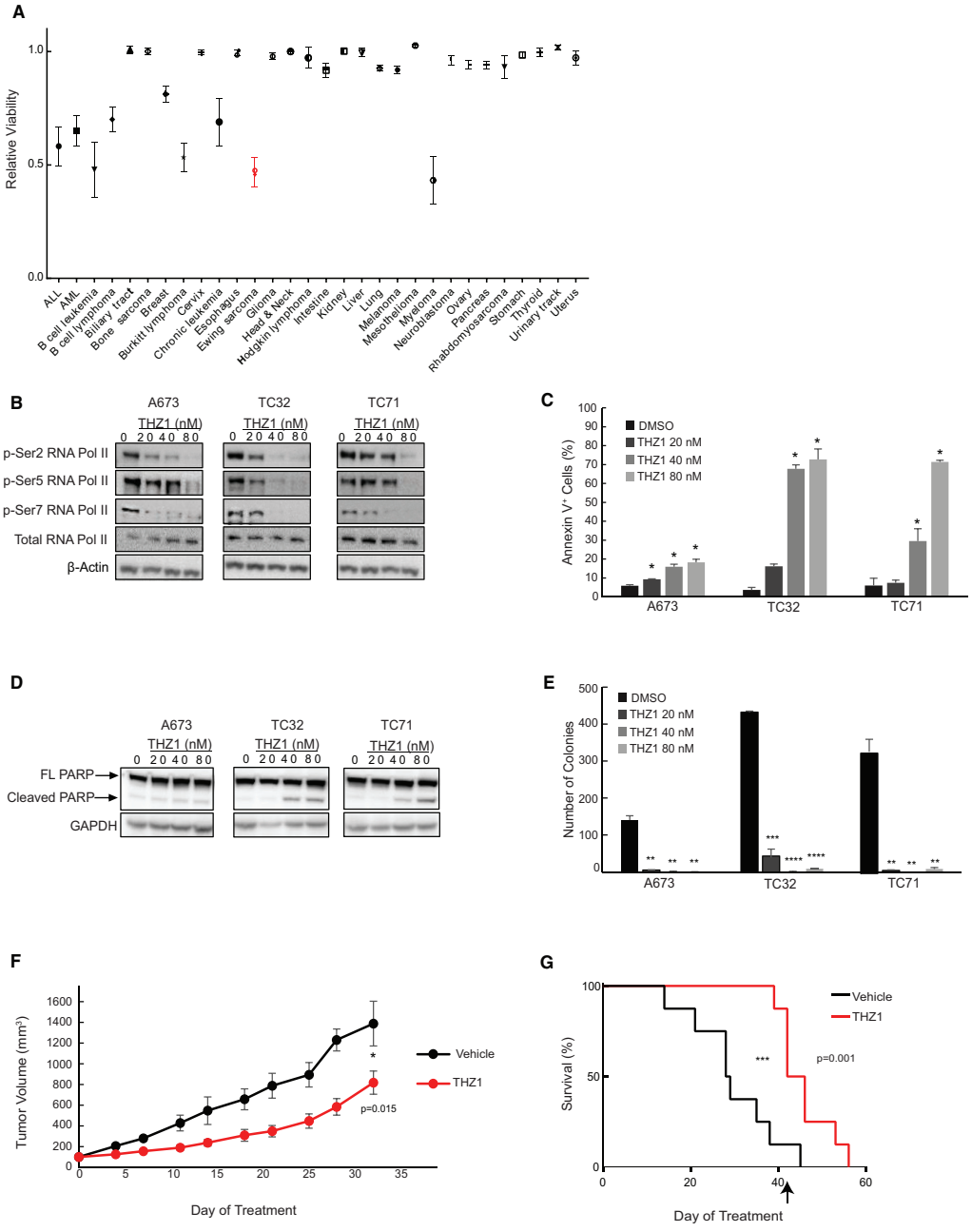

(legend on next page)

(Hu-Lieskovan et al., 2005; Smith et al., 2006). Moreover, three recent massively parallel sequencing efforts revealed that Ewing sarcoma tumors possess very low mutation rates, harboring few recurrent mutations other than EWS/ETS rearrangements (Brohl et al., 2014; Crompton et al., 2014; Tirode et al., 2014).

One approach to treating these tumors is the direct targeting of the aberrant transcription factor. With a few notable exceptions, however, this approach poses a significant drug discovery challenge. A second approach might target a synthetic lethal dependency imparted on the cell by virtue of the cancer-promoting genetic event, such as the use of poly(ADP-ribose) polymerase (PARP) inhibitors in *BRCA1*-and *BRCA2*-mutant cancers (Sonnenblick et al., 2015). A third approach might target basic transcriptional machinery with transcriptional inhibitors, such as the Food and Drug Administration-approved drug, actinomycin D, or compounds such as THZ1, a small-molecule covalent inhibitor of CDK7/12/13.

Initial studies demonstrated that CDK7/12/13 inhibition with THZ1 may be therapeutically beneficial in tumor types that are highly dependent on transcriptional programs for initiating a transformed phenotype (Kwiatkowski et al., 2014). These studies provided rationale for an inroad into treating cancers defined by aberrant transcription factors. For example, *MYCN*-amplified neuroblastoma cells were found to be highly responsive to THZ1 through suppression of the MYCN transcriptional program, and T cell acute lymphoblastic leukemia cells (T-ALL) were responsive to THZ1 through the repression of RUNX1 (Chipumuro et al., 2014; Kwiatkowski et al., 2014). THZ1 decreases the phosphorylation of the C-terminal domain (CTD) of RNA polymerase II (RNA Pol II), thereby preventing transcriptional initiation and elongation. Exquisite specificity is obtained through binding of the molecule to a cysteine residue adjacent to the ATP binding domain (Kwiatkowski et al., 2014). The capacity to perform at scale chemical genomic screening across over 1,000 cancer cell lines provided an unprecedented opportunity to discover new connections between response to THZ1 and the expression of other so-called "undruggable" targets.

RESULTS

Ewing Sarcoma Is Highly Sensitive to the CDK7/12/13 Inhibitor THZ1

THZ1, a covalent and potent inhibitor of CDK7/12/13 kinases involved in transcriptional regulation, recently emerged as a targeted strategy to impair aberrant transcription (Chipumuro et al., 2014; Christensen et al., 2014; Kwiatkowski et al., 2014). To identify biomarkers of sensitivity to THZ1, we screened THZ1 against a diverse panel of 1,081 cancer cell lines (Figure 1A) (Garnett et al., 2012; Kwiatkowski et al., 2014). Within the group of cell lines highly sensitive to low concentrations of THZ1 (defined by cell lines with viability <50% when treated with 9.76 nM THZ1), Ewing sarcoma cells were significantly enriched for response (Fisher's test, $p = 9 \times 10^{-9}$). In fact, Ewing sarcoma cell lines were collectively more sensitive to THZ1 than other cancer types previously reported to be highly sensitive to this molecule (Figure 1A). The mean viability for each tumor type screened with 9.76 nM THZ1 was as follows: Ewing sarcoma 47%, T-ALL 58%, lung cancer 92%, and neuroblastoma 96%. To assay the on-target activity of THZ1, we measured the phosphorylation of global pSer2/5/7 RNA Pol II levels at concentrations that inhibit Ewing sarcoma cell growth. THZ1 suppressed the phosphorylation of the CTD of RNA Pol II in a concentration-dependent manner (Figure 1B). Suppression of EWS/FLI did not affect the ability of THZ1 to repress these phosphorylation sites (Figure S1A). Furthermore, THZ1 induced apoptosis as demonstrated by an increase in the percentage of Annexin V^+ cells and PARP cleavage (Figures 1C and 1D) and strongly decreased the colony formation capacity of Ewing sarcoma cell lines (Figure 1E).

To establish the activity of THZ1 *in vivo*, TC32 Ewing sarcoma xenografts were treated with either vehicle control or 10 mg/kg of THZ1 delivered intraperitoneally twice per day. Treatment was stopped at day 42 and the remaining mice were followed for survival. THZ1 as a single agent significantly impaired tumor progression and increased overall survival (median survival = 28.5 days for vehicle and 44 days for the THZ1 arms) (Figures 1F and 1G). No weight loss-related toxicity was observed (Figure S1B).

A Primary Target of THZ1 Is CDK12 in Ewing Sarcoma

To elucidate preferential dependencies of cancer cells on CDK7, CDK12, and CDK13, we used genome-scale CRISPR-Cas9 screening across 341 cancer cell lines representing diverse cancer cell types (Meyers et al., 2017). We identified that *CDK7* disruption is pan-lethal with the depletion of guides targeting *CDK7*, similar to the depletion seen for known common essential genes in the screen, raising some concerns about the therapeutic window of a potent CDK7 inhibitor (Figure S2A). In contrast, CDK12 and CDK13 showed differential dependencies across the cell lines included in the screen (Figures S2B and S2C). We

Figure 1. Extensive Profiling of THZ1 Highlights Exceptional Sensitivity of Ewing Sarcoma Cells

(A) A diverse panel of 1,081 cancer cell lines was treated with DMSO or 9.76 nM THZ1 for 72 hr and assayed for cell viability. Shown are the mean relative viabilities ± SEM for each tumor type with at least eight cell lines screened. Ewing sarcoma cell lines are in red.

(B) Western blot demonstrating the effects of THZ1 on p-RNA Pol II in Ewing sarcoma cell lines at 6 hr. β-Actin, loading control.

(C) Concentration-dependent effects of THZ1 on the percentage of Annexin V^+ cells measured by flow cytometry at 24 hr. Data are presented as mean values ± SD of triplicate points (t test).

(D) Western blot demonstrating the effects of THZ1 on PARP cleavage at 24 hr. Glyceraldehyde 3-phosphate dehydrogenase (GAPDH), loading control.

(E) Colony formation in soft agar of Ewing sarcoma cell lines treated with THZ1 for 14 days. The experiment was conducted in biological triplicate. Data shown is a representative experiment of mean values ± SD of technical duplicates (t test).

(F) Tumor volume measurements of TC32 Ewing sarcoma xenografts treated with 10 mg/kg THZ1intraperitoneal (IP) or vehicle control (10% DMSO in D5W) IP twice daily (BID). Data are plotted out to day 32, when >50% of mice in the vehicle group were still alive and presented as mean values ± SD (n = 8 per arm) (t test).

(G) Kaplan-Meier survival curves for the experiment described in (F). Treatment was stopped on day 42 (arrow) and mice were followed for survival (log rank Mantel-Cox test).

*$p < 0.05$, **$p < 0.01$, ***$p < 0.001$, ****$p < 0.0001$. See also Figure S1.

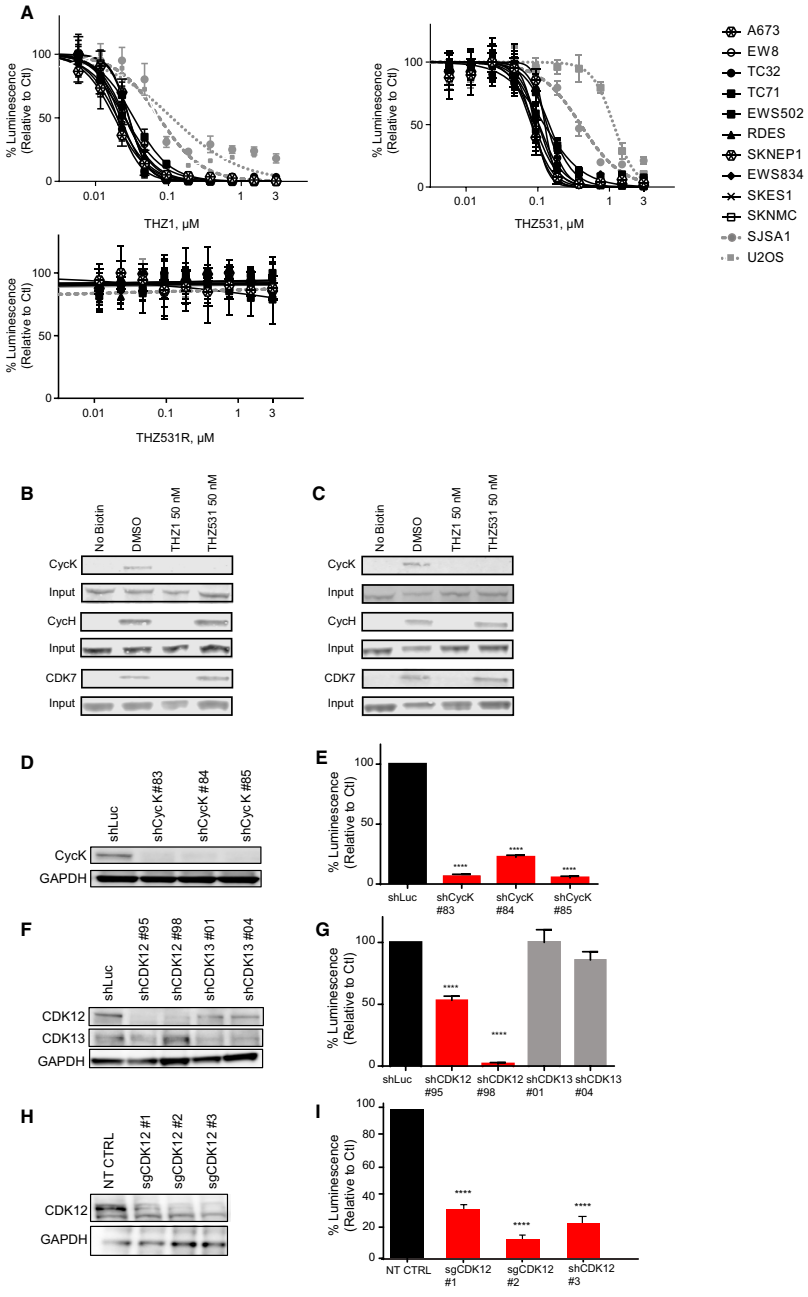

(legend on next page)

found that approximately 10.2% of the cell lines are dependent on CDK12 with a dependency score of < –0.5, compared with CDK7 and CDK13, where 100% and 3.8% of lines screened were dependent on the gene, respectively. Among the CDK12-dependent cell lines was SK-N-MC, the one Ewing sarcoma cell line included in the screen harboring an EWS/FLI rearrangement, with 3 of the 11 neuroblastoma cell lines included in the screen scoring between −0.4 and −0.5. The majority of neuroblastoma cell lines, as well as small-cell lung cancer (SCLC) and T-ALL cell lines, were not dependent on CDK12 for survival (Figure S2B). Furthermore, none of the Ewing sarcoma, neuroblastoma, T-ALL, or SCLC cell lines screened were dependent on CDK13 (Figure S2C). A full list of all of the CERES-dependency gene scores for CDK7, CDK12, and CDK13 across the 341 cancer cell lines is included in Table S1. These data suggest that the preferential sensitivity of Ewing sarcoma cells to THZ1 in our chemical genomics screen may be due to CDK12 and not CDK7 or CDK13 inhibition. They also suggest that a more selective CDK12/13 inhibitor would be preferentially toxic to Ewing sarcoma cells and may reduce potential toxicities associated with CDK7 inhibition. To develop more selective molecules, Zhang et al. (2016) used THZ1 as starting material for THZ531, a first-in-class covalent and selective CDK12 and CDK13 inhibitor, which targets a cysteine residue adjacent to the ATP binding site of CDK12 and CDK13. The authors reported that THZ531 inhibits CDK12 and CDK13 with half maximal inhibitory concentrations (IC_{50}) of 158 and 69 nM, respectively, whereas THZ531 inhibits CDK7 and CDK9 at 8.5 and 10.5 μM, respectively (Zhang et al., 2016). Furthermore, KiNativ profiling demonstrated that CDK12 and CDK13 were the primary targets of THZ531, with none of the other 211 kinases profiled demonstrating >55% inhibition (Zhang et al., 2016). To identify which kinase target of THZ1 is primarily responsible for the potent anti-viability effects observed, we treated a panel of Ewing sarcoma cell lines with three compounds: THZ1, a pan CDK7/12/13 inhibitor; THZ531, a CDK12/13 selective inhibitor; and THZ531R, a non-cysteine reactive analog with reduced anti-CDK12/13 activity (Figure 2A). We found that Ewing sarcoma cell lines were nearly as sensitive to THZ531 as they were to THZ1, with IC_{50} concentrations in the low nanomolar range with both small molecules in viability assays (Figure 2A; Table S2). The mean IC_{50} for THZ1 across Ewing sarcoma cell lines was 41.03 versus 90.4 nM for THZ531, demonstrating that CDK12/13 inhibition recapitulates much of the sensitivity to THZ1, although CDK7 inhibition may still contribute to the sensitivity to this molecule. In addition, Ewing sarcoma cell lines were completely insensitive to THZ531R (Figure 2A). Furthermore, Ewing sarcoma cell lines were 3- to 10-fold more sensitive to THZ1 and THZ531 than non-EWS/FLI-expressing osteosarcoma cell lines (Figure 2A; Table S2), suggesting that sensitivity to CDK7/12/13 inhibition may be enhanced in EWS/FLI rearranged cells. Interestingly, all ten Ewing sarcoma cell lines tested were uniformly sensitive to THZ1 and THZ531, indicating that CDK12/13 inhibition may be broadly effective as a treatment strategy for Ewing tumors defined by EWS/FLI rearrangements (Table S2).

To confirm the selectivity of these compounds in Ewing sarcoma cells, we performed THZ1-biotin immunoprecipitation of samples treated with THZ1 or THZ531 and probed for cyclin K (binding partner of CDK12/13) or cyclin H (binding partner of CDK7). We found that THZ531 has specificity for cyclin K-CDK12/13 complexes and not cyclin H-CDK7 complexes, as THZ1-biotin can pull down cyclin H-CDK7 complexes in samples pretreated with THZ531, but cannot pull down cyclin K-CDK12/13 complexes, as they are occupied by THZ531 (Figures 2B and 2C).

To provide further validation of the target of THZ531 in Ewing sarcoma cells, cyclin K was knocked down in A673 Ewing sarcoma cells (Figure 2D). Suppression of cyclin K using three different hairpins strongly suppressed the viability of these cells (Figures 2D and 2E). To further discriminate which CDK is responsible for the potent growth suppression with THZ531, we knocked down CDK12 and CDK13 using two different hairpins (Figure 2F). We found that genetic suppression of CDK12 decreased the viability of Ewing sarcoma cells (Figures 2F and 2G), while, in contrast, suppression of CDK13 had a minimal effect (Figures 2F and 2G). In addition, CRISPR-Cas9-mediated knock out of *CDK12* strongly reduced Ewing sarcoma cell viability (Figures 2H and 2I). Collectively, these results

Figure 2. The Activity of THZ1 in Ewing Sarcoma Cell Lines Is Attributed to CDK12 Inhibition

(A) Dose-response curves of Ewing sarcoma cell lines (black) and osteosarcoma cell lines (gray) treated with THZ1 (CDK7/12/13 inhibitor), THZ531 (CDK12/13 selective inhibitor), or THZ531R (derivative of THZ531 that lacks the covalent binding moiety) for 72 hr. Data are plotted as the percentage of luminescence relative to DMSO controls. The experiment was performed in biological triplicate. Results are presented as mean values of a representative experiment ± SD of eight technical replicates.

(B and C) THZ1-biotin IP of samples treated with THZ1 or THZ531 and probed for cyclin K (CycK) or cyclin H (CycH) in A673 cells (B) and TC32 cells (C). The experiment was performed in biological duplicate.

(D) Immunoblot of A673 cells infected with a luciferase small hairpin RNA (shRNA) control (shLuc) or shRNAs against cyclin K (shCycK) and probed for cyclin K expression 5 days post-infection. GAPDH, loading control.

(E) Relative viability of A673 cells infected with shLuc or shCycK 10 days post-infection. Data are plotted as the percentage of luminescence relative to shLuc control. The experiment was performed in biological triplicate. Results are presented as mean values of a representative experiment ± SD of eight technical replicates. Statistical significance is calculated for each individual hairpin compared with the control hairpin, t test.

(F) Immunoblot of A673 cells infected with a luciferase shRNA control or shRNAs against CDK12 or CDK13 5 days post-infection. GAPDH, loading control.

(G) Relative viability of cells infected with hairpins against luciferase, CDK12 or CDK13 10 days post-infection. Data are plotted as the percentage of luminescence relative to shLuc control. The experiment was performed in biological triplicate. Results are presented as mean values of a representative experiment ± SD of eight technical replicates. Statistical significance is calculated for each individual hairpin compared with the control hairpin, t test.

(H) Immunoblot of A673 cells infected with a non-targeting control single-guide RNA (sgRNA) (NT CTRL) or three different guide RNAs against *CDK12* (sgCDK12) 7 days post-infection. GAPDH, loading control.

(I) Relative viability of cells infected with an NT CTRL sgRNA or sgRNAs targeting *CDK12* 14 days post-infection. Data are plotted as the percentage of luminescence relative to NT control. The experiment was performed in biological triplicate. Results are presented as mean values of a representative experiment ± SD of eight technical replicates. Statistical significance is calculated for each individual hairpin compared with the control hairpin, t test.

****$p < 0.0001$. See also Figure S2 and Tables S1 and S2.

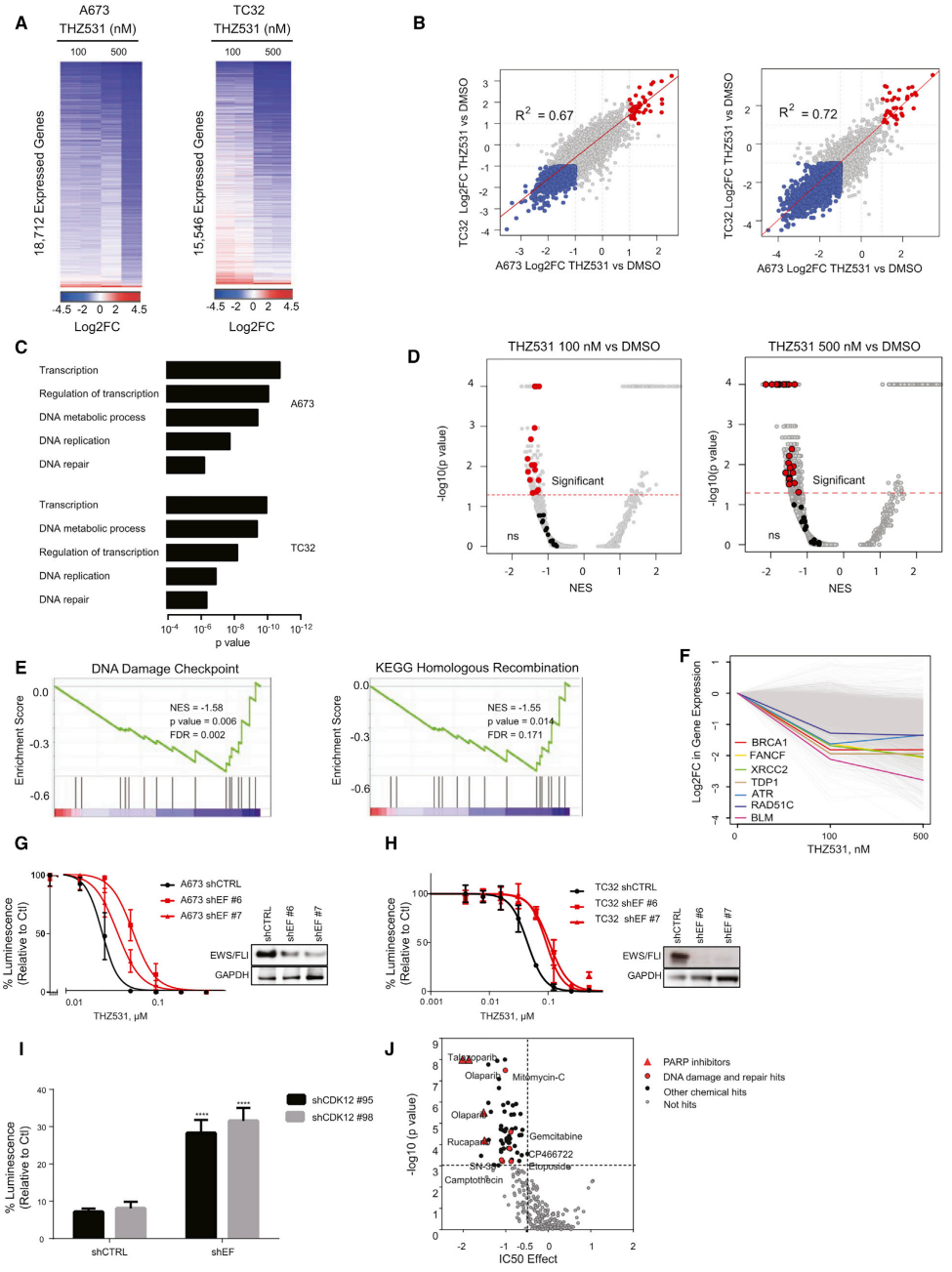

(legend on next page)

demonstrate that CDK12 inhibition underlies the enhanced sensitivity of Ewing sarcoma cells to THZ1, and, as such, we focused on the more selective compound, THZ531.

Cyclin K-CDK12 and cyclin K-CDK13 complexes were recently identified in human cells (Blazek et al., 2011). The cyclin K-CDK12 complex has been shown to regulate the phosphorylation of the CTD of RNA Pol II (Blazek et al., 2011). Consistent with the effects of THZ1, THZ531 reduced the phosphorylation of the RNA Pol II CTD at Ser2 and Ser5, but, in contrast, did not strongly reduce the phosphorylation at Ser7 (Figure S2D). In addition, THZ531 increased PARP cleavage and Annexin V^+ cell populations and decreased anchorage-independent growth in soft agar in Ewing sarcoma cells (Figures S2E–S2G).

THZ531 Treatment Preferentially Represses the Expression of DNA Repair-Related Genes in Ewing Sarcoma Cells

We next performed global gene expression profiling to investigate the effects of THZ531 on transcriptional programs in Ewing sarcoma. We profiled two highly sensitive EWS/FLI rearranged Ewing sarcoma cell lines, A673 and TC32, for which we have deep genomic characterization (Crompton et al., 2014). Samples were treated in duplicate with DMSO or THZ531 at 100 or 500 nM for 6 hr. THZ531 treatment globally downregulated steady-state mRNA levels in a concentration-dependent manner (Figure 3A). We observed profound gene expression suppression at 500 nM in both cell lines, with 22% and 27% of genes downregulated >2-linear-fold in A673 and TC32 cells, respectively (4,159 out of 18,712 genes in A673 cells and 4,207 out of 15,546 genes in TC32 cells) (Figure 3A). More modest effects on gene expression were observed at the 100 nM concentration with 10% and 6.7% of genes downregulated >2-fold in A673 and TC32 cells, respectively (1,876 out of 18,712 genes in A673 cells and 1,142 out of 15,546 genes in TC32 cells) (Figure 3A). Remarkably few genes were upregulated by THZ531 at either 100 or 500 nM, consistent with the known role of CDK12/13 in transcriptional initiation and elongation. The numbers of differentially expressed genes observed with THZ531 treatment is consistent with the differential expression observed with genetic depletion of *CDK12* (Liang et al., 2015). Gene expression changes between A673 and TC32 cells were strongly correlated at both 100 nM (R^2 = 0.67) and 500 nM (R^2 = 0.72) of THZ531 (Figure 3B). Venn diagrams demonstrate the significant overlap of down- and upregulated genes between the two cell lines (Figures S3A and S3B), indicating a common gene expression response to THZ531.

To elucidate candidate mechanisms of action of THZ531 in Ewing sarcoma, genes were ranked from most to least sensitive to 100 nM THZ531, and the top 5% of THZ531-sensitive genes (944 genes for A673 and 788 genes for TC32) were subjected to gene ontology enrichment using Database for Annotation, Visualization and Integrated Discovery functional annotation software analysis (Figure 3C). As expected, gene sets related to regulation of transcription and replication were enriched among THZ531-responsive genes. In addition, genes involved in DNA damage repair were identified as being preferentially downregulated by THZ531. We then performed gene set enrichment analysis for enrichment in the 5,499 gene sets from the MSigDB v5 collections, c2 (curated pathways and experimental gene sets) and c5 (gene ontology), as well as published EWS/FLI genes sets (Figure 3D) (Marques Howarth et al., 2014; Tomazou et al., 2015). Several DNA damage response (DDR) gene sets fell above the threshold of statistical significance and had negative normalized enrichment scores (Figure 3D), indicating that these gene sets were significantly downregulated by THZ531 treatment in both A673 and TC32 cells. DNA damage checkpoint and homologous recombination (HR) gene sets were among the most depleted by THZ531 treatment (Figure 3E). Furthermore, there was a noticeable lack of significant downregulation of EWS/FLI gene sets by THZ531 treatment in both Ewing sarcoma cell lines (Figure 3D). Lists of all DDR and EWS/FLI gene

Figure 3. THZ531 Treatment Globally Downregulates mRNA Levels with Enrichment for Suppression of DNA Damage/Repair-Related Genes

(A) A673 and TC32 cells were treated with THZ531 for 6 hr in duplicate. Heatmaps display the log2 fold change (Log2FC) in gene expression for THZ531 versus DMSO treatment.

(B) Log2FCs in gene expression in A673 cells (x axis) or TC32 cells (y axis) treated with 100 nM THZ531 versus DMSO (left) or 500 nM THZ531 versus DMSO (right). Genes are represented as dots. Dots corresponding to genes significantly downregulated by THZ531 in both A673 and TC32 lines are highlighted blue. Dots corresponding to genes significantly upregulated by THZ531 in both A673 and TC32 cells are highlighted red. The Log2FCs in gene expression in A673 cells versus TC32 cells are positively correlated with 100 nM THZ531 (R^2 = 0.67) and 500 nM THZ531 (R^2 = 0.72).

(C) Gene ontology analysis of the top 5% of sensitive genes to 100 nM THZ531 treatment.

(D) Volcano plot depicting gene set enrichment analysis (GSEA) for enrichment from the MSigDB v5 collections, c2, and c5, as well as published EWS/FLI genes sets, in the genes significantly downregulated by 100 nM THZ531 in both A673 and TC32 cells. DNA damage response (DDR) gene sets are highlighted in red and EWS/FLI1 gene sets are highlighted in black. Gene sets that fall above the red line are statistically significant. Positive normalized enrichment scores (NESs) indicate upregulation of genes sets, whereas negative NESs indicate downregulation of gene sets. ns, not significant.

(E) Individual GSEA plots for enrichment of the indicated gene sets among THZ531 downregulated genes.

(F) Graph showing the Log2FC in gene expression after 100 and 500 nM THZ531 treatment with select DDR genes highlighted.

(G and H) Dose-response curves of A673 shCTRL and shEWS/FLI (G) and TC32 shCTRL and shEWS/FLI cells (H) generated with two distinct hairpins treated with THZ531 for 72 hr. Data are plotted as the percentage of luminescence relative to DMSO controls. Experiments were conducted in biological triplicate. Results are presented as mean values of a representative experiment ± SD of eight technical replicates. Western blots demonstrating EWS/FLI knockdown are shown to the right of the dose-response curves.

(I) Relative viability of A673 shCTRL and shEWS/FLI cells infected with hairpins against CDK12 7 days post-infection. Data are plotted as the percentage of luminescence relative to shCTRL cells. The experiment was conducted in biological triplicate. Results are presented as mean values of a representative experiment ± SD of eight technical replicates. Statistical significance is calculated for the viability effect of each CDK12 hairpin in the context of shEWS/FLI compared with shCTRL. ****$p < 0.0001$, t test.

(J) EWS/FLI biomarker data from the Genomics of Drug Sensitivity in Cancer (http://cancerrxgene.org, release 21-41-36, June 2, 2017). Enrichment of drugs targeting DDR Pathways among drugs in which EWS/FLI is a biomarker of sensitivity was calculated by Two-tailed Fisher's exact test: odds ratios = 3.81, $p = 0.0078$. Significant hits cutoffs: IC_{50} effect < −0.5, $p < 0.001$. PARP inhibitors are shown as red triangles, additional DNA damage and repair drugs as red circles, and other chemical hits as black circles. Olaparib was screened at 5 and 10 nM. See also Figure S3 and Tables S3, S4, and S5.

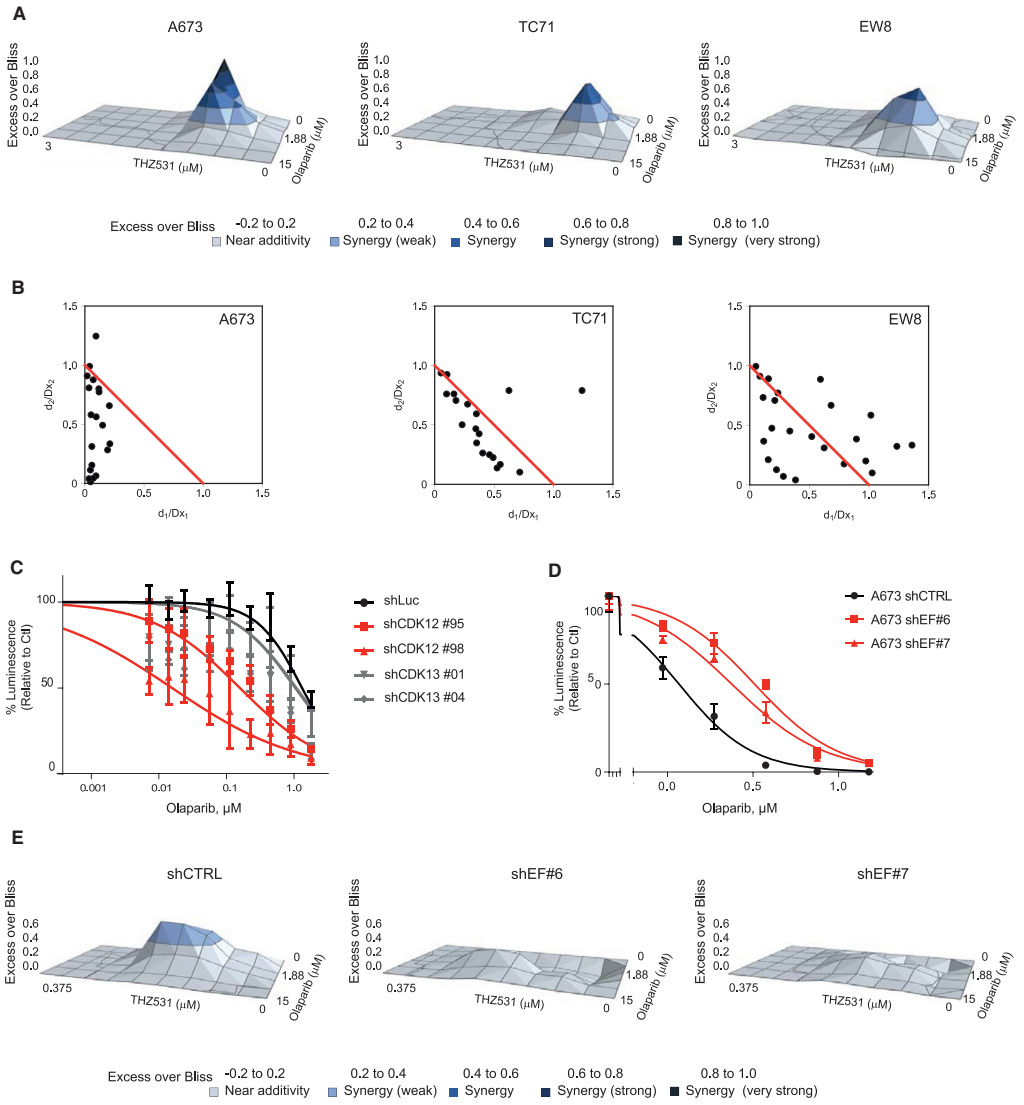

Figure 4. THZ531 Synergy with Olaparib Is EWS/FLI Dependent

(A) Excess over Bliss synergy plots for serial dilutions of THZ531 in combination with olaparib in A673, TC71, and EW8 cells. Excess over Bliss scores >0 indicate drug synergy, whereas negative scores indicate antagonism.

(B) Chou-Talalay normalized isobolograms of data presented in (A). Plots depict combination index scores over a range of concentrations of THZ531 and olaparib. The coordinates of the CI scores are d_1/D_{x1} and d_2/D_{x2}, where D_{x1} is the concentration of drug 1 (THZ531) that alone produces the fractional inhibition effect x, and D_{x2} is the concentration of drug 2 (olaparib) that alone produces the fractional inhibition effect x. CI < 1 = synergism, CI > 1 = antagonism. The red line displayed is the line of additivity.

(C) Dose-response curves of A673 cells infected with hairpins against luciferase, CDK12, or CDK13, and treated with olaparib for 5 days. Data are plotted as the percentage of luminescence relative to shLuc control. The experiment was conducted in biological duplicate. Results are presented as mean values of a representative experiment ± SD of eight technical replicates.

(legend continued on next page)

sets are included in Tables S3 and S4, and of all genes affected by THZ531 treatment in Table S5.

Several key genes regulating DDR were downregulated by THZ531 in A673 and TC32 cells (Figure 3F). We performed a leading-edge analysis to identify the genes that form the consensus among the DNA damage and repair gene signatures. We found that 33 genes belong to at least 4 of the enriched DNA damage and repair MSigDB gene sets, including several genes regulating HR and UV response (Figure S3C). Low-throughput validation of select genes (*BRCA1*, *RAD51*, *FANCF*, and *XRCC2*) by qPCR confirmed that THZ531 strongly suppresses expression of these genes (Figure S3D).

As THZ1 has been reported to preferentially repress the expression of super-enhancer (SE)-marked genes, we analyzed the effect of THZ531 on SE-marked gene expression (Chipumuro et al., 2014; Christensen et al., 2014; Kwiatkowski et al., 2014). Boxplots show the Log2FC in gene expression of all genes, typical enhancer-associated genes, SE genes, and EWS/FLI target genes following THZ531 treatment (Figure S3E). In this analysis, enhancers were ranked by H3K27Ac chromatin immunoprecipitation sequencing (ChIP-seq) signal, and EWS/FLI target genes were identified as (1) genes associated with EWS/FLI ChIP-seq signal and (2) genes with a decrease in transcript expression following EWS/FLI knockdown in A673 cells as described in (Riggi et al., 2014). Interestingly, we found that SE-associated genes and EWS/FLI target genes were not preferentially repressed by THZ531 compared with all genes. These data suggest that CDK12 and CDK13 do not preferentially regulate SE-marked or EWS/FLI target genes in Ewing sarcoma.

EWS/FLI Expression Imparts Sensitivity to CDK12 Inhibition and to Molecules Inducing DNA Damage

In light of the exceptional sensitivity of Ewing sarcoma cells to THZ531, we hypothesized that EWS/FLI may render cells more vulnerable to THZ531 and other DNA damage repair inhibitors. Indeed, DNA-damaging agents are currently used to treat patients with Ewing sarcoma, and Ewing sarcoma cell lines have been reported to be highly sensitive to PARP inhibitors (Gill et al., 2015). To test this hypothesis, we knocked down EWS/FLI using a TRIPZ-inducible system. We found that EWS/FLI suppression using two unique hairpins rendered TC32 and A673 cells less sensitive to THZ531 (Figures 3G and 3H). Furthermore, suppression of EWS/FLI can partially rescue the anti-viability effects of CDK12 knockdown (Figure 3I). To rule out the possibility that EWS/FLI knockdown renders resistance to THZ531 due to induction of cell-cycle arrest, we serum starved A673 and TC32 Ewing sarcoma cells to induce growth arrest (Figures S3F and S3G) and assayed sensitivity of these cells to THZ531. Importantly, unlike cells with EWS/FLI suppression, serum-starved cells do not display differential sensitivity to THZ531 (Figures S3H and S3I). Thus, the proliferative disadvantage of losing EWS/FLI is not responsible for the increased resistance to THZ531 as inducing growth arrest with serum starvation does not engender resistance to these molecules. These results suggest that the EWS/FLI oncoprotein imparts vulnerability to compounds that induce defects in DNA damage repair, and suggest that the presence of EWS/FLI itself is synthetic lethal with CDK12 inhibition in Ewing sarcoma cells.

We next mined the Genomics of Drug Sensitivity in Cancer database, a screen of 1,074 cancer cell lines treated with 265 anti-cancer drugs, to identify additional small molecules for which EWS/FLI is a biomarker of response (Yang et al., 2013). There was significant enrichment for drugs inducing DNA damage among the compounds in which EWS/FLI rearrangement was a biomarker of sensitivity (Figure 3J). Among these compounds were mitomycin C, etoposide, SN-38, camptothecin, and gemcitabine, all of which are chemotherapeutic agents that induce DNA damage. EWS/FLI was also a biomarker of sensitivity to the ATM inhibitor, CP466722, an interesting finding in light of a recent publication identifying ATR inhibitors as active in Ewing sarcoma (Nieto-Soler et al., 2016). In addition, as previously reported, EWS/FLI was a biomarker of sensitivity to three different PARP inhibitors (Figure 3J) (Garnett et al., 2012).

THZ531 Is Synergistic with PARP Inhibitors in Ewing Sarcoma

While THZ1 was active in a mouse model of Ewing sarcoma, treatment with THZ1 as a single agent did not cure mice of disease, suggesting that combination therapy will be necessary to achieve full efficacy. Therefore, we sought to identify clinically tractable synergistic combinations with THZ1 in Ewing sarcoma models. Ovarian tumors with loss-of-function mutations in *CDK12* have reduced BRCA1 levels, deficient HR, and are highly sensitive to PARP inhibition (Joshi et al., 2014). Moreover, it was recently reported that pan-CDK inhibition with dinaciclib can reverse PARP inhibitor resistance in BRCA-mutated triple-negative breast cancer (Johnson et al., 2016). In Ewing sarcoma, studies have demonstrated that EWS/FLI physically interacts with PARP1 and induces PARP1 expression (Brenner et al., 2012; Garnett et al., 2012; Stewart et al., 2014; Yang et al., 2013). These previous studies, in addition to our gene expression data identifying that THZ531 preferentially downregulates HR repair genes in Ewing sarcoma, led us to hypothesize that THZ531 would synergize with PARP inhibitors. We used the Bliss independence and Loewe additivity models to assess synergy. The Bliss independence model computes a quantitative measure, excess over Bliss, the difference between the observed combined effect and the expected combined effect of the two drugs (Bliss, 1956; Greco et al., 1995), while the Chou-Talalay combination index for the Loewe additivity model is a dose-effect approach that estimates the effect of combining two drugs based on the dose of each individual drug that produces the same quantitative effect (Chou, 2006; Chou and Talalay, 1984). We observed strong synergy between THZ531 and olaparib in several Ewing sarcoma cell lines, using both models across a wide range of concentrations (Figures 4A and 4B). Moreover,

(D) Dose-response curves of A673 shCTRL and shEWS/FLI cells treated with olaparib for 5 days. Data are plotted as the percentage of luminescence relative to DMSO controls. The experiment was conducted in biological triplicate. Results are presented as mean values of a representative experiment ± SD of eight technical replicates.

(E) THZ531 and olaparib excess over Bliss synergy plots in A673 shCTRL and shEWS/FLI cells. The experiment was conducted in biological triplicate. See also Figure S4.

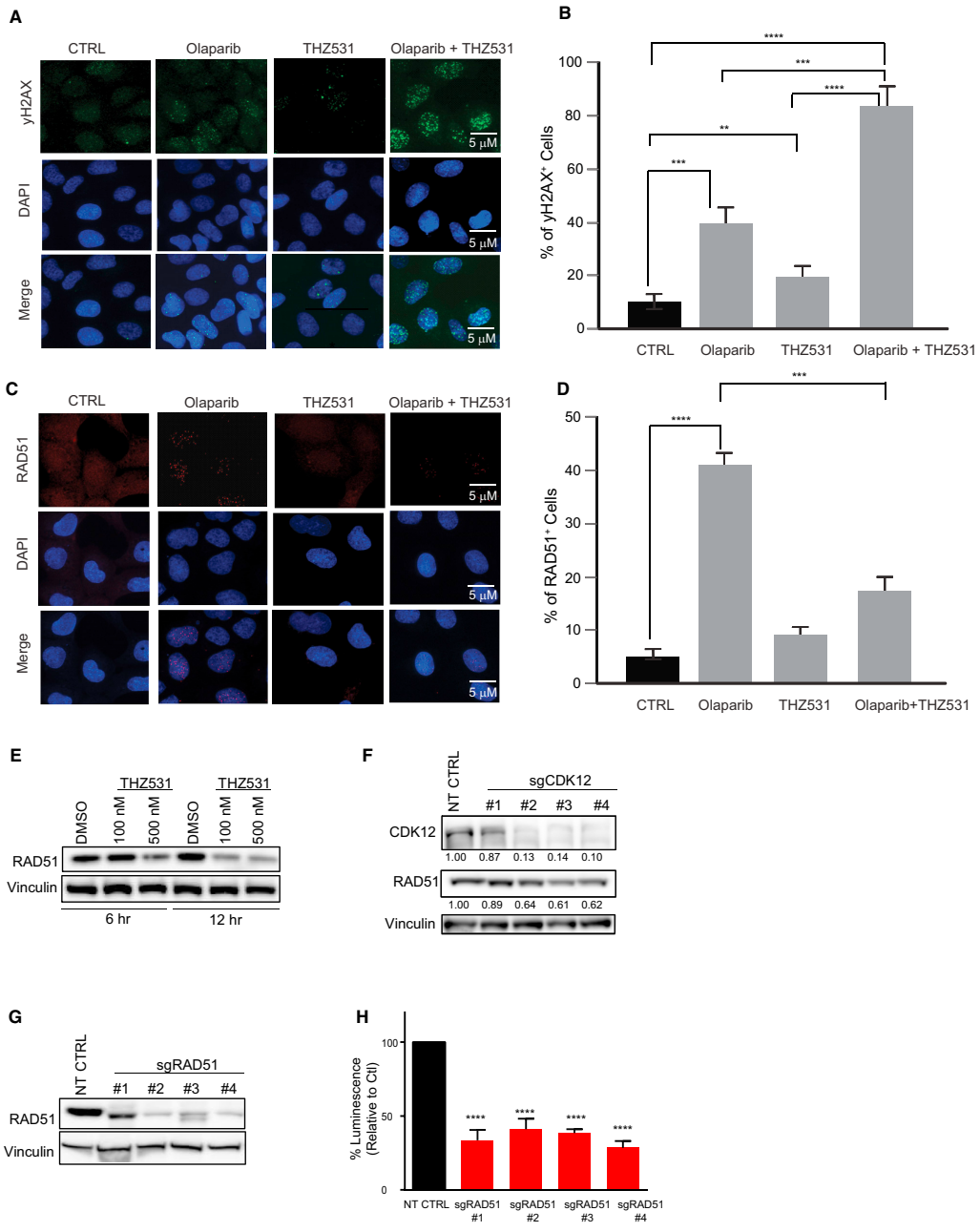

(legend on next page)

we observed that THZ531 strongly synergizes with cisplatin, mitomycin C, the ATR inhibitor VE821, and the ATM inhibitor KU5593, in Ewing sarcoma cells (Figures S4A–S4D). Importantly, THZ531 does not synergize with vincristine, a microtubule inhibitor not classified as a DNA-damaging agent (Figure S4E). These data provide further support that THZ531 mechanistically works through inhibiting DNA damage repair. Taken together, these findings suggest that Ewing sarcoma is a disease marked by DNA damage repair deficiency, rendering tumor cells highly sensitive to these combination strategies.

To confirm the on-target activity of THZ531 in this combination effect, we knocked down CDK12 and CDK13, treated these cells with olaparib, and assayed for cell viability. We found that genetic suppression of CDK12, but not CDK13, sensitizes cells to olaparib (Figure 4C). These data support that inhibition of CDK12 is responsible for the defects in DNA damage repair induced by THZ531. Furthermore, we demonstrated that suppression of EWS/FLI using two different hairpins renders cells more resistant to olaparib (Figure 4D), and when EWS/FLI is suppressed, synergy between THZ531 and olaparib is abrogated, consistent with the notion that EWS/FLI imparts vulnerability to defects in DNA repair (Figure 4E).

To further investigate the effects of these compounds on DNA damage and repair, we performed immunofluorescent analysis of γH2AX, an early sensor of DNA double-strand breaks. THZ531 and olaparib alone induced γH2AX foci staining in Ewing sarcoma cells (Figures 5A and 5B), and the combination synergistically induced γH2AX foci formation, suggesting that this combination impairs the ability of Ewing sarcoma cells to repair DNA damage. To evaluate the effects on HR repair, we assayed RAD51 foci staining, a key regulator of HR-mediated repair. We observed a striking increase in RAD51 foci staining in Ewing sarcoma cells treated with olaparib (Figures 5C and 5D). Interestingly, THZ531 prevented the induction of RAD51 foci formation in olaparib-treated Ewing sarcoma cells, suggesting that THZ531 is impairing HR and the ability of RAD51 to be recruited to sites of DNA damage. We found that both THZ531 treatment and knockout of *CDK12* led to a decrease in total RAD51 protein levels (Figures 5E and 5F). Furthermore, we observed a decrease in cell viability when *RAD51* was knocked out by CRISPR-Cas9 (Figures 5G and 5H).

The Combination of CDK7/12/13 and PARP Inhibitors Is Highly Active in Ewing Sarcoma

We next assayed the *in vivo* efficacy of combining a CDK12 inhibitor and olaparib in a mouse model of Ewing sarcoma. Because THZ531 is not optimized for *in vivo* studies, we used the parental compound, THZ1. We first confirmed synergy between the parental molecule and olaparib *in vitro* (Figure S5A). We then established an A673 xenograft mouse model of Ewing sarcoma and performed a 4-arm study with twice-daily treatment of vehicle, 10 mg/kg THZ1, 50 mg/kg olaparib, and the combination of olaparib + THZ1 delivered for 40 days. Olaparib and THZ1 as single agents each significantly decreased tumor growth rate and extended the survival of the mice (median survival: 18 days in vehicle, 32 days in THZ1, and 28 days in the olaparib groups) (Figures 6A and 6B). A striking decreased tumor growth rate was observed when both drugs were used in combination (Figure 6A), and the combination treatment significantly extended survival compared with the vehicle control or either single agent (Figure 6B). Seventy percent of mice in the combination arm were still alive by day 40 when treatment was ended (Figure 6B). Mice were followed out to day 150 without further treatment. At day 60, 40% (4 out of 10) of the mice in the combination group were still alive, whereas all of the mice in the vehicle and single agent arms had been sacrificed. Furthermore, 20% of tumors in the combination arm had regressed to where they were no longer palpable (Figure 6B). To test the generalizability of this treatment strategy in Ewing sarcoma, we performed combination *in vivo* studies in a second xenograft mouse model using TC71 cells, as well as in a patient-derived xenograft (PDX) mouse model of this disease. In the TC71 xenograft study, both THZ1 and olaparib significantly reduced the tumor growth rate and extended survival as single agents (Figures 6C and 6D), and the combination of THZ1 and olaparib significantly reduced tumor growth rate compared with either agent used alone (Figure 6C). The median survival of mice in the vehicle treated group was 30.5 days, compared with 42 days in the olaparib group, 38.5 days in the THZ1 group, and 66.5 days in the combination group (Figure 6D). Furthermore, we established a PDX mouse model of Ewing sarcoma with a type I EWS/FLI fusion from a tumor resected from the fibula of a 12-year-old patient at diagnosis (HSJD-ES-002). In this model, THZ1 as a single agent did not significantly reduce the tumor progression (Figure 6E), but did significantly increase overall survival (Figure 6F). Importantly, the combination of THZ1 and olaparib strikingly reduced tumor progression and increased median survival in this PDX (Figures 6E and 6F): vehicle, 23 days; olaparib, 42 days; THZ1, 44 days; and combination, 56 days. Taken together, this drug combination resulted in a more profound and durable response than treatment with either drug alone.

Complete blood counts of all mice treated with THZ1 and olaparib and the combination of these two drugs in the TC71 xenograft mouse model of Ewing sarcoma were performed

Figure 5. THZ531 and Olaparib Synergistically Induce DNA Damage in Ewing Sarcoma Cells

(A–D) γH2AX foci staining (A) and quantification (B), and Rad51 foci staining (C) and quantification (D) in A673 cells treated with olaparib (2 μM) or THZ531 (25 nM) alone and in combination for 72 hr. Nuclei are stained with DAPI. Scale bars represent 5 μM. One hundred cells per sample were counted and results are presented as mean values ± SD (t test). A cell was counted as positive if >10 foci per nucleus were identified.

(E) Immunoblot of A673 cell lysates treated with DMSO or THZ531 and probed for RAD51 expression. Vinculin, loading control.

(F) Immunoblot of A673 cells infected with an NT CTRL or guide RNAs targeting *CDK12* and probed for CDK12 and RAD51. Vinculin, loading control. Densitometric quantification is shown below the blots for CDK12 and RAD51. Values are normalized to the vinculin expression for each condition and then to the expression in the NT CTRL.

(G) Immunoblot of A673 cells infected with an NT CTRL or guide RNAs targeting *RAD51* 7 days post-infection. Vinculin, loading control.

(H) Viability of cells infected with sgRNAs against *RAD51* 14 days post-infection. Data are plotted as the percentage of luminescence relative to NT CTRL. The experiment was conducted in biological triplicate. Results are presented as mean values of a representative experiment ± SD of eight technical replicates (t test). $^{**}p < 0.01$, $^{***}p < 0.001$, $^{****}p < 0.0001$.

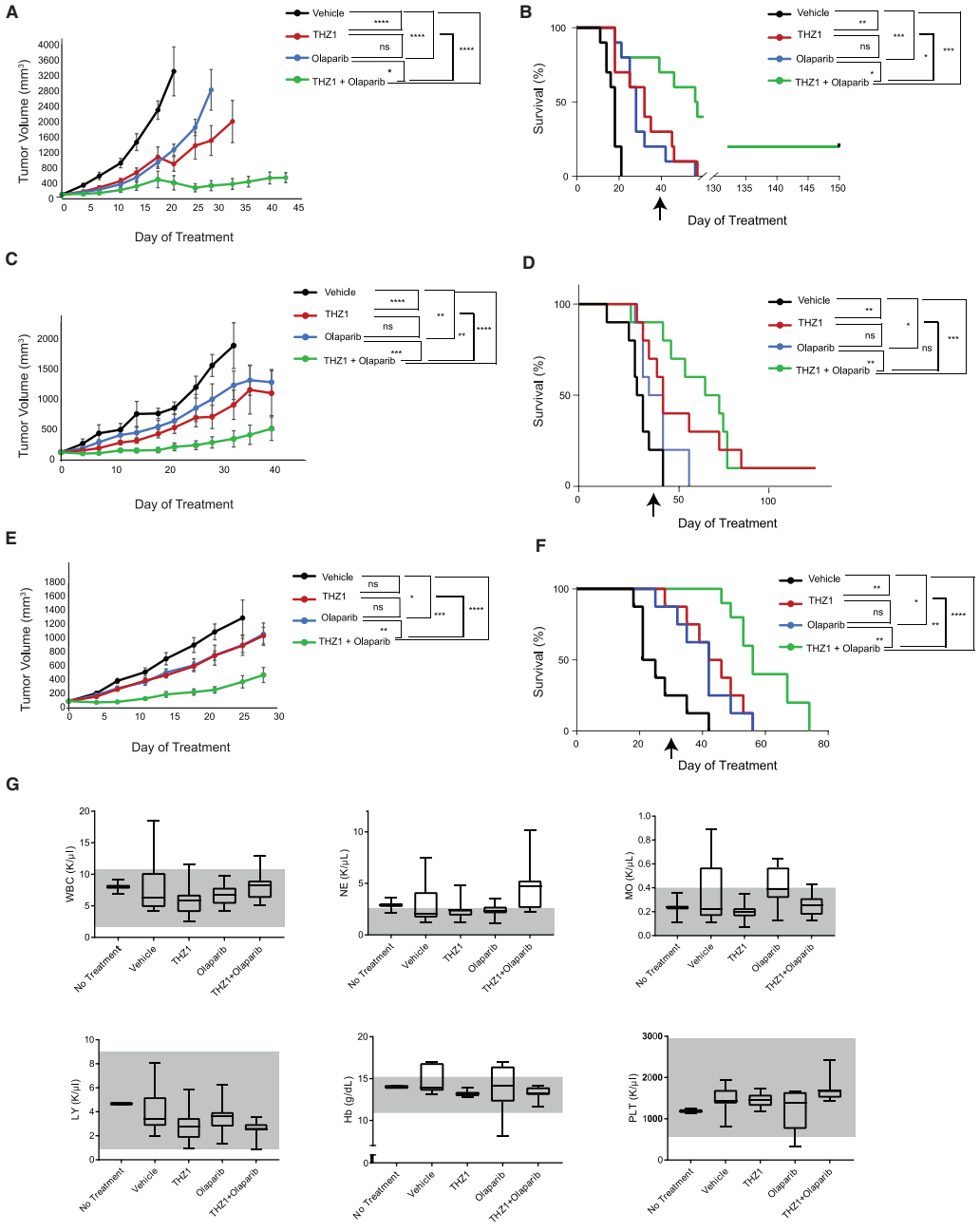

(legend on next page)

(Figure 6G). Importantly, we did not observe any hematopoietic toxicities after up to 40 days of treatment. Significant weight loss was also not observed in any of the three mouse models tested over long-term treatment (Figures S5B–S5D).

DISCUSSION

Pediatric, and even a subset of adult, cancers possess remarkably quiet genomes, which are defined by sentinel genetic lesions (Lawrence et al., 2013). In principle, targeting these key lesions should make for a propitious therapeutic strategy; however, because most of the driver events involve transcription factors or loss of tumor suppressors, only a minority have been successfully pharmacologically addressed. For example, chromosomal translocations that result in EWS/ETS rearrangements characterizing Ewing sarcoma tumors have yet to be successfully targeted. EWS/FLI is a master transcription factor that activates an oncogenic transcriptional program. Unfortunately, targeting this transcription factor fusion protein has been a drug discovery challenge. Here, we demonstrate that synthetic lethal dependencies can be identified in the context of sentinel genetic lesions using chemical genomics. We determined that EWS/FLI incurs a synthetic lethal relationship with molecules that are involved in DNA damage/repair. Such a strategy could be applied broadly to other cancers with exceptionally simple genomic landscapes.

DNA-damaging agents, such as doxorubicin and etoposide, form the backbone of Ewing sarcoma therapy. Moreover, Ewing sarcoma is highly radiation responsive, suggesting that Ewing sarcoma is particularly sensitive to DNA damage. Intriguingly, three independent studies reported that Ewing sarcoma is sensitive to PARP inhibitors (Brenner et al., 2012; Garnett et al., 2012; Stewart et al., 2014; Yang et al., 2013). In one study, PARP1 was found to physically interact with EWS/FLI and act as a transcriptional co-regulator of the oncogenic transcription factor fusion protein (Brenner et al., 2012). Furthermore, EWS/FLI was found to induce PARP1 expression in a positive feedforward loop (Brenner et al., 2012). In a second study, a chemical genomics screen across 639 cancer cell lines was conducted to identify new genotype:chemosensitivity relationships in cancer (Garnett et al., 2012; Yang et al., 2013). The connection between EWS/ETS rearranged Ewing sarcoma and response to PARP inhibitors was highlighted. Suppressing EWS/FLI in Ewing sarcoma cells was reported to render resistance to PARP inhibition, a finding which we recapitulate in the current study (Garnett et al., 2012). In our own study of the exquisite sensitivity to the CDK7/12/13 inhibitor THZ1, we found that CDK12 was an essential target for their selective sensitivity, and mechanistically, suppression of RAD51 expression impaired the growth of EWS/FLI-expressing Ewing sarcoma cells. Our data are consistent with prior studies demonstrating that CDK12 regulates the expression of DNA damage repair genes, most notably, *BRCA1*, *ATR*, *FANCI*, and *FANCD2* (Blazek et al., 2011). Furthermore, CDK12 was shown to bind to these HR-related genes, and was necessary for the phosphorylation of the CTD of RNA Pol II at Ser2 at these genes (Ekumi et al., 2015).

While additional studies will be necessary to dissect the precise mechanisms by which EWS/FLI sensitizes Ewing sarcoma cells to compounds that induce DNA damage and/or prevent its repair, the results of these studies are readily translatable. Clinical trials testing PARP inhibitors in patients with BRCA-deficient tumors have demonstrated anti-tumor efficacy and provide an example of successfully exploiting synthetic lethal relationships for therapeutic benefit (Kaelin, 2005; Sonnenblick et al., 2015). The promising activity of PARP inhibitors in trials for HR-deficient tumors, and the convergence of multiple groups demonstrating PARP inhibitor activity in Ewing sarcoma, prompted much interest in their clinical testing in this disease, one for which there are no approved targeted therapeutics, and for which cure rates remain quite poor for patients with metastatic or relapsed disease. Despite promising preclinical data demonstrating sensitivity of Ewing sarcoma cells to PARP inhibitors (Norris et al., 2014; Vormoor and Curtin, 2014), a phase II clinical trial testing olaparib in patients with relapsed/refractory Ewing sarcoma failed to demonstrate antitumor efficacy (Choy et al., 2014). These disappointing results highlighted the need to identify agents to use in combination with PARP inhibitors to improve their efficacy.

In the current study, we hypothesized that a CDK12 inhibitor would synergize with a PARP inhibitor because *CDK12*

Figure 6. THZ1 and Olaparib Are Strongly Synergistic in Several Mouse Models of Ewing Sarcoma

(A) Tumor volume measurements of an A673 xenograft mouse model treated with vehicle, 10 mg/kg THZ1 IP BID, 50 mg/kg olaparib PO BID, or the combination of olaparib + THZ1. Treatment was stopped on day 40. Data for a given time point were plotted if >50% of mice in the group were alive. Data are plotted as mean values ± SD (n = 10 per arm).

(B) Kaplan-Meier survival curves for the experiment described in (A). Arrow indicates treatment end date.

(C) Tumor volume measurements of a TC71 xenograft mouse model treated with vehicle, 10 mg/kg THZ1 IP BID, 50 mg/kg olaparib PO BID, or the combination of olaparib + THZ1. Treatment was stopped on day 40. Data for a given time point were plotted if >50% of mice in the group were alive. Data are plotted as mean values ± SD (n = 10 per arm).

(D) Kaplan-Meier survival curves for the experiment described in (C). Arrow indicates treatment end date.

(E) Tumor volume measurements of a PDX mouse model of Ewing sarcoma treated with vehicle, 10 mg/kg THZ1 IP BID, 50 mg/kg olaparib PO BID, or the combination of olaparib + THZ1. Treatment was stopped on day 28. Data for a given time point were plotted if >50% of mice in the group were alive. Data are plotted as mean values ± SD (n = 8 per arm).

(F) Kaplan-Meier survival curves for the experiment described in (E). Arrow indicates treatment end date. ns, not significant, *p < 0.05, **p < 0.01, ***p < 0.001, ****p < 0.0001. Two-way ANOVA with Tukey *post hoc* test was performed for tumor volume graphs and log rank Mantel-Cox test was performed for survival curves.

(G) Complete blood count analysis of TC71 xenografted mice treated as in (C) at time of sacrifice. Mice were sacrificed when tumors reached 2 cm in length, and, in some cases, mice were off treatment at time of sacrifice. Two mice that were never on treatment were included as additional controls. The gray areas mark the normal range for each blood cell count and are measured in thousands per cubic milliliter (K/μL) of blood. WBC, white blood cells; NE, neutrophils; MO, monocytes; LY, lymphocytes; Hb, hemoglobin; PLT, platelets.

Data are presented as mean values with whiskers representing min and max values and the outer edges of the boxes representing the 25th percentile (lower quartile) and 75th percentile (upper quartile). ns, not significant, *p < 0.05, **p < 0.01, ***p < 0.001, ****p < 0.0001. See also Figure S5.

loss-of-function mutations in ovarian cancer have rendered sensitivity to PARP inhibitors (Bajrami et al., 2014; Joshi et al., 2014). Indeed, THZ531/THZ1 and olaparib were highly synergistic *in vitro*, and THZ1 and olaparib were highly active in combination *in vivo* with a subset of the mice remarkably "cured" of disease without bone marrow toxicity. It is important to note that some of the anti-proliferative effects of THZ1 *in vivo* may not be due solely to CDK12 inhibition, as the molecule also targets CDK7 and CDK13, and the optimization of CDK12 selective inhibitors for *in vivo* studies is still needed. However, the strong synergy observed between THZ1 and olaparib is likely mediated by THZ1's inhibitory effects on CDK12, which our data suggest impairs HR repair. With this class of compounds in early-phase clinical trials, this study has translational potential for patients with Ewing sarcoma, and provides the preclinical validation for second-generation clinical trials. Moreover, this combination is predicted to be broadly applicable for cancers with *BRCA1/2* mutations, which are highly sensitive to PARP inhibitors.

STAR★METHODS

Detailed methods are provided in the online version of this paper and include the following:

- KEY RESOURCES TABLE
- CONTACT FOR REAGENT AND RESOURCE SHARING
- EXPERIMENTAL MODEL AND SUBJECT DETAILS
  - Cell Lines
  - In Vivo Tumor Models
- METHOD DETAILS
  - Western Blotting
  - Quantitative PCR
  - Compounds
  - THZ1-biotin Immunoprecipitation
  - Genome-Scale CRISPR-Cas9 Screening
  - RNA Extractions and Synthetic RNA Spike-in
  - Gene Expression Profiling
  - Gene Set Enrichment Analysis
  - Comparative Marker Analysis
  - Super-Enhancer Analysis
  - Immunofluorescence
  - Colony Formation Assays
  - Annexin V/PI Staining
  - shRNA and CRISPR Studies
  - Cell Viability and Synergy Studies
  - Chou-Talalay Combination Index for Loewe Additivity
  - The Bliss Independence Method
- QUANTIFICATION AND STATISTICAL ANALYSES
- DATA AND SOFTWARE AVAILABILITY

SUPPLEMENTAL INFORMATION

Supplemental Information includes five figures and six tables and can be found with this article online at https://doi.org/10.1016/j.ccell.2017.12.009.

ACKNOWLEDGMENTS

This work was supported by the Brian MacIsaac Sarcoma Foundation (K.S.), the Ty Louis Campbell Foundation (K.S.), the National Cancer Institute (1R35 CA210030) (K.S.), the St. Baldrick's Foundation (Robert J. Arceci Innovation Award) (K.S.), the NIH (HG002668) (R.A.Y.), and the Koch Institute and Dana–Farber/Harvard Cancer Center Bridge Grant (R.A.Y.). A.B.I. is a Damon Runyon Foundation Fellow (DRSG:12-15). N.S.G., T.Z., and N.K. are co-inventors on a patent that covers THZ531, which has been licensed to a company founded by N.S.G. and R.A.Y.

AUTHOR CONTRIBUTIONS

Conceptualization, A.B.I., K.S., N.S.G., R.A.Y., D.C., and C.H.B.; Formal Analysis, G.A., B.J.A., and N.V.D.; Investigation, A.B.I., B.S., E.J.W., A.S.C., A.L., P.K., and C.H.B.; Resources, N.K., T.Z., and J.M.; Writing – Original Draft, A.B.I. and K.S.; Writing – Review & Editing, A.B.I., K.S., N.K., and B.J.A.; Funding Acquisition, K.S. and R.A.Y.

Received: August 30, 2016
Revised: September 15, 2017
Accepted: December 19, 2017
Published: January 18, 2018

SUPPORTING CITATIONS

The following references appear in the Supplemental Information: Hong et al. (2016); Sanjana et al. (2014).

REFERENCES

Bajrami, I., Frankum, J.R., Konde, A., Miller, R.E., Rehman, F.L., Brough, R., Campbell, J., Sims, D., Rafiq, R., Hooper, S., et al. (2014). Genome-wide profiling of genetic synthetic lethality identifies CDK12 as a novel determinant of PARP1/2 inhibitor sensitivity. Cancer Res. *74*, 287–297.

Blazek, D., Kohoutek, J., Bartholomeeusen, K., Johansen, E., Hulinkova, P., Luo, Z., Cimermancic, P., Ule, J., and Peterlin, B.M. (2011). The cyclin K/Cdk12 complex maintains genomic stability via regulation of expression of DNA damage response genes. Genes Dev. *25*, 2158–2172.

Bliss, C.I. (1956). The calculation of microbial assays. Bacteriol. Rev. *20*, 243–258.

Brenner, J.C., Feng, F.Y., Han, S., Patel, S., Goyal, S.V., Bou-Maroun, L.M., Liu, M., Lonigro, R., Prensner, J.R., Tomlins, S.A., and Chinnaiyan, A.M. (2012). PARP-1 inhibition as a targeted strategy to treat Ewing's sarcoma. Cancer Res. *72*, 1608–1613.

Brohl, A.S., Solomon, D.A., Chang, W., Wang, J., Song, Y., Sindiri, S., Patidar, R., Hurd, L., Chen, L., Shern, J.F., et al. (2014). The genomic landscape of the Ewing sarcoma family of tumors reveals recurrent STAG2 mutation. PLoS Genet. *10*, e1004475.

Chipumuro, E., Marco, E., Christensen, C.L., Kwiatkowski, N., Zhang, T., Hatheway, C.M., Abraham, B.J., Sharma, B., Yeung, C., Altabef, A., et al. (2014). CDK7 inhibition suppresses super-enhancer-linked oncogenic transcription in MYCN-driven cancer. Cell *159*, 1126–1139.

Chou, T.C. (2006). Theoretical basis, experimental design, and computerized simulation of synergism and antagonism in drug combination studies. Pharmacol. Rev. *58*, 621–681.

Chou, T.C., and Talalay, P. (1984). Quantitative analysis of dose-effect relationships: the combined effects of multiple drugs or enzyme inhibitors. Adv. Enzyme Regul. *22*, 27–55.

Choy, E., Butrynski, J.E., Harmon, D.C., Morgan, J.A., George, S., Wagner, A.J., D'Adamo, D., Cote, G.M., Flamand, Y., Benes, C.H., et al. (2014). Phase II study of olaparib in patients with refractory Ewing sarcoma following failure of standard chemotherapy. BMC Cancer *14*, 813.

Christensen, C.L., Kwiatkowski, N., Abraham, B.J., Carretero, J., Al-Shahrour, F., Zhang, T., Chipumuro, E., Herter-Sprie, G.S., Akbay, E.A., Altabef, A., et al. (2014). Targeting transcriptional addictions in small cell lung cancer with a covalent CDK7 inhibitor. Cancer Cell *26*, 909–922.

Crompton, B.D., Stewart, C., Taylor-Weiner, A., Alexe, G., Kurek, K.C., Calicchio, M.L., Kiezun, A., Carter, S.L., Shukla, S.A., Mehta, S.S., et al. (2014). The genomic landscape of pediatric Ewing sarcoma. Cancer Discov. *4*, 1326–1341.

Ekumi, K.M., Paculova, H., Lenasi, T., Pospichalova, V., Bosken, C.A., Rybarikova, J., Bryja, V., Geyer, M., Blazek, D., and Barboric, M. (2015). Ovarian carcinoma CDK12 mutations misregulate expression of DNA repair genes via deficient formation and function of the Cdk12/CycK complex. Nucleic Acids Res. *43*, 2575–2589.

Garnett, M.J., Edelman, E.J., Heidorn, S.J., Greenman, C.D., Dastur, A., Lau, K.W., Greninger, P., Thompson, I.R., Luo, X., Soares, J., et al. (2012). Systematic identification of genomic markers of drug sensitivity in cancer cells. Nature *483*, 570–575.

Gill, S.J., Travers, J., Pshenichnaya, I., Kogera, F.A., Barthorpe, S., Mironenko, T., Richardson, L., Benes, C.H., Stratton, M.R., McDermott, U., et al. (2015). Combinations of PARP inhibitors with temozolomide drive PARP1 trapping and apoptosis in Ewing's sarcoma. PLoS One *10*, e0140988.

Greco, W.R., Bravo, G., and Parsons, J.C. (1995). The search for synergy: a critical review from a response surface perspective. Pharmacol. Rev. *47*, 331–385.

Hong, A.L., Tseng, Y.Y., Cowley, G.S., Jonas, O., Cheah, J.H., Kynnap, B.D., Doshi, M.B., Oh, C., Meyer, S.C., Church, A.J., et al. (2016). Integrated genetic and pharmacologic interrogation of rare cancers. Nat. Commun. *7*, 11987.

Hu-Lieskovan, S., Heidel, J.D., Bartlett, D.W., Davis, M.E., and Triche, T.J. (2005). Sequence-specific knockdown of EWS-FLI1 by targeted, nonviral delivery of small interfering RNA inhibits tumor growth in a murine model of metastatic Ewing's sarcoma. Cancer Res. *65*, 8984–8992.

Johnson, S.F., Cruz, C., Greifenberg, A.K., Dust, S., Stover, D.G., Chi, D., Primack, B., Cao, S., Bernhardy, A.J., Coulson, R., et al. (2016). CDK12 inhibition reverses de novo and acquired PARP inhibitor resistance in BRCA wild-type and mutated models of triple-negative breast cancer. Cell Rep. *17*, 2367–2381.

Joshi, P.M., Sutor, S.L., Huntoon, C.J., and Karnitz, L.M. (2014). Ovarian cancer-associated mutations disable catalytic activity of CDK12, a kinase that promotes homologous recombination repair and resistance to cisplatin and poly(ADP-ribose) polymerase inhibitors. J. Biol. Chem. *289*, 9247–9253.

Kaelin, W.G., Jr. (2005). The concept of synthetic lethality in the context of anti-cancer therapy. Nat. Rev. Cancer *5*, 689–698.

Kennedy, A.L., Vallurupalli, M., Chen, L., Crompton, B., Cowley, G., Vazquez, F., Weir, B.A., Tsherniak, A., Parasuraman, S., Kim, S., et al. (2015). Functional, chemical genomic, and super-enhancer screening identify sensitivity to cyclin D1/CDK4 pathway inhibition in Ewing sarcoma. Oncotarget *6*, 30178–30193.

Kwiatkowski, N., Zhang, T., Rahl, P.B., Abraham, B.J., Reddy, J., Ficarro, S.B., Dastur, A., Amzallag, A., Ramaswamy, S., Tesar, B., et al. (2014). Targeting transcription regulation in cancer with a covalent CDK7 inhibitor. Nature *511*, 616–620.

Lawrence, M.S., Stojanov, P., Polak, P., Kryukov, G.V., Cibulskis, K., Sivachenko, A., Carter, S.L., Stewart, C., Mermel, C.H., Roberts, S.A., et al. (2013). Mutational heterogeneity in cancer and the search for new cancer associated genes. Nature *499*, 214–218.

Liang, K., Gao, X., Gilmore, J.M., Florens, L., Washburn, M.P., Smith, E., and Shilatifard, A. (2015). Characterization of human cyclin-dependent kinase 12 (CDK12) and CDK13 complexes in C-terminal domain phosphorylation, gene transcription, and RNA processing. Mol. Cell. Biol. *35*, 928–938.

Loven, J., Orlando, D.A., Sigova, A.A., Lin, C.Y., Rahl, P.B., Burge, C.B., Levens, D.L., Lee, T.I., and Young, R.A. (2012). Revisiting global gene expression analysis. Cell *151*, 476–482.

Marques Howarth, M., Simpson, D., Ngok, S.P., Nieves, B., Chen, R., Siprashvili, Z., Vaka, D., Breese, M.R., Crompton, B.D., Alexe, G., et al. (2014). Long noncoding RNA EWSAT1-mediated gene repression facilitates Ewing sarcoma oncogenesis. J. Clin. Invest. *124*, 5275–5290.

Meyers, R.M., Bryan, J.G., McFarland, J.M., Weir, B.A., Sizemore, A.E., Xu, H., Dharia, N.V., Montgomery, P.G., Cowley, G.S., Pantel, S., et al. (2017). Computational correction of copy-number effect improves specificity of CRISPR-Cas9 essentiality screens in cancer cells. Nat. Genet. *49*, 1779–1784.

Monterrubio, C., Paco, S., Vila-Ubach, M., Rodriguez, E., Glisoni, R., Lavarino, C., Schaiquevich, P., Sosnik, A., Mora, J., and Carcaboso, A.M. (2015). Combined microdialysis-tumor homogenate method for the study of the steady state compartmental distribution of a hydrophobic anticancer drug in patient-derived xenografts. Pharm. Res. *32*, 2889–2900.

Mootha, V.K., Lindgren, C.M., Eriksson, K.F., Subramanian, A., Sihag, S., Lehar, J., Puigserver, P., Carlsson, E., Ridderstrale, M., Laurila, E., et al. (2003). PGC-1alpha-responsive genes involved in oxidative phosphorylation are coordinately downregulated in human diabetes. Nat. Genet. *34*, 267–273.

Stewart, S.A., Dykxhoorn, D.M., Palliser, D., Mizuno, H., Yu, E.Y., An, D.S., Sabatini, D.M., Chen, I.S., Hahn, W.C., Sharp, P.A., et al. (2003). Lentivirus-delivered stable gene silencing by RNAi in primary cells. RNA *9*, 493–501.

Nieto-Soler, M., Morgado-Palacin, I., Lafarga, V., Lecona, E., Murga, M., Callen, E., Azorin, D., Alonso, J., LopezContreras, A.J., Nussenzweig, A., and Fernandez-Capetillo, O. (2016). Efficacy of ATR inhibitors as single agents in Ewing sarcoma. Oncotarget *7*, 58759–58767.

Norris, R.E., Adamson, P.C., Nguyen, V.T., and Fox, E. (2014). Preclinical evaluation of the PARP inhibitor, olaparib, in combination with cytotoxic chemotherapy in pediatric solid tumors. Pediatr. Blood Cancer *61*, 145150.

Ordonez, J.L., Amaral, A.T., Carcaboso, A.M., Herrero-Martin, D., del Carmen Garcia-Macias, M., Sevillano, V., Alonso, D., Pascual-Pasto, G., San-Segundo, L., Vila-Ubach, M., et al. (2015). The PARP inhibitor olaparib enhances the sensitivity of Ewing sarcoma to trabectedin. Oncotarget *6*, 18875–18890.

Riggi, N., Knoechel, B., Gillespie, S.M., Rheinbay, E., Boulay, G., Suva, M.L., Rossetti, N.E., Boonseng, W.E., Oksuz, O., Cook, E.B., et al. (2014). EWS-FLI1 utilizes divergent chromatin remodeling mechanisms to directly activate or repress enhancer elements in Ewing sarcoma. Cancer Cell *26*, 668–681.

Sanjana, N.E., Shalem, O., and Zhang, F. (2014). Improved vectors and genome-wide libraries for CRISPR screening. Nat. Methods *11*, 783–784.

Smith, R., Owen, L.A., Trem, D.J., Wong, J.S., Whangbo, J.S., Golub, T.R., and Lessnick, S.L. (2006). Expression profiling of EWS/FLI identifies NKX2.2 as a critical target gene in Ewing's sarcoma. Cancer Cell *9*, 405–416.

Sonnenblick, A., de Azambuja, E., Azim, H.A., Jr., and Piccart, M. (2015). An update on PARP inhibitors – moving to the adjuvant setting. Nat. Rev. Clin. Oncol. *12*, 27–41.

Stewart, E., Goshorn, R., Bradley, C., Griffiths, L.M., Benavente, C., Twarog, N.R., Miller, G.M., Caufield, W., Freeman, B.B., 3rd, Bahrami, A., et al. (2014). Targeting the DNA repair pathway in Ewing sarcoma. Cell Rep. *9*, 829–841.

Tirode, F., Surdez, D., Ma, X., Parker, M., Le Deley, M.C., Bahrami, A., Zhang, Z., Lapouble, E., GrosseteteLalami, S., Rusch, M., et al. (2014). Genomic landscape of Ewing sarcoma defines an aggressive subtype with co-association of STAG2 and TP53 mutations. Cancer Discov. *4*, 1342–1353.

Tomazou, E.M., Sheffield, N.C., Schmidl, C., Schuster, M., Schonegger, A., Datlinger, P., Kubicek, S., Bock, C., and Kovar, H. (2015). Epigenome mapping reveals distinct modes of gene regulation and widespread enhancer reprogramming by the oncogenic fusion protein EWS-FLI1. Cell Rep. *10*, 1082–1095.

Vormoor, B., and Curtin, N.J. (2014). Poly(ADP-ribose) polymerase inhibitors in Ewing sarcoma. Curr. Opin. Oncol. *26*, 428–433.

Yang, W., Soares, J., Greninger, P., Edelman, E.J., Lightfoot, H., Forbes, S., Bindal, N., Beare, D., Smith, J.A., Thompson, I.R., et al. (2013). Genomics of Drug Sensitivity in Cancer (GDSC): a resource for therapeutic biomarker discovery in cancer cells. Nucleic Acids Res. *41*, D955–D961.

Zhang, T., Kwiatkowski, N., Olson, C.M., Dixon-Clarke, S.E., Abraham, B.J., Greifenberg, A.K., Ficarro, S.B., Elkins, J.M., Liang, Y., Hannett, N.M., et al. (2016). Covalent targeting of remote cysteine residues to develop CDK12 and CDK13 inhibitors. Nat. Chem. Biol. *12*, 876–884.

STAR★METHODS

KEY RESOURCES TABLE

REAGENT or RESOURCE	SOURCE	IDENTIFIER
Antibodies		
CDK7	Cell Signaling Technology	Cat# 2090; RRID:AB_2077140
CDK12	Cell Signaling Technology	Cat# 11973; RRID:AB_2715688
CDK13 (CDC2L5)	Bethyl Laboratories	Cat# A301-458A; RRID:AB_960967
Cyclin K	Abcam	Cat# ab85854; RRID:AB_1860218
Cyclin H	Abcam	Cat# ab10542; RRID:AB_297282
phospho-Ser2-RNA-Polymerase II	Bethyl	Cat# A300-654A; RRID:AB_519341
phospho-Ser5-RNA-Polymerase II	Bethyl	Cat# A304-408A; RRID:AB_2620602
phospho-Ser7-RNA-Polymerase II	Millipore	Cat# 04-1570; RRID:AB_10618152
Total RNA-Polymerase II	Santa Cruz	Cat# sc-900; RRID:AB_2167474
PARP	Cell Signaling Technology	Cat# 9542; RRID:AB_2160739
RAD51	Cell Signaling Technology	Cat# 8875; RRID:AB_2721109
FLI	Abcam	Cat# Ab15289; RRID:AB_301825
Vinculin	Abcam	Cat# Ab18058; RRID:AB_444215
GAPDH	Santa Cruz	Cat# sc-137179; RRID:AB_2232048
beta-Actin	Cell Signaling Technology	Cat# 3700; RRID:AB_2242334
Anti-Mouse IgG, HRP-linked	Fisher Scientific	Cat# 45-000-680; RRID:AB_2721110
Anti-Rabbit IgG, HRP-linked	Fisher Scientific	Cat# 45-000-683; RRID:AB_2721111
Anti-rat IgG, HRP-linked	Cell Signaling Technology	Cat# 7077; RRID:AB_10694715
Bacterial and Virus Strains		
Stbl3 Chemically Competent E. coli	Life Technologies	C737303
Chemicals, Peptides, and Recombinant Proteins		
TaqMan Gene Expression Master Mix	Life Technologies	4369016
M-MLV Reverse Transcriptase	Thermo Fisher Scientific	PRM1705
PhosSTOP Phosphatase Inhibitor	Roche Diagnostic	4906837001
Cell Lysis Buffer	Cell Signaling Technology	9803S
Complete, EDTA-free Protease Inhibitor Tablet	Roche Diagnostic	6327-4
SuperSignal West Dura Chemiluminescent	Thermo Fisher Scientific	34076
RPMI 1640	Thermo Fisher Scientific	MT10040CV
DMEM With L-Glutamine	Thermo Fisher Scientific	MT10013CM
Fetal Bovine Serum	Sigma Aldrich	F2442
Penicillin Streptomycin	Thermo Fisher Scientific	MT30002CI
Penicillin-Streptomycin-L-Glutamine	Thermo Fisher Scientific	MT30009CI
Sodium Pyruvate	Life Technologies	11360070
Puromycin	Invivogen	ant-pr-1
Fugene 6	Promega	E2691
Tet System Approved FBS	Clontech	631367
Precision Plus Protein Kaleidoscope Prestained Protein Standards	Bio-Rad Laboratories	161-0395
THZ1	Gray Laboratory (DFCI)	N/A
THZ531	Gray Laboratory (DFCI)	N/A
THZ531R	Gray Laboratory (DFCI)	N/A
Olaparib (*in vitro*)	Selleck Chemicals	S1060
Olaparib (*in vivo*)	ApexBIO	A4154

(*Continued on next page*)

Continued

REAGENT or RESOURCE	SOURCE	IDENTIFIER
Critical Commercial Assays		
RNeasy Mini kit	Qiagen	74104
Bio-Rad Protein Assay	Bio-Rad Laboratories	500-0006
Cell-TiterGlo luminescent assay kit	Promega	G7573
Annexin V: FITC Apoptosis Detection Kit	BD Pharmingen	556547
Maxi prep kit	Qiagen	12663
Deposited Data		
Gene expression data	GEO	GSE82270, https://www.ncbi.nlm.nih.gov/geo/query/acc.cgi?acc=GSE82270
Experimental Models: Cell Lines		
Human: A673	Golub Lab, DFCI	N/A
Human: TC32	Golub Lab, DFCI	N/A
Human: TC71	Golub Lab, DFCI	N/A
Human: EW8	Golub Lab, DFCI	N/A
Human: EWS502	Fletcher Lab, BWH	N/A
Human: RDES	Golub Lab, DFCI	N/A
Human: SKNEP1	Golub Lab, DFCI	N/A
Human: EWS834	Fletcher Lab, BWH	N/A
Human: SKES1	Golub Lab, DFCI	N/A
Human: SKNMC	Golub Lab, DFCI	N/A
Human: SJSA1	Hahn Lab, DFCI	N/A
Human: U2OS	Hahn Lab, DFCI	N/A
Human cancer cell lines included in the CRISPR-Cas9 screen (Figure S2A–S2C)	Meyers et al., 2017	N/A
Human cancer cell lines included in the THZ1 cancer cell line profiling (Figure 1A)	Kwiatkowski et al., 2014, www.cancerRXgene.org	N/A
Experimental Models: Organisms/Strains		
Mouse: Nu/Nu Nude Female	Charles River Laboratories	Crl: Nu-Foxn1nu
PDX mouse model	Mora Lab, Sant Joan de Déu Hospital	HSJD-ES-002
Oligonucleotides		
TaqMan Probe: RPL13A	Life Technologies	Hs04194366_g1
TaqMan Probe: BRCA1	Life Technologies	Hs01556193_m1
TaqMan Probe: Rad51	Life Technologies	Hs01556193_m1
TaqMan Probe: FANCF	Life Technologies	Hs00256030_s1
TaqMan Probe: XRCC2	Life Technologies	Hs03044154_m1
sgRNA sequences, see Table S6	This Study	N/A
shRNA sequences, see Table S6	This Study	N/A
Recombinant DNA		
pCMV8.2	pCMV8.2 was a gift from Didier Trono (unpublished)	pCMV delta R8.2, Addgene Plasmid #12263
pCMV-VSV-G	pCMV-VSV-G was a gift from Dr. Robert Weinberg (Stewart et al., 2003 Apr;9(4):493-501)	pCMV-VSV-G, Addgene Plasmid #8454
Software and Algorithms		
PRISM	GraphPad Software	Version 7
GSEA	Mootha et al., 2003	v2.1.0
ImageJ	NIH	https://imagej.nih.gov/ij/

CONTACT FOR REAGENT AND RESOURCE SHARING

Requests for resources and reagents should be directed to and will be fulfilled by the Lead Contact, Kimberly Stegmaier (kimberly_stegmaier@dfci.harvard.edu)

EXPERIMENTAL MODEL AND SUBJECT DETAILS

Cell Lines

A673 cells (female) were cultured in DMEM + 10% FBS + 1 mM sodium pyruvate + 1% PSQ. TC32 (female), TC71 (male) and SJSA1 (male) cells were cultured in RPMI + 10% FBS +1% PSQ. EW8 (male), U2OS (female), and SKNMC (female) cells were cultured in DMEM + 10% FBS + 1% PSQ. EWS502 cells (female) were cultured in DMEM + 15% FBS + 1% PSQ. RDES (male), EWS834 (female), and SKNEP1 (female) cells were cultured in DMEM + 20% FBS + 1% PSQ. SKES1 (male) cells were cultured in McCoys5a + 15% FBS + 1% PSQ. Whole exome sequencing, RNA sequencing and STR genotyping of all Ewing sarcoma cell lines used in these studies were previously performed to validate cell line identity (Crompton et al., 2014).

In Vivo Tumor Models

A PDX mouse model of Ewing sarcoma with a type I EWS/FLI fusion was established from a tumor resected from the fibula of a 12 year old patient at diagnosis (HSJD-ES-002). HSJD-ES-002 was established in athymic nude mice (Harlan, Barcelona, Spain) as previously described (Monterrubio et al., 2015; Ordonez et al., 2015). Informed consent for the use of clinical data and biological material was obtained from the patient and all studies were approved by the ethics review committee at the Sant Joan de Déu Hospital in Esplugues de Llobregat. All dosing studies were performed at the Dana-Farber Cancer Institute, and all animal protocols were approved by the Dana-Farber Cancer Institute Animal Care and Use Committee. Nude mice were maintained according to institutional guidelines.

Single Agent THZ1 Study

Three million TC32 Ewing sarcoma cells were implanted subcutaneously into the right flank of 7-8 week old female nude mice. Following engraftment, mice with palpable tumors were divided into two groups and treated with 10 mg/kg THZ1 or vehicle control administered IP BID. Tumors were measured twice per week and mice were followed for survival. Statistical significance was determined by Log-rank test for survival curves.

THZ1 and Olaparib Combination Study

Three million A673 or TC71 cells were subcutaneously implanted into the right flanks of 7-8 week old nude female mice. For PDX studies, 1 mm^3 viably frozen tumor chunks were dipped in matrigel and implanted into the right flanks via minor surgery. When tumors measured 100-150 mm^3, mice were divided into four groups: vehicle control, THZ1, olaparib, and THZ1 and olaparib in combination. THZ1 was administered IP BID at 10 mg/kg, and olaparib was administered PO BID at 50 mg/kg. Tumors were measured twice per week and mice were followed for survival. Statistical significance was determined by log-rank test for survival curves.

METHOD DETAILS

Western Blotting

Cells were lysed in Cell Signaling Lysis Buffer (Cell Signaling Technology) supplemented with Complete, EDTA free Protease Inhibitor Cocktail (Roche Diagnostics) and PhosSTOP Phosphatase Inhibitor (Roche Diagnostics). Protein concentrations were determined by the Bradford protein assay. Protein samples were separated by SDS-PAGE and transferred to PVDF membranes. Membranes were incubated with primary antibodies directed against CDK7 (Cell Signaling Technology Cat. No. 2090S), CDK12 (Cell Signaling Technology Cat. No. 11973), CDK13 (Bethyl Cat. No. A301-458A), Cyclin K (Abcam ab130475), p-Ser2-RNA-Pol II (Bethyl Cat. No. A300654A), p-Ser5-RNA-Pol II (Bethyl Cat. No. A300-655A), p-Ser7-RNA-Pol II (Millipore Cat. No. 04-1570), total RNA-Pol II (Santa Cruz Cat. No. sc-17798), PARP (Cell Signaling Technology Cat. No. 9542), RAD51 (Cell Signaling Technology Cat. No. 8875), FLI1 (Santa Cruz Biotechnology Cat. No. sc-356), Vinculin (Abcam Cat. No. ab18058), GAPDH (Santa Cruz Biotechnology Cat. No. sc-137179), and β-Actin (Cell Signaling Technology Cat. No. cs3700). Horseradish peroxidase (HRP) conjugated secondary antibodies were used. Blots were visualized by enhanced chemi-luminescence (ThermoFisher Scientific).

Quantitative PCR

RNA was extracted from cells with the RNeasy Kit and on-column DNA digestion (Qiagen). cDNA was prepared using M-MLV Reverse Transcriptase (ThermoFisher Scientific). Taqman probes for *RPL13A* (Hs01926559_g1), *BRCA1* (Hs01556193_m1), *RAD51* (Hs00427442_m1), *FANCF* (Hs00256030_s1), and *XRCC2* (Hs03044154_m1) were obtained from Life Technologies. Data were collected in technical and biological triplicate and analyzed using the ΔΔCT method.

Compounds

THZ1, THZ1R, THZ531, and THZ531R were synthesized by the Gray Laboratory (Dana-Farber Cancer Institute). Olaparib was obtained from Selleck Chemicals (Cat. No. S1060) for *in vitro* studies, and ApexBio (Cat. No. A4154) for *in vivo* studies. For the *in vivo* studies, THZ1 was solubilized in 10% DMSO, 90% D5W, and olaparib was solubilized in 10% DMSO, 90% HPBCD.

THZ1-biotin Immunoprecipitation

Cells were treated with THZ1 or THZ531 for 6 hr and lysed with 50 mM Hepes pH 7.4, 150 mM NaCl, 1% NP40, 5 mM EDTA, and protease and phosphatase inhibitors. Samples were incubated with 1 μM THZ1-biotin or DMSO overnight at 4°C. Streptavidin beads were added to each sample and incubated for 2 hr at 4°C. Samples were washed in lysis buffer and SDS loading dye was added to each sample and boiled at 95°C before loading onto western blot gels.

Genome-Scale CRISPR-Cas9 Screening

The genome-scale CRISPR-Cas9 screen was conducted using the Broad Institute's Avana library and analyzed using the CERES algorithm as previously described (Meyers et al., 2017). The data used for the analysis of CDK7, CDK12, and CDK13 included the gene effects as predicted by the CERES algorithm.

RNA Extractions and Synthetic RNA Spike-in

RNA was extracted from equal numbers of Ewing sarcoma cells using the RNeasy kit (Qiagen) according to the manufacturer's instructions. A fixed amount of External RNA Controls Consortium (ERCC) RNA Spike-In Mix (Ambion, 4456739) was added to the total RNA (Loven et al., 2012).

Gene Expression Profiling

Gene expression profiling was performed with spiked-in RNA samples using Human PrimeView arrays (Affymetrix) as previously described (Kwiatkowski et al., 2014). For gene expression studies, the CEL data files were subjected to the quality control tests based on distance between arrays, array intensity distribution and variance mean dependence, which are implemented in the ArrayQuality R package available at Bioconductor v 3.2 (www.bioconductor.org). All CEL files passed the test. CEL files were processed as previously described (Kwiatkowski et al., 2014). Briefly, the raw expression values for each probe were summarized using Mas5, and Mas5-normalized probe set values were normalized across samples using Loess normalization with ERCC probes as the reference subset. The probe with the highest average signal was taken for each RefSeq transcript. Replicates were averaged for each transcript. All probe sets with an average log2 expression below 4 were considered under-expressed and they were designated as "filtered". Out of the 49,293 probe sets on the Affymetrix PrimeView Human Gene Expression Array, 44,125 probe sets remained after filtering. The data from the 44,125 probe sets was further collapsed to 11,963 non-redundant genes with distinct GRCh37/hg19 HUGO symbols, by assigning to each gene the probe set with the maximum average expression intensity. These genes were considered expressed for Figures 3A and 3F. For each cell line, significant hits were selected based on the cutoffs: 1 for absolute fold change, 0.05 for permutation p value, and 0.05 for False Discovery Rate. Transcript fold-changes were performed by log2-transforming the transcript values in both samples plus one pseudo-count and subtracting the log2-transformed values. In Figure 3F, the top 30% of transcripts ranked by DMSO signal were taken.

Gene Set Enrichment Analysis

The Database for Annotation, Visualization and Integrated Discovery (DAVID) v6.7 and the GSEA v2.1.0 software were used to identify functional associations of the molecular phenotypes induced by THZ531 at 100 nM vs. vehicle and by THZ531 at 500 nM vs. vehicle. Gene sets with less than 15 genes or more than 500 genes were excluded from the analysis. Gene sets with an FDR $\leq$ 0.25 and a nominal p value $\leq$ 0.05 were considered significant hits. The enrichment results for THZ531 at 100 nM vs. vehicle and for THZ531 at 500 nM vs. vehicle were visualized on GSEA plots and heatmaps for selected gene signatures. The molecular gene set signatures of THZ531 100 nM and THZ531 500 nM vs. vehicle were visualized as dots in the volcano plots of normalized enrichment scores (NES) vs. –log10(p value) scores.

Comparative Marker Analysis

The Comparative Marker Selection module from GenePattern v3.9.6 was employed to identify individual genes that were differentially expressed between treated and vehicle conditions. The analysis was performed on the log2 normalized expression data by applying a 2-sided signal-to-noise ratio (SNR) test followed by 1000 permutations of phenotype labels. The settings for the SNR parameters were log-transformed-data:yes, complete:no, balanced:no, smooth p values: yes. Gene signatures (down and up) for 100 nM THZ531 vs. vehicle and 500 nM THZ531 vs. vehicle were defined separately for each of the A673 and TC32 cell lines based on the cut-offs SNR permutation p value $\leq$ 0.05, Benjamini-Hochberg false discovery rate (FDR) $\leq$ 0.05, and absolute fold change [FC] $\geq$ 2. A *core* molecular signature for the differential expression of A673 and TC32 cell lines was defined by overlapping the lists of genes which are significantly differentially expressed (down and up, respectively) in either cell line. The significance of the overlap of the lists of genes differentially expressed in A763 vs. TC32 cell lines was estimated based on the two-tailed Fisher test. The correlation between the expression fold changes induced by THZ531 vs. vehicle in the A673 and TC32 cell lines was estimated by fitting a linear regression model. The differentially expressed genes induced by THZ531 in the A673 and TC32 cell lines were visualized as highlighted dots in scatter plots of log2 fold change of expression.

Super-Enhancer Analysis

The TC32 enhancer and FLI1 region/gene target data were created and published by the Stegmaier lab (Kennedy et al., 2015). The A673 enhancer and FLI1 region/gene target data were created and published by the Rivera lab (Riggi et al., 2014). Peaks were called

using MACS 1.4.2 with corresponding input control and two parameter sets: -p 1e-9 –keep-dup=1 and -p 1e-9 –keep-dup=all. The collapsed union of peaks was used as input for ROSE. ROSE was run with parameters -t 1000 -s 12500 and corresponding input control. ROSE-defined enhancers were assigned to the single nearest expressed gene whose transcription start site was closest to the center of the enhancer. Expressed genes are defined as the top 2/3 of RefSeq transcripts ranked by their promoter H3K27ac levels, where promoters are defined as 1kb regions centered on each transcription start site and H3K27ac level is calculated using bamToGFF (https://github.com/BradnerLab/pipeline) with parameters -e 200 -m 1 -r -d.

Leading Edge Analysis

The leading edge analysis implemented in the GSEA platform http://software.broadinstitute.org/gsea/index.jsp was employed to analyze the collection of ''leading edge'' genes, (i.e., the genes which simultaneously (i) are in multiple significantly enriched DNA Damage and DNA Repair gene sets and (ii) are differentially expressed by the THZ531 100 nM treatment vs. vehicle). The collection of 33 leading edge genes that belong to at least four DNA Damage and DNA Repair gene sets enriched in the THZ531 vs. vehicle signature was visualized.

Immunofluorescence

Cells were fixed with 4% paraformaldehyde for 10 minutes at RT, permeabilized with ice cold methanol for 5 minutes at -20°C, and blocked in 3% BSA in PBS for 30 minutes at RT. Cells were then incubated in primary antibodies against RAD51 (Abcam, clone 14B4), or γH2AX (S139, Millipore, clone JBW301). Alexa-Fluor conjugated secondary antibodies were used (Life Technologies). Cell nuclei were stained using DAPI reagent (Cell Signaling Technology Cat. No. 8961). One hundred cells per sample were counted. A cell was counted as γH2AX or RAD51 positive only if >10 foci per nucleus were identified.

Colony Formation Assays

A base layer of 1:9 6% agar in media was poured into 24 well plates. Cells were plated in a 0.3% agar/media solution on top of the base layer at a concentration of 15,000 cells/well. Cells were fed with growth media on the first and sixth day after plating, stained with MTT, and imaged once colonies were visible. Colonies were counted using Image Quant (GE Healthcare).

Annexin V/PI Staining

Apoptosis was measured using the Annexin V: FITC Apoptosis Detection Kit per the manufacturer's protocol (BD Pharmingen, San Jose, CA, USA).

shRNA and CRISPR Studies

Lentivirus was generated by transfecting 293T cells with the appropriate lentiCRISPRv2 sgRNA vector or the appropriate pLKO shRNA vector, and the packaging plasmids pCMV8.9 and pCMV-VSVG, using Fugene 6 per the manufacturer's instructions (Promega). Forty-eight hrs after transfection, media containing virus was filtered through a 0.45 μM filter. Ewing sarcoma cell lines were transduced in 10 cm plates with 3 ml virus, 3 ml of growth media and 8 μg/ml polybrene (Sigma-Aldrich). Forty-eight hrs post-infection, cells were selected in puromycin–containing media. Five days post-selection (CRISPR studies) or three days post-selection (shRNA studies), cells were harvested for protein, colony formation and viability assays. CRISPR guide sequences were designed using the Broad Institute's sgRNA designer tool
(http://www.broadinstitute.org/rnai/public/analysis-tools/sgrna-design-v1).

EWS/FLI knockdown was achieved using a TRIPZ inducible lentiviral vector system. Cells with either an shRNA against EWS/FLI or non-targeting control were treated with doxycycline every 48 hr for seven days. EWS/FLI knockdown was confirmed by western blotting. See Table S6 for a list of all shRNA and sgRNA sequences and vector information.

Cell Viability and Synergy Studies

Cells were seeded onto 384-well tissue culture treated plates at a density of 25,000 cells/ml. After treatment with a compound or a combination of compounds, cells were analyzed for cell viability on days zero, three, five, and seven, using the Cell-TiterGlo luminescent assay (Promega) per the manufacturer's instructions. Luminescence was read on a Fluostar Omega Reader (BMG Labtech).

Chou-Talalay Combination Index for Loewe Additivity

Loewe additivity is a dose-effect model which states that additivity occurs in a two-drug combination if the sum of the ratios of the dose vs. the median-effect for each individual drug is 1. In this model, *combination index* (CI) scores estimate the interaction between the two drugs. If CI < 1, the drugs have a synergistic effect and if CI > 1, the drugs have an antagonistic effect. CI = 1 means the drugs have additive effect. Chou and Talalay (Chou and Talalay, 1984) showed that Loewe equations are valid for enzyme inhibitors with similar mechanisms of action – either competitive or non-competitive toward the substrate. The combination index (*CI*) coefficients were computed based on the Chou-Talalay Median Effect model as implemented in *CalcuSyn* v2.11 (http://www.biosoft.com/w/calcusyn.htm). The degree of interaction between drugs was estimated according to the classification presented by Chou-Talalay (Chou and Talalay, 1984). The CI scores were computed for the range of concentrations of drug combinations where the effect of an individual drug was less than a fractional inhibition of 0.9. If the fractional inhibition score in paired combination with DMSO and with the other drug is > 0.9, this dose was eliminated from the analysis since the additional effect of the second drug could not be reliably calculated.

The Bliss Independence Method

Bliss independence (Bliss, 1956) is an effect-based strategy that compares the effect resulting from the combination of two drugs directly to the effects of its individual components.

The model predicts that if the individual drugs have the inhibitory effects f_1 and f_2 then the expected combined effect of the two drugs is:

$$E(f_{12}) = 1 - (1 - f_1)\,(1 - f_2) = f_1 + f_2 - f_1\,f_2$$

The difference between the observed combined effect f_{12} and the *expected* combined effect of the two drugs is called the Excess over Bliss (eob): $eob = f_{12} - E(f_{12})$

Positive eob values are indicative of a synergistic interaction, whereas negative eob values are indicative of antagonistic behavior. Null *eob* values indicate no drug interaction.

QUANTIFICATION AND STATISTICAL ANALYSES

GSEA v2.1.0, GraphPad PRISM 7, R 3.2.3 and Python 2.7.2 software packages were used to perform the statistical analyses. Statistical tests used are specified in the Figure legends. Errors bars represent standard deviation, unless otherwise stated. The threshold for statistical significance is $P < 0.05$, unless otherwise specified.

DATA AND SOFTWARE AVAILABILITY

Gene expression data have been deposited to GEO (accession no: GSE82270).

It can be accessed at:
https://www.ncbi.nlm.nih.gov/geo/query/acc.cgi?acc=GSE82270

12 - References

1. Ewing, J., *The Classic: Diffuse endothelioma of bone. Proceedings of the New York Pathological Society. 1921;12:17.* Clin Orthop Relat Res, 2006. **450**: p. 25-7.
2. Gaspar, N., et al., *Ewing Sarcoma: Current Management and Future Approaches Through Collaboration.* J Clin Oncol, 2015. **33**(27): p. 3036-46.
3. Stahl, M., et al., *Risk of recurrence and survival after relapse in patients with Ewing sarcoma.* Pediatr Blood Cancer, 2011. **57**(4): p. 549-53.
4. Cotterill, S.J., et al., *Prognostic factors in Ewing's tumor of bone: analysis of 975 patients from the European Intergroup Cooperative Ewing's Sarcoma Study Group.* J Clin Oncol, 2000. **18**(17): p. 3108-14.
5. Rodriguez-Galindo, C., et al., *Prognostic factors for local and distant control in Ewing sarcoma family of tumors.* Ann Oncol, 2008. **19**(4): p. 814-20.
6. Burningham, Z., et al., *The epidemiology of sarcoma.* Clin Sarcoma Res, 2012. **2**(1): p. 14.
7. Kovar, H., et al., *The second European interdisciplinary Ewing sarcoma research summit--A joint effort to deconstructing the multiple layers of a complex disease.* Oncotarget, 2016. **7**(8): p. 8613-24.
8. Esiashvili, N., M. Goodman, and R.B. Marcus, Jr., *Changes in incidence and survival of Ewing sarcoma patients over the past 3 decades: Surveillance Epidemiology and End Results data.* J Pediatr Hematol Oncol, 2008. **30**(6): p. 425-30.
9. Grunewald, T.G.P., et al., *Ewing sarcoma.* Nat Rev Dis Primers, 2018. **4**(1): p. 5.
10. Tu, J., et al., *The Histogenesis of Ewing Sarcoma.* Cancer Rep Rev, 2017. **1**(2).
11. Cidre-Aranaz, F. and J. Alonso, *EWS/FLI1 Target Genes and Therapeutic Opportunities in Ewing Sarcoma.* Front Oncol, 2015. **5**: p. 162.
12. May, W.A., et al., *Ewing sarcoma 11;22 translocation produces a chimeric transcription factor that requires the DNA-binding domain encoded by FLI1 for transformation.* Proc Natl Acad Sci U S A, 1993. **90**(12): p. 5752-6.
13. Delattre, O., et al., *Gene fusion with an ETS DNA-binding domain caused by chromosome translocation in human tumours.* Nature, 1992. **359**(6391): p. 162-5.
14. Lessnick, S.L., et al., *Multiple domains mediate transformation by the Ewing's sarcoma EWS/FLI-1 fusion gene.* Oncogene, 1995. **10**(3): p. 423-31.
15. May, W.A., et al., *The Ewing's sarcoma EWS/FLI-1 fusion gene encodes a more potent transcriptional activator and is a more powerful transforming gene than FLI-1.* Mol Cell Biol, 1993. **13**(12): p. 7393-8.
16. Brohl, A.S., et al., *The genomic landscape of the Ewing Sarcoma family of tumors reveals recurrent STAG2 mutation.* PLoS Genet, 2014. **10**(7): p. e1004475.
17. Crompton, B.D., et al., *The genomic landscape of pediatric Ewing sarcoma.* Cancer Discov, 2014. **4**(11): p. 1326-41.
18. Tirode, F., et al., *Genomic landscape of Ewing sarcoma defines an aggressive subtype with co-association of STAG2 and TP53 mutations.* Cancer Discov, 2014. **4**(11): p. 1342-53.
19. Gollavilli, P.N., et al., *EWS/ETS-Driven Ewing Sarcoma Requires BET Bromodomain Proteins.* Cancer Res, 2018. **78**(16): p. 4760-4773.

20. Lin, L., et al., *Super-enhancer-associated MEIS1 promotes transcriptional dysregulation in Ewing sarcoma in co-operation with EWS-FLI1.* Nucleic Acids Res, 2019. **47**(3): p. 1255-1267.
21. Souza, B.K., et al., *Targeting Histone Deacetylase Activity to Arrest Cell Growth and Promote Neural Differentiation in Ewing Sarcoma.* Mol Neurobiol, 2018. **55**(9): p. 7242-7258.
22. Longhi, A., et al., *Late effects of chemotherapy and radiotherapy in osteosarcoma and Ewing sarcoma patients: the Italian Sarcoma Group Experience (1983-2006).* Cancer, 2012. **118**(20): p. 5050-9.
23. Buchdunger, E., et al., *Inhibition of the Abl protein-tyrosine kinase in vitro and in vivo by a 2-phenylaminopyrimidine derivative.* Cancer Res, 1996. **56**(1): p. 100-4.
24. DuBois, S.G., et al., *Ushering in the next generation of precision trials for pediatric cancer.* Science, 2019. **363**(6432): p. 1175-1181.
25. Dang, C.V., et al., *Drugging the 'undruggable' cancer targets.* Nat Rev Cancer, 2017. **17**(8): p. 502-508.
26. Erkizan, H.V., et al., *A small molecule blocking oncogenic protein EWS-FLI1 interaction with RNA helicase A inhibits growth of Ewing's sarcoma.* Nat Med, 2009. **15**(7): p. 750-6.
27. Barrangou, R., et al., *CRISPR provides acquired resistance against viruses in prokaryotes.* Science, 2007. **315**(5819): p. 1709-12.
28. Bolotin, A., et al., *Clustered regularly interspaced short palindrome repeats (CRISPRs) have spacers of extrachromosomal origin.* Microbiology, 2005. **151**(Pt 8): p. 2551-61.
29. Mojica, F.J., et al., *Intervening sequences of regularly spaced prokaryotic repeats derive from foreign genetic elements.* J Mol Evol, 2005. **60**(2): p. 174-82.
30. Pourcel, C., G. Salvignol, and G. Vergnaud, *CRISPR elements in Yersinia pestis acquire new repeats by preferential uptake of bacteriophage DNA, and provide additional tools for evolutionary studies.* Microbiology, 2005. **151**(Pt 3): p. 653-63.
31. Cong, L., et al., *Multiplex genome engineering using CRISPR/Cas systems.* Science, 2013. **339**(6121): p. 819-23.
32. Mali, P., et al., *RNA-guided human genome engineering via Cas9.* Science, 2013. **339**(6121): p. 823-6.
33. Shalem, O., et al., *Genome-scale CRISPR-Cas9 knockout screening in human cells.* Science, 2014. **343**(6166): p. 84-87.
34. Shalem, O., N.E. Sanjana, and F. Zhang, *High-throughput functional genomics using CRISPR-Cas9.* Nat Rev Genet, 2015. **16**(5): p. 299-311.
35. Wang, T., et al., *Genetic screens in human cells using the CRISPR-Cas9 system.* Science, 2014. **343**(6166): p. 80-4.
36. Hart, T., et al., *High-Resolution CRISPR Screens Reveal Fitness Genes and Genotype-Specific Cancer Liabilities.* Cell, 2015. **163**(6): p. 1515-26.
37. Tzelepis, K., et al., *A CRISPR Dropout Screen Identifies Genetic Vulnerabilities and Therapeutic Targets in Acute Myeloid Leukemia.* Cell Rep, 2016. **17**(4): p. 1193-1205.
38. Aguirre, A.J., et al., *Genomic Copy Number Dictates a Gene-Independent Cell Response to CRISPR/Cas9 Targeting.* Cancer Discov, 2016. **6**(8): p. 914-29.
39. Garnett, M.J., et al., *Systematic identification of genomic markers of drug sensitivity in cancer cells.* Nature, 2012. **483**(7391): p. 570-5.

40. Leroy, B., M. Anderson, and T. Soussi, *TP53 mutations in human cancer: database reassessment and prospects for the next decade.* Hum Mutat, 2014. **35**(6): p. 672-88.
41. Lane, D.P., *Cancer. p53, guardian of the genome.* Nature, 1992. **358**(6381): p. 15-6.
42. Hanahan, D. and R.A. Weinberg, *Hallmarks of cancer: the next generation.* Cell, 2011. **144**(5): p. 646-74.
43. Malkin, D., et al., *Mutations of the p53 tumor suppressor gene occur infrequently in Wilms' tumor.* Cancer Res, 1994. **54**(8): p. 2077-9.
44. Kato, M.V., et al., *Loss of heterozygosity on chromosome 17 and mutation of the p53 gene in retinoblastoma.* Cancer Lett, 1996. **106**(1): p. 75-82.
45. Hendy, O.M., et al., *Frequency and prognostic significance of murine double minute protein-2 overexpression and p53 gene mutations in childhood acute lymphoblastic leukemia.* Hematology, 2009. **14**(6): p. 335-40.
46. Hof, J., et al., *Mutations and deletions of the TP53 gene predict nonresponse to treatment and poor outcome in first relapse of childhood acute lymphoblastic leukemia.* J Clin Oncol, 2011. **29**(23): p. 3185-93.
47. Ognjanovic, S., et al., *Low Prevalence of TP53 Mutations and MDM2 Amplifications in Pediatric Rhabdomyosarcoma.* Sarcoma, 2012. **2012**: p. 492086.
48. Pishas, K.I., et al., *Nutlin-3a is a potential therapeutic for ewing sarcoma.* Clin Cancer Res, 2011. **17**(3): p. 494-504.
49. Wang, Y., et al., *CDK7-dependent transcriptional addiction in triple-negative breast cancer.* Cell, 2015. **163**(1): p. 174-86.
50. Kwiatkowski, N., et al., *Targeting transcription regulation in cancer with a covalent CDK7 inhibitor.* Nature, 2014. **511**(7511): p. 616-20.
51. Cao, K. and A. Shilatifard, *Inhibit globally, act locally: CDK7 inhibitors in cancer therapy.* Cancer Cell, 2014. **26**(2): p. 158-9.
52. Franco, H.L. and W.L. Kraus, *No driver behind the wheel? Targeting transcription in cancer.* Cell, 2015. **163**(1): p. 28-30.
53. Delmore, J.E., et al., *BET bromodomain inhibition as a therapeutic strategy to target c-Myc.* Cell, 2011. **146**(6): p. 904-17.
54. Riggi, N., et al., *EWS-FLI1 utilizes divergent chromatin remodeling mechanisms to directly activate or repress enhancer elements in Ewing sarcoma.* Cancer Cell, 2014. **26**(5): p. 668-681.
55. Smith, R., et al., *Expression profiling of EWS/FLI identifies NKX2.2 as a critical target gene in Ewing's sarcoma.* Cancer Cell, 2006. **9**(5): p. 405-16.
56. Braun, B.S., et al., *Identification of target genes for the Ewing's sarcoma EWS/FLI fusion protein by representational difference analysis.* Mol Cell Biol, 1995. **15**(8): p. 4623-30.
57. Deneen, B., H. Hamidi, and C.T. Denny, *Functional analysis of the EWS/ETS target gene uridine phosphorylase.* Cancer Res, 2003. **63**(14): p. 4268-74.
58. Lessnick, S.L., C.S. Dacwag, and T.R. Golub, *The Ewing's sarcoma oncoprotein EWS/FLI induces a p53-dependent growth arrest in primary human fibroblasts.* Cancer Cell, 2002. **1**(4): p. 393-401.
59. Thompson, A.D., et al., *EAT-2 is a novel SH2 domain containing protein that is up regulated by Ewing's sarcoma EWS/FLI1 fusion gene.* Oncogene, 1996. **13**(12): p. 2649-58.

60. May, W.A., et al., *EWS/FLI1-induced manic fringe renders NIH 3T3 cells tumorigenic.* Nat Genet, 1997. **17**(4): p. 495-7.
61. Chipumuro, E., et al., *CDK7 inhibition suppresses super-enhancer-linked oncogenic transcription in MYCN-driven cancer.* Cell, 2014. **159**(5): p. 1126-1139.
62. Christensen, C.L., et al., *Targeting transcriptional addictions in small cell lung cancer with a covalent CDK7 inhibitor.* Cancer Cell, 2014. **26**(6): p. 909-922.
63. Ordonez, J.L., et al., *The PARP inhibitor olaparib enhances the sensitivity of Ewing sarcoma to trabectedin.* Oncotarget, 2015. **6**(22): p. 18875-90.

13 - Acknowledgements

I would like to thank Dr. Kimberly Stegmaier for the supervision, mentoring, and formative and fun time in the lab. Thank you for making all this happen and affording me opportunities I never thought possible - forever grateful.

I would like to thank Professor Christoph Klein for years' worth of encouragement, support and guidance. Thank you for all your help and advice on countless occasions.

Dr. Mandy Balboni Iniguez for being the best teacher in the lab I can imagine and the blast we had working together on these projects. Thank you for showing me what it means to be a good scientist.

A very warm thank you to Dr. Loren Walensky for the optimism and positive energy, and endlessly helpful discussions, resources, and insights.

Dr. Franziska Wachter for mentorship and friendship.

A big thank you to everyone in the Stegmaier lab especially Linda, Amy, Neekesh, Gabriela, Amanda, Emily, Alex, Sam, Sarah, and Anjali, as well as Annie and Greg from the Walensky lab.

Professor Martin Fischer for supporting my break from medical school to do research.

Thank you for the financial support to Deutscher Akademischer Austauschdienst (DAAD), and for the financial support for a previous research project to BI Fonds.

Finally and especially, thank you to my parents, my brother Stefan, and Anna for all the love and support.